THE UNIVERSITY OF CHICAGO

LEVERAGING MACROPHAGES TO DEVELOP CANCER THERAPEUTICS

A DISSERTATION SUBMITTED TO

THE FACULTY OF THE DIVISION OF THE BIOLOGICAL SCIENCES

AND THE PRITZKER SCHOOL OF MEDICINE

IN CANDIDACY FOR THE DEGREE OF

DOCTOR OF PHILOSOPHY

COMMITTEE ON CANCER BIOLOGY

BY

CHANG CUI

CHICAGO, ILLINOIS

MARCH 2021

DEDICATION

This dissertation is dedicated to:

Robert Zhang, my husband, for his patience, his trust, and his presence every step of the way.

Lev Becker, my lifelong mentor, for teaching me, amongst many things, how to dress my mind in a tuxedo.

TABLE OF CONTENTS

LIST OF FIGURES

LIST OF ABBREVIATIONS

ADCs – antibody-drug conjugates

ARG1 – arginase 1

ATM – Adipose tissue macrophages

BMDM – bone marrow-derived macrophages.

CSF1 – colony-stimulating factor 1

CSF1R – colony-stimulating factor 1 receptor

CTL – cytotoxic T lymphocytes

CTLA4 – cytotoxic T-lymphocytes-associated protein 4

CTSL/B/Z/D/E – cathepsins L/B/Z/D/E

DC – dendritic cells

DQ-OVA – Ovalbumin degradation assay

ECM – extracellular matrix

GEM: genetically engineered mouse

HDACs – histone deacetylase inhibitors

HMDM – human monocyte-derived macrophages

IFNγ – interferon-gamma

IL4/10/12/6/1b – interleukin 4/10/12/6/1beta

iNOS/NOS2 – nitric oxide synthase

IR – insulin resistance

IRF3 – interferon regulatory transcription factor 3

Kla – Histone lysine lactylation

LIPA – lysosomal acid lipase

LMNB1 – lamin B1

LPS – liposaccharide

Mab(s) – Monoclonal antibody/antibodies

MARCO – macrophage receptors with collagenous structure

M0 – Unstimulated monocyte or bone marrow-derived macrophage

M1 – "Classically activated macrophage" – monocyte or bone marrow-derived macrophage treated with IFNγ and LPS

M2 – "Alternatively activated macrophage" – monocyte or bone marrow-derived macrophage treated with IL-4

MHCI/II – Major histocompatibility complex class I/II

MMe – metabolically activated

MMPs – matrix metallopeptidases

MMR – macrophage mannose receptor

MSR1 – macrophage scavenger receptor 1

MSRN – macrophage sterol-responsive network

NFκB – Nuclear factor kappa B

NO – nitric oxide

PD1 – programmed cell death protein 1

PDL1 – programmed death-ligand 1

SCARB1 – scavenger receptor class B member 1

SIRPα – signal regulatory protein-a

STAT1/3/6 – Signal transducer and activator of transcription 1/3/6

STING – stimulator of interferon genes

T2D – Type 2 Diabetes

TAMs – tumor-associated macrophages

TFEB – transcription factor EB

Th1/2 – Type 1/2 T helper cells

TIF – tumor interstitial fluid

TLR – Toll-like receptor

TME – Tumor microenvironment

TNBC – triple-negative breast cancer

TNFR – tumor necrosis factor receptor

TRAIL – TNF-related apoptosis-inducing ligand

VEGFα – vascular endothelial growth factor alpha

ACKNOWLEDGMENTS

Everything I have accomplished in the past five and a half years has been facilitated by countless people: every member in the Becker lab, countless faculty and students across divisions, our collaborators, technicians in core facilities, administrative staff, cleaning and safety crew on campus, and hundreds of other dedicated people who have devoted their time and effort to make my research feasible and my grad school experience joyful. I could go on for pages mentioning names of individuals I owe thanks to but will limit the list to the handful of people below. Without their efforts, I wouldn't have been where I am and who I am today.

My first thank is to Lev Becker, whom I considered my boss, my friend, and my family. In the past five and a half years, there were countless moments filled with excitement, frustration, inspiration, or tension, but none were regret or resentment. Joining the Becker lab is one of my best decisions so far and becoming the first graduate student that Lev has mentored from year one is indeed my ultimate honor. Honestly, it was never a hard decision. Once I saw how he fueled a deep and abiding curiosity in himself and how he treated others, regardless of their status, I knew he would inspire people around him and build a culture of trust and respect.

Lev is a living example of a relentless pursuit of perfection. From both the philosophy he follows in conducting science and the way he delivers them via talks or writing. No detail is too small for him; he needs us to get all the little things right before interpreting any results. For instance, he personally demonstrated how to use a multichannel pipette and set up a home-made gel filtration column, he went over buffer concentration and pH for optimizing various assays, he demanded all raw measurements from protein concentration to tumor growth until I could handle everything correctly. When it comes to writing a manuscript or composing a talk, Lev's refusal to accept inadequacy even stands out more. Every paper or talk has way too many versions, each

of which represents their unique way to shine the science. He would go back and forth and compare and contrast to figure out the best way how a single piece of data fits in not only to serve the bigger picture but also carry the story along the way. He is good at doing science, but more importantly, he is good at selling it even fields where he has no roots yet. Undoubtfully, this requires a mental power to conceptualize both the mechanistic detail and the overarching promise. Formatting is another topic that I really think Lev want beyond seriousness. I don't think I will ever forget the 85.04 pt as figure standard, 7pt bold for the y-axis, and adobe blue instead of prism blue for most of the control group. Honestly, it could be exhausting and frustrating sometimes. But it was also inspiring, which far outweighed frustration. Because I know how much he cares about making things right and great, I simply want to live up to his expectation and do more.

Beyond the time he spends on my education and projects, he gave me access to his thinking and decision making, such as how to formulate a model from various pieces of data, what is the most efficient way to connect individual value points in a presentation or a write-up. It will never be an exaggeration to say that he taught me how to see in a way I hadn't be able to see before. I've learned his unique creative process where you can identify a pattern without knowledge and boundaries and connect ideas that fit in a bigger context. What is more invaluable is the ability to see a grand view as well as the granular details at the same time and consider how one affects the other. Lev walked me through this in a visionary's eye.

One of our common traits is that we both take immense personal pride in the work we do. This could be why my time with him has been genuinely pleasant. I appreciate all the lessons he consciously or subconsciously taught me, and I try my best to comprehend them. Thinking back

on the many lessons I learned, I would say it eventually comes down to one core value — "always give your mind a tuxedo to wear".

I would also thank Catherine Reardon (Kate) for sharing this journey with me from start to finish, for doing so much more than just giving me guidance on experiments and work-related diligence, and for years of endless listening and tremendous support. It is Kate who taught me that a loving heart is the truest wisdom.

Kelly Schoenfelt has also been with me from the beginning. As our lab mom, I couldn't thank her enough for many of the fundamental techniques she taught me, for her dedication to create an efficient lab environment, and for her optimism towards plenty of expected or unexpected occasions.

Alexandria Hoffman (Alex, I got it right!) is undoubtedly the best bench mate ever. She demonstrated patience to deduce my broken English and tolerated my invasive style of experimentation using our shared bench and fridge.

Anna Tang and Guolin Zhou helped me tremendously at the most intense time of my research, and both have been invaluable to me and to the rise of my projects.

Kasturi Chakraborty (Kaz), I cannot express enough my deep gratitude for your collaboration (lol) and your friendship. Although we met late, it has been a great sharing lessons, memories, and experiences with you.

Janie and Pete Booker are one of the strongest, caring, and sweet couples I have ever met. You two will always have the most special place in my heart.

Others I want to mention here include Geoffrey Greene, Yamuna Krishnan, Kay Macleod, Peter Savage, Seungmin Hwang Ernst Lengyel, Hilary Kenny, Megan Mcnerney, Ani Solanki, Lindsey Luat, Karin Peterson, Tomas Vaisar, Lucy Godley, Lisa McCune, Mark Eckert,

Seungmin Hwang, Wenchao Liu, Di Zhang, Xiang Yuan, Ariane Blank, Payal Tiwari, Jessica Fessler, Sravya Tumuluru. Their warmness, wisdom, and perspective made my grad school experience at the University of Chicago unique and memorable.

ABSTRACT

Tumor-associated macrophages (TAMs) are the most prevalent immune cell in the tumor microenvironment. Their high abundance in tumors has been strongly correlated with poor prognosis and patient survival across many cancer types. Despite their exhibition of immune stimulating M1-like phenotypes at an early stage of cancer development, TAMs mainly adopt an immunosuppressive M2-like phenotype. Extensive evidence has shown that M2-like TAMs support cancer cell survival, dampen cytotoxic adaptive immunity, promote angiogenesis, and facilitate tumor metastasis. Because of their negative influence in almost every step of tumorigenesis, targeting M2-like TAMs represents an emerging anti-cancer therapeutic strategy. However, our ability to exploit TAMs therapeutically has been stymied by two challenges: 1) an incomplete understanding of targetable pro-tumorigenic pathways and 2) limited knowledge of the mechanisms producing their M2-like phenotype. Overcoming these two challenges is required to develop effective TAM-targeting therapeutics and identify patients that might benefit from them. Studies in Chapter 2 (aiming to tackle the first challenge) not only identified lysosomal cysteine protease activity in TAMs as an important immune checkpoint in regulating antigen cross-presentation in cancer but further described a DNA nanodevice that can be targeted with organelle-level precision to alleviate this checkpoint in TAMs and achieve immunomodulation *in vivo*. Studies in Chapter 3 (aiming to tackle the second challenge) not only demonstrated a metabolic pathway to promote M2-like phenotypes in TAMs through a novel epigenetic mechanism, but also provided a rationale for repurposing LDHA inhibitors to target TAMs using the lactate-Kla-M2 pathway as a biomarker. Collectively, our studies clarify mechanisms contributing to the pro-tumorigenic functions of TAMs and seeded an approach to therapeutically target them.

CHAPTER ONE: A COMPREHENSIVE INTRODUCTION

Historical milestones of macrophage discovery, origins, and activation

Macrophages, along with their phagocytic capability during infection, were first discovered by a Russian zoologist Élie Metchnikoff over 120 years ago (Cavaillon, 2011; Metschnikoff, 1884; Tauber, 2003). Having observed that sticking rose thorns in starfish larvae could cause many phagocytic cells in their hemolymph, Metchnikoff had the intuition that phagocytosis might be a cellular defense mechanism against infection. He started to work on the concept that those phagocytes were actively participating in inflammation to fight pathogens and that inflammation should not be considered as a detrimental event (Cavaillon, 2011; Metchnikoff and Metchnikoff, 1873; Tauber and Chernyak, 1991). Although other scientific papers also reported similar phenomena of phagocytosis around the same time or even earlier, Metchnikoff's work on describing the phagocyting macrophages was the most detailed and documented (Ambrose, 2006; Cavaillon, 2011).

During the next five decades (after the initial discovery in 1884), researchers began to explore the origin of tissue resident macrophages. From both *in vitro* and *in vivo* experiments, scientists achieved a key realization that monocytes in the blood could migrate into the damaged tissue and accumulate there with appearances similar to those of tissue resident macrophages (Carrel and Ebeling, 1922; Clark and Clark, 1930; Ebert and Florey, 1939). This notion that macrophages were differentiated from blood monocytes became the prevailing view for the next 40 years. In the early 1980s, some evidence suggested that tissue resident macrophages were independent of circulating monocytes (Sawyer et al., 1982; Schulz et al., 2012). But it was not until recently that research equipped with more advanced genetic tools, such as lineage tracing,

demonstrated that many of the resident tissue macrophages were established during embryonic development, specifically derived from the yolk sac and the fetal liver (Ginhoux et al., 2010; Hoeffel et al., 2012; Schulz et al., 2012). However, whether embryonic and blood-derived macrophages possess specialized function remained to be explored (Epelman et al., 2014).

In addition to the origin of macrophages, the development of new technologies after World War II allowed research to more closely examine the biological roles of phagocytes in the disease setting. One milestone discovery was by George Mackaness in the early 1960s. He observed that macrophages from mice immunized with *Listeria monocytogenes* had distinct structures compared to those from the non-immunized mice (Mackaness, 1962; North and Mackaness, 1963). Mackaness further showed that those macrophages remained hypersensitive and acquired resistance to reinfection (Mackaness, 1962). This work introduced the concept of macrophage activation.

In the next 40 years, several studies reported that the supernatant from antigen-stimulated lymphocytes could robustly enhance pathogen killing activity of both murine and human macrophages (Anderson et al., 1976; Borges and Johnson, 1975; Fowles et al., 1973; Nathan et al., 1971, 1973). After a decade of hard searching, Carl Nathan finally identified interferon-gamma (IFNγ) as the lymphokine that could activate macrophages to acquire a boosted antimicrobial activity (Nathan, 1983). This finding was immediately integrated with the hypothesis that there were two types of T helper cells proposed by Robert Coffman and his colleagues (Mosmann et al., 1986). Research linked the secretion of IFNγ from Type 1 T helper cells (Th1) with the antimicrobial activity (intracellular infection) of activated macrophages and later referred to this type of activation as classical activation. The effect on macrophages by Type 2 T helper cells (Th2), which were involved in extracellular parasite clearance and allergy

response, was studied by Siamon Gordon and his team. They discovered that Th2-derived interleukin 4 (IL-4) potently enhanced murine macrophage mannose receptor (MMR) and suppressed pro-inflammatory cytokine expression (Doyle et al., 1994; Stein et al., 1992). This was later referred to as an alternative activation.

Classical and alternative activation were termed as M1 and M2 to mimic the Th cell nomenclature, but studies had soon realized that this terminology is more relevant for describing macrophage activation phenotype rather than the stimulus. Charles Mills observed that with the same stimulus (IFNγ and/or liposaccharide (LPS)), macrophages from prototypical Th1 strains of mice (e.g., C57BL/6, B10D2) showed increased nitric oxide synthases (iNOS) expression to produce nitric oxide (NO) whereas those from Th2 stains (e.g., BALB/c, DBA/2) showed increased arginase expression to produce ornithine (Mills et al., 2000). The discovery of differences in arginine metabolism between M1- and M2-activated macrophages prompted researchers to ask how the cytokine system contributed to similar/different phenotypes under physiological conditions.

While studying macrophage activation under physiological conditions, researchers gradually realized that such a binary classification does not represent the complex *in vivo* phenotypes. In the early 2000s, Alberto Mantovani and his colleagues presented the concept of a continuum of macrophage activation (Mantovani et al., 2002, 2004). This concept was first presented in the context of cancer: tumor-associated macrophages (TAMs) mainly adopt an M2-like phenotype (Mantovani et al., 2002). Later studies further acknowledged that M1 and M2 were just the two extreme ends of the continuum of macrophage activation and extended this concept to macrophage plasticity and heterogeneity in various diseases (Mantovani et al., 2004; Martinez and Gordon, 2014; Murray, 2017).

With rapidly growing research in this field, one challenge that stood out was the lack of consensus on how to define macrophage activation, which is commonly thought to be interchangeable with the term "polarization". This impeded the appropriate experimental designs both *in vitro* and *in vivo*, causing various interpretations and contentious statements about their pathophysiological functions (Hume, 2015; Murray et al., 2014). Peter Murray and his colleagues attempted to unify the polarization/activation terminology in 2014 (Murray et al., 2014). In cancer, for example, TAMs heterogeneity began to resolve and better characterized through genetics, microarray analysis, and purification methods (Cassetta et al., 2019; Qian and Pollard, 2010). Nowadays, the concept of macrophage activation has evolved to be a complex field that not only intersects with most physiological and pathological scenarios, but also provides conceptual understanding to guide therapeutic development.

Macrophage heterogeneity and plasticity in tissue homeostasis and disease progression

Macrophages are present in almost all tissues in various forms and play important roles in shaping tissue architectures, maintaining homeostasis, and orchestrating tissue-repair response (Okabe and Medzhitov, 2016; Wynn et al., 2013). One of the most appreciated features is that they display unique epigenetic and transcriptomic profiles and thus specialize in different tasks in each tissue (Gautier et al., 2012; Lavin et al., 2014). For example, Kupffer cells (macrophages in the liver) are involved in both immunogenic and tolerogenic responses, such as microbial clearance, toxin removal, and lipid metabolism (Ju et al., 2003; Remmerie and Scott, 2018; Seki et al., 2000). Osteoclasts (macrophages in the bone) mainly function in bone resorption during remodeling (Teitelbaum and Ross, 2003). Microglia (macrophages in the brain) are crucial in synaptic pruning for normal brain development (Paolicelli et al., 2011; Parkhurst et al., 2013).

Macrophages in the intestines regulate gastrointestinal motility as well as maintain mucosal homeostasis in the face of microbiota (Bain and Mowat, 2014; Muller et al., 2014). Therefore, macrophages are an incredibly diverse set of cells that have roles in almost every aspect of an organism's biology.

As plastic as they can be, macrophages within the same tissue have the capability of quickly adjusting their phenotype along the M1/M2 activation spectrum (Murray, 2017; Okabe and Medzhitov, 2016). For instance, during an early stage of infection, macrophages recognize and destroy a wide range of pathogens. They secrete pro-inflammatory cytokines and/or present antigens to alert the adaptive immune system (Shi and Pamer, 2011). Once the infection is cleared, macrophages adjust their phenotype to an immunosuppressive state to heal the wound and repair the tissue. (Mills et al., 2014; Nathan and Ding, 2010). Such plasticity not only reinforces their integral role in maintaining homeostasis, but also indicates their necessary functions in response to environmental stimuli. Consequently, macrophage dysfunction, i.e., under-or over-activation, that impairs functional heterogeneity and adaptation results in a causal association of macrophages with many diseases, including cancer, atherosclerosis, obesity/type 2 diabetes, asthma, arthritis, and susceptibility to infections (Cassetta and Pollard, 2018; Chawla et al., 2011; Moore and Tabas, 2011; Olefsky and Glass, 2010; Vitale et al., 2019; Wynn and Barron, 2010; Wynn et al., 2013) [1].

Obesity is associated with low-grade chronic inflammation that potentiates insulin resistance (IR). This leads to an increased insulin secretion by β-cells, causing a state of hyperinsulinemia to control blood glucose levels. If unmanaged, IR progress to type 2 diabetes

[1] Our lab aims to understand how disease-specific changes to tissues trigger specific pathways in macrophages to drive pathogenesis. I am fortunate to be involved in obesity/T2D and atherosclerosis projects, and thus provide a brief background in the following two paragraphs. Macrophages in cancer, which is the main focus of my Ph.D studies will be presented as a separate section.

(T2D), in which the increased insulin is unable to compensate for the degree of IR (Petersen and Shulman, 2018). Evidence since the 1990s has suggested a strong link among inflammation, obesity, and IR. Inhibiting pathways that drive inflammatory signaling and/or production in adipose tissue improves IR (Han et al., 2013; Hotamisligil et al., 1993, 1996; Olefsky and Glass, 2010; Saberi et al., 2009; Wei et al., 2016). Macrophages, which accumulate in obese adipose tissue, have been identified as a key player in the inflammation in potentiating IR (Weisberg et al., 2003; Xu et al., 2003). Murine studies showed that ablating pro-inflammatory adipose tissue macrophages (ATMs) or targeting pathways (e.g., TLR4, JNK) that support inflammation in ATMs improved insulin sensitivity and glucose tolerance (Arkan et al., 2005; Han et al., 2013; Saberi et al., 2009). Such inflamed ATM profile is often referred to as M1-activated phenotypes. Nevertheless, studies from our laboratory showed that ATMs adopt a metabolically activated (MMe) macrophage phenotype during obesity (Kratz et al., 2014). The MMe phenotype is distinct from the pro-inflammatory M1 phenotype present during infection. Using a proteomic approach, we showed that markers of M1 activation are absent on ATM from obese humans. MMe is driven by independent pro- and anti-inflammatory pathways, which regulate the balance between cytokine production and lipid metabolism. We further demonstrated that MMe macrophages could perform both detrimental and beneficial functions depending on the stages of obesity progression (Coats et al., 2017). Ongoing studies in the laboratory aim to dissect the signaling pathways underlying the activation of MMe macrophages. Understanding this mechanism is important because it allows us to specifically target the pro-inflammatory pathway in obesity/T2D without affecting the ability of macrophages to fight infections (M1-activated pro-inflammatory profile).

Another macrophage dysfunction-related inflammatory disease that our lab studies and I was fortunate to be involved in is atherosclerosis (Beckman et al., 2002; Gore et al., 2015; Haffner et al., 1998). Macrophages with excess cholesterol accumulation (foam cells) have been causatively linked to the initiation, progression, and rupture of atherosclerotic plaques (Li and Glass, 2002; Moore et al., 2013). Our previous work provided additional mechanistic understanding by identifying a "macrophage sterol-responsive network" (MSRN) that is important for foam cell formation and the development of atherosclerosis (Becker et al., 2010). Beyond deciphering pathways of atherosclerosis development, research has also tried to gain knowledge of how risk factors promote this disease. One major risk factor of atherosclerosis is T2D. However, the underlying mechanism has not been fully understood. This is mainly due to the difficulty of distinguishing macrophage pathways driven by hypercholesterolemia from those regulated by concomitant obesity/IR. To overcome this obstacle, many recent efforts, including ours, have combined genetic and dietary intervention in atherosclerotic mouse models (Daugherty et al., 2017; Guerrini and Gennaro, 2019; Hartvigsen et al., 2007; Reardon et al., 2018). Our work identified IFNγ, potentially through a noncanonical signaling pathway, as a T2D-specific driver of atherosclerosis by regulating proteins in the MSRN leading to foam cell formation (Reardon et al., 2018). Others have identified additional critical components in macrophages that drive diabetes-accelerated atherosclerosis (Kanter et al., 2020).

The above examples of how macrophages regulate disease progression illustrate their heterogeneous and plastic properties. More importantly, they emphasize that not all inflammatory phenotypes (non-resolving inflammation such as cancer is discussed below) are born equal. Although the upstream triggers involve the same molecules, the downstream effector pathways could have dramatic differences and thus overall outcome. Thus, therapeutics that are

tailored to precisely target disease driven pathway or a specific subcellular compartment within them would be necessary and have great potential.

Macrophages and cancer

Over the past decades, extensive research has increasingly recognized that tumor biology, especially metastatic dissemination and resistance to cancer treatment, cannot be fully understood when only examining the intrinsic proprieties of the cancer cells. Instead, it must be conferred by non-malignant cells as well as the non-cellular component that make up the tumor microenvironment (TME) (Cassetta and Pollard, 2018; Hanahan and Weinberg, 2011). The cellular component of the TME constitutes numerous cell types, among which leukocytes account for a large portion of total tumor mass (Gentles et al., 2015; Stankovic et al., 2018; Thorsson et al., 2018). As early as 100 years ago, evidence suggested that immune cells were able to react to the presence of cancer cells and reject tumors at early onset. This led scientists to formulate the hypothesis of cancer immunosurveillance (Burnet, 1971; Ehrlich, 1909; Gajewski et al., 2013). However, subsequent evidence showed that once cancer progresses, these tumor-infiltrating immune cells are modified to support tumor growth and suppress immune cell-mediated toxicity (Gajewski et al., 2013; Lengauer et al., 1998; Loeb et al., 2003). Such recognition that immunity plays a dual role in cancer progression refined the cancer immunosurveillance hypothesis to “cancer immunoediting” (Dunn et al., 2004a).

Cancer immunoediting is a dynamic process composed of three phases: elimination, equilibrium, and escape. In brief, elimination represents the classic concept of cancer immunosurveillance. Equilibrium is the adaption of tumor cells to increase resistance to immune attack by genetic instability/mutation/selection. This is probably the longest of the three phases

and ultimately contributes to the reduced immunogenicity and increased heterogeneity of tumors. The escape phase could be considered as the final win for cancer cells, where they acquire the ability to grow and progress (Dunn et al., 2004b, 2004a). Although many immune cells participate in this process, tumor-associated macrophages (TAMs) have been shown to be one of the most crucial contributors to this cancer immunoediting process (Cassetta and Pollard, 2018; O'Sullivan et al., 2012).

TAMs are the most abundant infiltrating leukocyte in almost all solid tumors (Cassetta and Pollard, 2018; Thorsson et al., 2018). Such increased infiltration largely originates from bone marrow-derived monocytes that are recruited through inflammatory signals, such as monocytes chemoattractant protein-1 (CCL2), released by cancer cells (Arwert et al., 2018; Qian et al., 2011). Yet, in cancers such as gliomas and those of the pancreas, TAMs can also be derived from erythroid-myeloid progenitors developed in the yolk sac at the embryonic stage (Chen et al., 2017; Zhu et al., 2017). But regardless of origin, the TME promotes these progenitors to differentiate into TAMs, which constitutes a heterogeneous population and perform diverse functions during tumorigenesis (Cassetta and Pollard, 2018).

At an early stage of cancer development, TAMs exhibit M1-like antitumor properties. They produce cytokines, such as IFNγ, to coordinate with adaptive immune cells (e.g., stimulate $CD8^+$ T cell proliferation and activation) and activate an antitumor adaptive immune response (Biswas and Mantovani, 2010; Evans and Alexander, 1970; Ong et al., 2012; Tsung et al., 2002). As the biggest "eaters" in our immune system, macrophages also possess phagocytosis ability that can directly kill cancer cells (Kroemer et al., 2013; Munn and Cheung, 1990; Salmi, 2017). This phagocytosis ability has been recently leveraged in combination with other therapeutic agents to eliminate tumor cells (Gholamin et al., 2017; Gül et al., 2014). In addition, several

studies, including ours, have shown that TAMs are capable of cross-presenting tumor antigen to active cytotoxic T cell response (Asano et al., 2011; Singhal et al., 2019). Considering their abundance in tumors, their cross-presentation activity makes them attractive to serve as a communication bridge to alert the adaptive immunity (a function classically ascribed to DCs). Furthermore, the abscopal effect, raised from the clinical observation that tumors regress at distant sites upon irradiation of the primary sites, has also been linked to the antitumor properties of TAMs (Klug et al., 2013).

However, those beneficial properties to oppose tumorigenesis do not represent the dominant phenotype of TAMs. With tumor progression, TAMs mainly adopted an M2-like pro-tumorigenic function. This dominantly pro-tumorigenic function also reflects on patients' clinical outcomes. Studies showed that their increased abundance in tumors is strongly correlated with both poor prognosis and patient survival in many cancer types (Joyce and Pollard, 2009; Mei et al., 2016; Tang, 2013; Yin et al., 2017; Zhao et al., 2017).

TAMs contribute to almost every step of tumorigenesis. At initiation stages, they supply bioactive molecules to create a "fertile" TME for cancer cells to survive and thrive (Mantovani et al., 2008; Wang et al., 2019). These bioactive molecules include growth factors, such as epidermal growth factor (EGF), to sustain tumor cell proliferating signaling, and survival factors, such as WNT, to limit cell death and maintain tumor stemness. They also include inflammatory cytokines, such as IL-6, and reactive oxygen species, such as nitric oxide, to create a mutagenic microenvironment. Studies have shown that in comparison to the normal inflammatory response during infection, which is resolved after the environmental insult is eliminated, the chronically inflamed TME that TAMs nourished presents no functional restoration. This leads to increased

DNA damage with existing congenic stress cause more mutation and genomic instability, proceeding tumor malignancy (Greten and Grivennikov, 2019; Kawanishi et al., 2017).

Beyond “fertilizing the soil”, TAMs support tumor angiogenesis. They produce pro-angiogenic factors, such as vascular endothelial growth factors A (VEGFA), and angiogenic CXC chemokines (CXCL8/12) to trigger rapid formation of new vessels, which provide a constant supply of oxygen and nutrients for tumor cells (Bergers and Benjamin, 2003; Lin and Pollard, 2007; Owen and Mohamadzadeh, 2013). Unlike normal blood vessels, those newly formed tumor vessels are immature and leaky. These abnormalities further contribute to other pro-tumorigenic characteristics, such as interstitial hypertension, hypoxia, and acidosis. Besides, these factors that TAMs secrete have also been reported to interfere with the delivery of therapeutic drugs, rendering tumor cells resistant to both radiation and some forms of cytotoxic therapy (Owen and Mohamadzadeh, 2013; Wenes et al., 2016).

In addition to directly benefiting cancer cells, TAMs negatively modulate other immune cells in the tumor, which indirectly contributes to tumorigenesis (Biswas and Mantovani, 2010; Mantovani et al., 2017). TAMs express T cell checkpoint ligands, such as PDL1 and CD80/86, which directly inhibit T cell functions. They also secrete enzymes, such as arginase (ARG1) and indoleamine 2,3-dioxygenase (IDO) to inhibit T cell proliferation (Dannenmann et al., 2013; Munn et al., 1999; Rodriguez et al., 2003, 2004; Saio et al., 2001). Their secretion of IL10 and TGFβ have also been shown to inhibit both $CD4^+$ and $CD8^+$ T cells yet induce regulatory T cell expansion (Curiel et al., 2004; Liu et al., 2011; Serafini et al., 2008). Further, TAMs are able to obstruct the activation of NK cells by expressing non-classical major histocompatibility complex HLA-E to interact with CD94 (Morandi and Pistoia, 2014). Together, those interactions with

other immune cells in the TME create an immunosuppressive environment where cancer cells can escape immune surveillance and proceed to establish metastases.

To facilitate cancer cell metastasis, another task TAMs take on is extracellular matrix (ECM) remodeling. ECM is a major structural support of the TME and is comprised of a network of biochemically distinct components. It is highly dynamic and able to shape communication among cells in the TME through a broad range of biophysical and biochemical changes. In general, there are three different mechanisms of ECM remodeling: 1) ECM deposition and post-translational modification, which alters the abundance, composition, or biochemical properties of ECM components; 2) ECM degradation, which releases bioactive ECM fragments and ECM-bound factors to alleviate migration barriers; 3) force-mediated ECM modification, where integrins apply mechanical force to align ECM fibres to open-up passages for cell migration (Henke et al., 2019; Winkler et al., 2020). TAMs are an important source of ECM remodeling proteases (Joyce et al., 2004). They induce proteolytic clearance of ECM component through upregulating metalloproteinase (MMP) production, accompanied by increased endocytosis and lysosomal degradation of collagen (Madsen et al., 2017). In addition to ECM degradation, TAMs contribute to ECM deposition. They increase the synthesis and assembly of collagens, resulting in cross-linking and linearization near invasive tumors. Such alteration increases tumor stiffness, which further promotes cell migration and invasion (Afik et al., 2016; Kai et al., 2019).

Therefore, understanding the diverse phenotypes of TAMs at different stages of cancer development as well as the mechanism by which they influence cancer and non-cancer cells within the TME is essential for designing therapeutic strategies and best leveraging their ability to eliminate tumors.

Current strategies of targeting tumor-associated macrophages

Currently, TAM-targeting strategies can be generally divided into three categories. One is to prevent their accumulation in tumors by either depleting TAMs or inhibiting macrophage/monocyte recruitment. Depleting macrophages by either genetic ablation of macrophage colony-stimulating factor 1 ($CSF1^{op/op}$) or antibody/chemical-based methods (anti-CSF1R/anti-F4/80 antibody or clodrosome treatment) in various murine tumor models has shown some promise in limiting tumor growth (Duong et al., 2018; Hiraoka et al., 2008; Lin et al., 2001, 2006; Miselis et al., 2008; Ries et al., 2014; Zeisberger et al., 2006). Hence, many small molecules or monoclonal antibodies (mAbs) therapies have been proposed, some of which have moved into clinical trials (Cassetta and Pollard, 2018; Poh and Ernst, 2018). For instance, trabectedin, in addition to its cancer cell killing capacity through the TNF-related apoptosis-inducing ligand (TRAIL)-mediated apoptosis pathway, induced TAM apoptosis (Germano et al., 2013; Liguori et al., 2016). Bisphosphonates, which are a class of drugs typically used for treating osteoporosis and complications arising from bone metastases, have also been widely used for depleting macrophages (Rogers and Holen, 2011; Van Acker et al., 2016). Especially, clodronate and zoledronic acid, a non-nitrogen or nitrogen-containing-bisphosphonate respectively, were preferentially taken up by macrophages *in vivo*, resulting in decreased TAM accumulation and reduced tumor burden (depletion efficacy varies depending on administration route and tissue, but is ~30-50%) (Daubiné et al., 2007; Hiraoka et al., 2008; Marra et al., 2011; Zeisberger et al., 2006). Moreover, CSF1 plays a crucial role in macrophage survival and proliferation. And CSF1-receptor (CSF1R) activation leads to macrophage accumulation in the tumor (the first study was in diffuse-type giant cell tumor) (Cannarile et al., 2017; Ries et al., 2014; Stanley et al., 1997). Thus, mAbs or small molecules to inhibit CSF1-CSF1R and CCL2-

CCR2 axes to prevent macrophage recruitment to both primary and metastatic tumors have also gained traction (Grossman et al., 2018; Manthey et al., 2009; Ries et al., 2014; Strachan et al., 2013).

The second category is to impede their immunosuppressive effects on other immune cells in the TME by directly targeting the molecules TAMs secrete or express. For instance, T cell proliferation and subsequent effector function rely on a sufficient L-arginine supply. Because M2-like TAMs express a high level of ARG1, which enzymatically depletes L-arginine from the environment and suppresses T cell functions, inhibitors to neutralize ARG1, such as CB-1158, have been in development (Cassetta and Pollard, 2018; Rodriguez et al., 2004; Steggerda et al., 2017). Checkpoint blockade inhibitors are another example. Effector T cells need to overcome intrinsic negative regulation pathways signaled through immune checkpoint receptors such as programmed cell death protein (PD1) or cytotoxic T-lymphocytes-associated protein 4 (CTLA4) (Waldman et al., 2020). In many cancer types, tumor cells express their ligand (PDL1 for PD1 and CD80/CD86 for CTLA4) to silence T cell function. Nevertheless, those ligands are also abundantly expressed on infiltrating immune cells, especially on TAMs, the most abundant immune cells in tumors (Sharma and Allison, 2015). Hence, the administration of many checkpoint inhibitors is also targeting TAMs in addition to malignant cells (Kleinovink et al., 2017).

The third category is through macrophage reprogramming, which is also the most advantageous pathway due to the opportunity to rebalance the infiltrating immune cells in the TME (compared to strategies in the first category) in a more proactive way (compared to strategies in the second category). Admittedly, macrophage reprogramming is a broad concept. Here, it is mainly referring to as shifting TAMs away from an M2-like phenotype and towards an

M1-like phenotype. Many targets have been proposed and explored. For instance, CD47 interacts with the signal regulatory protein-a (SIRPa), mainly expressed by macrophages, to prevent myosin IIA accumulation at the phagocytic synapse. Because this signaling pathway serves as an anti-phagocytosis or "do not eat me" signals, many cancer cells overexpress CD47 to escape phagocytosis by macrophages (Barclay and Van den Berg, 2014; Okazawa et al., 2005). Studies have shown that targeting this signal stimulates TAMs' antitumor phagocytic response and attenuate tumor growth in several murine tumor models (Edris et al., 2012; Gholamin et al., 2017; Xiao et al., 2015). Currently, two anti-CD47 monoclonal antibodies (mAb; Hu5F9G4 and CC-90002) and one soluble recombinant SIRPa-crystallizable fragment fusion protein (TTI-621) are being tested in clinical trials (Liu et al., 2015).

Toll-like receptor (TLR) agonist is another promising direction for reprogramming TAMs. Because TLRs play crucial roles in the detection of microbial infection and the induction of immune and inflammatory responses, different TLR synthetic ligands have been tested in various cancer models to skew macrophage polarization towards an M1-like phenotype to promote tumor regression (Adams, 2009; Medzhitov and Janeway, 2000). Two TLR7 agonists (Imiquimod and 852A) have shown efficacy in many murine models and are currently being tested on several cancers in clinical trials (Adams et al., 2012; Bubna, 2015; Dudek et al., 2007; Rodell et al., 2018). Similarly, the TLR9 ligand IMO-2055 has shown great promise when used alone or in combination with other therapies (Agrawal, 2008; Melisi et al., 2014; Sagiv-Barfi et al., 2018).

There are many other emerging strategies to reprogram TAMs. Targeting CD40, a receptor that belongs to the tumor necrosis factor receptor (TNFR) superfamily, showed profound TAM reprogramming and elicited an antitumor T cell response (Hoves et al., 2018;

Perry et al., 2018; Vonderheide, 2018). Anti-MARCO antibody, which targets macrophage receptors with collagenous structure (MARCO), induces antitumor activity of TAMs in multiple pre-clinical models. The underlying mechanism was dependent on the interaction of the Fc portion of the anti-MARCO antibody with the inhibitory Fc receptor on TAMs (Georgoudaki et al., 2016). These findings revisit the concept of mAb-mediated cytotoxicity via the Fc receptor (Clynes et al., 1998, 2000; Kang and Jung, 2019). In addition, the histone deacetylase inhibitor (HDACs) TMP195 led to the recruitment of highly phagocytotic and antitumorigenic TAMs and increased the efficacy of immunotherapy and chemotherapy (Guerriero et al., 2017). Some transcription factors, such as STAT1, STAT3, STAT6, and NFκB, were also proposed as targets for reprogramming TAMs (Baer et al., 2016; Kumar et al., 2016; Kusmartsev and Gabrilovich, 2005; Xin et al., 2009; Yan et al., 2016). Yet, many drugs are not designed to specifically target TAMs, and many targeted molecules are also expressed by other cell types. Hence, when interpreting the effect on tumor growth, one needs to take into consideration the off-target effects, which might be either synergetic or adversary or both depending on the dose, delivery method, and tumor models.

The contribution of my studies

There are two general approaches to explore targeting TAMs therapeutically. One approach is to identify targetable pro-tumorigenic pathways in M2-like TAMs, and the other is to understand the mechanism producing M2-like TAMs. In other words, one is to correct their bad behavior to prevent further damage, and the other is to prevent them from behaving badly in the first place.

My studies in Chapter 2 identified lysosomal cysteine protease activity in TAMs are

responsible for destroying tumor-associated antigens, resulting in a failure to activate $CD8^+$ T cells. I proposed that their failure to instruct $CD8^+$ T cells represents an important blockade in antitumor immunity. And because elevated lysosomal cysteine protease levels in tumors correlates with poor prognosis in many cancers, most of which are characterized by a preponderance of TAMs, the identification of this targetable pro-tumorigenic pathway in M2-like TAMs may have broad therapeutic implications. My studies in Chapter 3 extrapolated the concept obtained from an infection setting and applied it to cancer, and demonstrated that hypoxia induces a pro-tumorigenic M2-like phenotype in TAMs through LDHA-mediated lactate production. And this lactate-histone lactylation (Kla) pathway is considered as one mechanism producing M2-phenotypes. Because hypoxia is the most common feature of aggressive tumors, targeting this pathway to lowering lactate production by TAMs may also have broad implications.

CHAPTER TWO: ELEVATED LYSOSOMAL CYSTEINE PROTEASE ACTIVITY IN TUMOR-ASSOCIATED MACROPHAGES RESTRAINS ANTITUMOR IMMUNITY

Introduction

Tumor-associated macrophages (TAMs) are the most prevalent immune cell in the tumor microenvironment (Cassetta and Pollard, 2018). TAMs predominantly adopt an anti-inflammatory M2-like phenotype that contributes to tumor development through multiple mechanisms. M2-like TAMs overexpress growth factors (eg. VEGFa) that promote angiogenesis, proteases (eg. MMPs) that facilitate metastatic dissemination, and inhibitory molecules (eg. ARG1, IL-10, PDL1) that suppress adaptive immune responses (Cassetta and Pollard, 2018; Mantovani et al., 2017; Noy and Pollard, 2014). Moreover, depleting TAMs in pre-clinical models attenuated tumor growth and metastasis (Cotechini et al., 2015; Poh and Ernst, 2018), and high TAM abundance correlates with poor survival in patients across many cancer types (Gentles et al., 2015; Mantovani et al., 2017; Takeya and Komohara, 2016). For these reasons, M2-like TAMs are an emerging target for anti-cancer therapy development (Cassetta and Pollard, 2018; DeNardo and Ruffell, 2019; Mantovani et al., 2017; Poh and Ernst, 2018; Vitale et al., 2019).

Although the M2-like TAM phenotype predominates during tumor progression, TAMs are heterogeneous and their phenotype can be dynamically controlled by environmental cues including hypoxia, crosstalk with cancer cells, or stimuli derived from stromal or other immune cells in the tumor microenvironment (Poh and Ernst, 2018). During early stages of tumor development, TAMs are considered to acquire a pro-inflammatory M1-like phenotype that opposes tumorigenesis by killing cancer cells and secreting immune-activating cytokines

(Mantovani et al., 2017; Singhal et al., 2019). Moreover, recent studies showed that TAMs isolated from early human lung tumors can cross-present antigens to directly activate $CD8^+$ cytotoxic T lymphocytes (CTLs) (Singhal et al., 2019).

$CD8^+$ CTL activation via antigen cross-presentation has proven effective at eliminating tumors (Fehres et al., 2014; Kurts et al., 2010). In this process, innate immune cells acquire tumor antigens by phagocytosing cancer cells and display them on MHC class I molecules to activate $CD8^+$ CTLs. Although this function has been traditionally ascribed to tumor dendritic cells (DCs) (Joffre et al., 2012), many types of macrophages can cross-present antigens (albeit less efficiently than DCs), including TAMs isolated from early human lung tumors (Cruz-Leal et al., 2018; Embgenbroich and Burgdorf, 2018; Shen et al., 2004; Singhal et al., 2019). Given that TAMs are far more abundant and phagocytic than DCs in tumors (Cassetta and Pollard, 2018; Noy and Pollard, 2014), harnessing their ability to directly activate $CD8^+$ CTLs to attack tumors would be advantageous. However, there are two major impediments to enable such an approach. the first is an incomplete understanding the mechanisms limiting antigen cross-presentation by M2-like TAMs and the second is a paucity of technologies to target therapeutics to TAMs *in vivo*.

Here I identify a mechanism that limits antigen cross-presentation by M2-like TAMs. Using unbiased proteomics, I found that M2-like TAMs are characterized by elevated cysteine protease activity specifically in their lysosomes which hampers antigen cross-presentation and therefore prevents the effective activation of $CD8^+$ CTLs. I reasoned that if one could chemically inhibit cysteine proteases specifically in lysosomes, it might act as a potential therapeutic. DNA scaffolds have enabled the targeted delivery of chemical imaging agents to lysosomes in phagocytic cells in culture or in live worms by exploiting scavenger receptor mediated

endocytosis (Chakraborty et al., 2017; Dan et al., 2019; Surana et al., 2011; Veetil et al., 2017). Since there has been no other synthetic scaffolds that can deliver cargo with organelle-level precision and cell-type specificity in whole organisms, we therefore collaborated with Dr. Yamnua Krishnan's group and adopted their DNA nanotechnology to create a DNA nanodevice (E64-DNA) that carries the cysteine protease inhibitor E64 as a payload. E64-DNA preferentially localizes to TAMs via scavenger receptor-mediated endocytosis and traffics to lysosomes in these cells. By inhibiting cysteine protease activity specifically in lysosome in TAMs, E64-DNA improves antigen cross-presentation, which in turn, activates $CD8^+$ T cells to oppose tumorigenesis. My studies identify elevated lysosomal activity in M2-like TAMs as an important innate immune blockade in antitumor immunity that can be targeted by DNA nanotechnology.

Materials and Methods

Regulatory. Animal studies were approved by the Institutional Animal Care and Use Committee (ACUP #72209, #72504) at the University of Chicago. Cancer cell lines were approved by the Institutional Biosafety Committee (IBC #1503).

Mouse models. 6-7-week-old C57BL/6 female mice, LysMcre knock in mice, OT-1 mice, *Scarb1*-/-, *Cd36*-/- and *Msr1*-/- mice were purchased from The Jackson Laboratory. $Tfeb^{fl/fl}$ mice were a gift from Dr. Andrea Ballabio. pMel mice were a gift from Dr. Melody Swartz, University of Chicago. Myeloid cell specific *Tfeb*-/- mice (m*Tfeb*-/-) and their littermate controls (*fl/fl*) were generated by crossing $Tfeb^{fl/fl}$ mice with $LysMcre^{+/-}$ mice. Mouse genotype was confirmed by PCR using the following primers: forward, GTAGAACTGAGTCAAGGCATACTGG; reverse, GGGTCCTACCTACCACAGAGCC; loxp-

R, CTTCGTATAATGTATGCTATACGAAG). Mice were housed in the specific pathogen free animal facility at the Gordon Center for Integrative Science building at the University of Chicago.

Cell Lines. E0771 cells were a gift from Dr. Marsha Rosner, University of Chicago. LLC1 cells were purchased from ATTC (CRL-1642^{TM}). B16F10 cells were a gift from Dr. Thomas Gajewski, University of Chicago. B16.OVA cells were a gift from Dr. Jeffrey Hubbell, University of Chicago. Cells were cultured in Dubecco's Modified Eagles Medium (DMEM; HyClone) containing 10% heat-inactivated FBS (Gemini Bio Products) and 1% penicillin/streptomycin (Gibco).

Bone marrow-derived macrophage (BMDM) isolation and activation. BMDMs were differentiated from bone marrow stem cells with L-cell conditioned media for six days as previously described (Kratz et al., 2014). For M1 activation, BMDMs were treated with LPS (5ng/mL) and IFNγ (12ng/mL) for 24hrs. For M2 activation, BMDMs were treated with IL-4 (20ng/mL, R&D Systems) for 48hrs.

Adipose tissue macrophage (ATM) isolation. Adipose tissue was digested with Type 1 Collagenase (Worthington, 1mg/mL) at 37ºC with shaking at 160rpm for 45mins. Digested tissue was filtered through a 100μm cell strainer, incubated in RBC lysis buffer for 5 min, and passed through a 40μm cell strainer. ATMs were isolated using CD11b microbeads (Miltenyi Biotec) as previously described (Kratz et al., 2014) and purity was assessed by flow cytometry.

Murine tumor processing. Tumors were digested with Type 4 Collagenase (Worthington, 3mg/mL) and hyaluronidases (Sigma, 1.5mg/mL) at 37ºC with horizontal shaking at 200rpm for 45 mins (E0771) or 30 mins (LLC1 and B16F10). Digested tumor was filtered through a 100μm cell strainer, incubated in RBC lysis buffer for 5 min, and passed through a

40μm cell strainer. **For tumor immune cell analyses**, cells were labeled with various antibodies and analyzed by flow cytometry. **For sorting**, cells were resuspended in isolation buffer (0.1% BSA/PBS, 2mM EDTA), layered onto Ficoll-Paque^{TM} PLUS (GE Healthcare), and centrifuged at 450xg for 30mins. Mononuclear cells were obtained by collecting the middle white layer. Enriched mononuclear cells were stained with antibodies and M1-like and M2-like tumor-associated macrophages (TAMs) were sorted using a BD FACS Aria Fusion cell sorter. **For isolation of pooled TAMs**, TAMs were isolated using CD11b microbeads (Miltenyi Biotec) according to manufacturer's instruction, and purity was assessed by flow cytometry. **Antibodies used include**: CD45 (47-0451), CD11b (25-0112), MHCII (11-5321), Ly6C (12-5932), CD4 (17-0041), CD8 (12-0081), CD44 (25-0441) from ThermoFisher Scientific; CD3 (560527), CD62L (561917), CD11c (561241), Gr1(553129) from BD Biosciences, and Ly6G (127614), CD103 (121415), CD206 (141706) from BioLegend. Viability was assessed by calcein blue AM (BD Biosciences). Flow data were quantified by FlowJo v.10.4.1.

Isolation and activation of human peripheral blood monocyte-derived macrophage (HMDM). Monocytes were purified from the buffy coat using CD14 microbeads (MiltenylBiotec) and differentiated into HMDMs using human M-CSF (125ng/mL, R&D Systems) for 7 days as previously described (Kratz et al., 2014). For M1 activation, HMDMs were treated with LPS (100ng/mL, Sigma) and IFNγ (1ng/mL, R&D Systems) for 48hrs. For M2 activation, HMDMs were treated with IL-4 (10ng/mL, R&D Systems) and IL-10 (10ng/mL), R&D Systems for 48hrs.

Human breast tumor tissue processing and immune analysis. Human breast tumor tissue was cut into ~100mg pieces, each of which was digested in HBSS $Ca2^{+}$/$Mg2^{+}$ buffer containing TL (14U/ml) and DL (28U/ml) (Roche) and DNAse I (15mg/mL) at 37ºC with

horizontal shaking at 200rpm for 45mins, adapted from previously described (Cassetta et al., 2019). Digested tumors were filtered through a 100μm cell strainer, incubated in RBC lysis buffer for 5 min, passed through a 40μm cell strainer, and resultant cells were resuspended in isolation buffer (0.1% BSA/PBS, 2mM EDTA). For DQ-OVA degradation assays, cells were incubated with DQ-ovalbumin (see below) and DQ-OVA fluorescence was quantified in $CD45^+CD11b^+CD14^+CD163^+$ TAMs. Antibodies used include: CD11b (17-0118-41) from ThermoFisher Scientific; CD45 (557748), CD163 (563887), CD14 (347497), CD206 (321120), HLA-DR (560651) from BD Biosciences. Viability was assessed by Calcein blue AM (BD Biosciences). Flow data were quantified by FlowJo v.10.4.1.

Thioglycolate-elicited peritoneal macrophage isolation. Peritoneal macrophages were isolated as previously described (Reardon et al., 2018). Briefly, peritoneal macrophages were collected by lavaging the peritoneal cavity with PBS containing 2% endotoxin-free BSA (Sigma) 5 days after 4% thioglycolate injection (3 mL/mouse). Purity was assessed by flow cytometry.

Cytosolic and nuclear extractions. For cytosolic extraction, cell pellets were resuspended in 5X volume of cytoplasmic extraction buffer (10mM HEPES, 10mM KCl, 0.1 mM EDTA, 0.3% NP-40, protease inhibitors), incubated on ice for 5 mins with vortexing, and centrifuged at 3500*xg* for 5 mins at 4ºC, and the supernatant was harvested. For nuclear extraction, cell pellets were washed twice with 5X volume of cytoplasmic extraction buffer without NP-40, resuspended with 1X volume of nuclear extraction buffer (20mM HEPES, 0.4M NaCl, 1mM EDTA, 25% glycerol, protease inhibitors), incubated on ice for 10 mins with vortexing, centrifuged at 900x*g* for 5 mins at 4ºC, and the supernatant was harvested.

Analysis of lysosome number. Macrophages were seeded on imaging dishes (Cellvis). After attachment, cells were stained with anti-LAMP1 antibody to mark lysosomes,

followed by a DyLight 594 secondary antibody and DAPI for nuclear staining. Fluorescence images were acquired with a Nikon Eclipse Ti2 microscope with the following settings: objective magnification 90x, objective numerical aperture 0.45, room temperature, emission wavelengths of 457.5nm (DAPI), 535.0nm (GFP), and 610 nm (RFP), Camera Nikon DS-Qi2, and NIS-Element Version 5.02 software. Analysis was performed using brightfield to denote the area and perimeter of the cell. LAMP1 was imaged in RFP and thresholding was set using bright spot detection. Adjacent cells were separated using a watershed function centered on the nucleus. LAMP1 signal was quantified using number of LAMP1 signals per unit of cell area.

Analysis of lysosomal degradation by DQ-OVA. Lysosomal degradative capacity of macrophages was assessed by a DQ-OVA degradation assay according to manufacturer's instruction. Briefly, 0.2 million cells were incubated with 10μg/mL of DQ-OVA at room temperature for 15mins, washed, and incubated at 37ºC for another 15mins. DQ-OVA fluorescence was quantified by flow cytometry.

Analysis of lysosome pH. Lysosomal pH of macrophages was assessed by LysoTracker™ Red DND-99 according to manufacturer's instructions. In brief, 0.5 million cells were incubated with 100nM lysotracker at 37ºC for 1h. Signals were quantified by flow cytometry.

***In vitro* cell viability assay.** TAMs were plated in complete growth media and treated with vehicle, DNA, E64, or E64-DNA (100nM) for 72h, and cell viability was assessed by Calcein-AM (4ng/mL). Fluorescence was measured at 495nm/516nm using a Synergy HT Multi-Mode Microplate Reader (Biotek).

***In vitro* cell proliferation assay**. E0771 cells were seeded in a 96 well clear bottom plate (Greiner Bio-One) at 2000 cells/well. plate was placed into the IncuCyte® S3 live-cell analysis

system and allow the plate to warm to 37 °C for 30min prior to scanning. Each well was scanned every 4h, and the % of confluency was analyzed by IncuCyte analysis software.

Western blot analyses. Cells were lysed with 1% SDS containing protease and phosphatase inhibitors (Sigma), and protein was quantified with the BCA Protein Assay Kit (Pierce). Proteins (10-20μg) were resolved on 10%, 12.5%, or 15% SDS-PAGE gels depending on the target protein, transferred to PVDF membranes (Millipore), blocked with 5% BSA (Sigma) in 0.1% TBS/Tween-20 at RT for 2hrs, stained with primary and secondary antibodies, and visualized using the ECL detection kit (Biorad) and a LI-COR imager.

Antibodies – Antibodies against murine CTSL (af1515, R&D Systems), CTSB (3171, CST), Tubulin (2125, CST), CTSZ (sc-376976, Santa Cruz Biotechnology), BLOC1S1 (SC-515444, Santa Cruz Biotechnology), LIPA (sc-58374, Santa Cruz Biotechnology). LMNB1 (13435, CST), IRF3 (sc-33641, Santa Cruz Biotechnology), p-IRF3 (29047, CST), TBK1 (5483, CST), p-TBK1 (3504, CST), LC3 (L7543, Sigma), p62 (nbp1-49954, Novus Biologicals), CTSE (SC-166500, Santa Cruz Biotechnology), CTSD (SC-377124, Santa Cruz Biotechnology).

Shotgun proteomics. Whole cell lysates from M1 and M2 BMDMs were collected in 4% sodium deoxycholate (SDC) in 10mM Tris, 1 mM EDTA, pH 7.4 for trypsin digestion. Samples were denatured by heating at 56ºC and reduced with 5mM dithiothreitol (DTT) for 1h, alkylated with 15mM iodoacetamide for 30 min at room temperature in the dark, and excess iodoacetamide was quenched with an additional 5mM DTT. Samples were digested with trypsin (Promega, Madison, WI) at 1:20 w/w ratio overnight at 37°C with mixing. After digestion, SDC was precipitated by addition of 1% trifluoroacetic acid and insoluble material was removed by centrifugation at 14,000x*g* for 10min. Samples were then desalted by solid phase extraction

using Oasis HLB 96-well μElution Plate, dried down, stored at -80°C, and reconstituted with 0.1% formic acid in 5% acetonitrile to a peptide concentration of 0.1μg/μL for LC-MS analysis.

LC/MS analyses. Digested peptides were injected onto a trap column (40x0.1mm, Reprosil C18, 5μm, Dr.Maisch, Germany), desalted for 5 min at a flow of 4μL/min, and separated on a pulled tip analytical column (300 x 0.075 mm, Reprosil C18, 1.9 μm, Dr.Maisch, Germany) with a 3 segment linear gradient of acetonitrile, 0.1%FA (B) in water, 0.1%FA (A) as follows: 0-2 min 1-5%B, 2-150 min 5-25%B, 150-180 min 25-35%B followed by column wash at 80% B and re-equilibration at a flow rate 0.4μL/min (Waters NanoACQUITY UPLC). Tandem MS/MS spectra were acquired on Orbitrap Fusion Lumos (Thermo Scientific) operated in data-dependent mode on charge states 2-4 with 2s cycle time, dynamic exclusion of 30s, HCD fragmentation (NCE 30%) and MS/MS acquisition in the Orbitrap. MS spectra were acquired at a resolution 120,000 and MS/MS spectra (precursor selection window 1.6Da) at a resolution of 30,000 (for PMN media) or 15,000 (in-gel digests, recombinant peptides). Peptides and proteins were identified using the Comet search engine (Eng et al., 2015) with PeptideProphet and ProteinProphet validation. Search criteria included a 20ppm tolerance window for precursors and products, fixed Cys alkylation, and variable Met oxidation.

Measurement of gene expression by qRT-PCR. Cell pellets were lysed in RLT buffer, total RNA was isolated using the RNAeasy kit (Qiagen) with on-the-column DNAse digestion (Qiagen), converted to cDNA using reverse transcription kit (Qiagen), and amplified using QuantiTect SYBR Green PCR Kits (Qiagen). The following murine primers were used:
18s forward: GCCGCTAGAGGTGAAATTCTT, reverse: CGTCTTCGAACCTCCGACT.
Ctsb forward: CTGCGCGGGTATTAGGAGT, reverse: CAGGCAAGAAAGAAGGATCAAG.
Cstl forward: AGACCGGCAAACTGATCTCA, reverse: ATCCACGAACCCTGTGTCAT.
Ctsz forward: GGCCAGACTTGCTACCATCC, reverse: ACACCGTTCACATTTCTCCAG.

Lipa forward: CTGGTGAGGAACACTCGGTC, reverse: AGCCGTGCTGAAGATACACAA.

Lgmn forward: ATTCCTGACGAGCAGATCATAGT, reverse: GTGCCGTTAGGTCGGTTGA.

Tnfa forward: CACCACGCTCTTCTGTCTACTG, reverse: GCTACAGGCTTGTCACTCGAA.

Il1b forward: AACTCAACTGTGAAATGCCACC, reverse: CATCAGGACAGCCCAGGTC.

Nos2 forward: GCTCCTCTTCCAAGGTGCTT, reverse: TTCCATGCTAATGCGAAAGG.

Arg1 forward: CTCCAAGCCAAAGTCCTTAGAG, reverse: AGGAGCTGTCATTAGGGACATC.

Il10 forward: GCTCTTACTGACTGGCATGAG, reverse: CGCAGCTCTAGGAGCATGTG.

Fizz1 forward: CCTGCTGGGATGACTG, reverse: TGGGTTCTCCACCTCTTCAT.

Gapdh forward: TGGCCTTCCGTGTTCCTAC, reverse: GAGTTGCTGTTGAAGTCGCA.

Cd11b forward: CCATGACCTTCCAAGAGAATGC, reverse: ACCGGCTTGTGCTGTAGTC.

Sqstm1 forward: GAGTAACACTCAGCCAAGCA, reverse: TTCACCTGTAGATGGGTCCA.

Map1lc3b forward: TTGCAGCTCAATGCTAACCA, reverse: GGCATAAACCATGTACAGGA.

Vps11 forward: AAAAGAGAGACGGTGGCAATC, reverse: AGCCCAGTAACGGGATAGTTG.

Uvrag forward: CTGACAGAAAAGGAGCGAGA, reverse: GGATGGCATTGGAGATGTGA.

Atg9b forward: CCATCCCACAATGATACACACC, reverse: CCTCTAGCCGTTCATAGTCCT.

Vps18 forward: AGTACGAGGACTCATTGTCCC, reverse: TGGGCACTTACATACCCAGAAT.

Becn1 forward: AGGTACCGACTTGTTCCCTA, reverse: TCCATCCTGTACGGAAGACA.

The following human primers were used:

18S forward: CCCAACTTCTTAGAGGGACAAG, reverse: CATCTAAGGGCATCACAGACC.

CTSB froward: GAGCTGGTCAACTATGTCAACA, reverse: GCTCATGTCCACGTTGTAGAAGT.

CTSL forward: AAACTGGGAGGCTTATCTCACT, reverse: GCATAATCCATTAGGCCACCAT.

CTSZ forward: ACCAATGTGGGACATGCAATG, reverse: TTTGCGTAGATTTCTGCCATCA.

LIPA forward: CCCACGTTTGCACTCATGTC, reverse: CCCAGTCAAAGGCTTGAAACTT.

LGMN forward: TCCGGCAAAGTCCTGAAGAG, reverse: GGCAGCAGTAGTTGCATAAACA.

TNFA forward: CAGCCTCTTCTCCTTCCTGAT, reverse: GCCAGAGGGCTGATTAGAGA.

IL1B forward: TCTGTACCTGTCCTGCGTGT, reverse: ACTGGGCAGACTCAAATTCC.

IL12 forward: GCGGAGCTGCTACACTCTC, reverse: CCATGACCTCAATGGGCAGAC.

NOS2 forward: CAGCGGGATGACTTTCCAAG, reverse: AGGCAAGATTTGGACCTGCA.

CD206 forward: GGCGGTGACCTCACAAGTAT, reverse: ACGAAGCCATTTGGTAAACG.

ARG1 forward: GGCAAGGTGATGGAAGAAAC, reverse: AGTCCGAAACAAGCCAAGGT.

IL10 forward: GGGAGAACCTGAAGACCCTC, reverse: ATAGAGTCGCCACCCTGATG.

MMP12 forward: CATGAACCGTGAGGATGTTGA, reverse: GCATGGGCTAGGATTCCACC.

***In vitro* peptide digestion by lysosomal aspartic and cysteine proteases.** $gp100_{25\text{-}33}$ (1.5μg) was incubated with vehicle (Veh), lysosomal cysteine protease s (0.1μg CTSB and 0.1μg CTSL), or LAPs (0.1μg CTSD and 0.1μg CTSE) in pH 5 sodium acetate buffer at 37°C for 3h. Degradation was stopped by diluting the digested solution with cell culture media to 10μg/mL at pH 7.4. Diluted digested solution was added to TAMs to assess antigen presentation and $CD8^+$ T cell activation.

Nucleic acid synthesis. Amine labeled 38-mer DNA (D1), Alexa 647 labeled complementary DNA strand (D2), RNA (R1) and Alexa 647 labeled RNA strand (R2) were obtained from IDT. HPLC-purified oligonucleotides were dissolved in Milli-Q water to make 100μM stock solutions and quantified using an ultraviolet spectrophotometer and stored at − 20 °C. To prepare a DNA or RNA duplex sample (i.e. D1-D2, or R1-R2), 50μM of each complementary strand were mixed in equimolar ratios in 20 mM sodium phosphate buffer (pH 7.2) containing 100 mM KCl. The resultant solution was heated to 90 °C for 15 min, cooled to room temperature at 5°C per 15 min, and kept at 4°C overnight.

D1: ATCAACACTGCACACCAGACAGCAAGATCCTATATATA

D2: Alexa647TATATATAGGATCTTGCTGTCTGGTGTGCAGTGTTGAT

R1: AUCAACACUGCACACCAGACAGCAAGAUCCUAUAUAUA

R2: Alexa647UAUAUAUAGGAUCUUGCUGUCUGGUGUGCAGUGUUGAU

E64-DNA or PepA-DNA synthesis. E64 (Selleckchem) or Pepestin A (PepA, GoldBio) was conjugated to the amine labeled DNA duplex via EDC coupling. Briefly, 2mM E64 was incubated with *N*-hydroxysuccinimide (NHS) and 1-ethyl-3-(-3-dimethylaminopropyl) carbodiimide hydrochloride (EDC, each 2 equivalents excess) in 10mM MES buffer at pH 5.0 for 1 hour at room temperature. The solution was then added to the DNA duplex sample in two rounds and incubated for 24 hours. To remove excess E64, NHS and EDC the reaction mixture was pass through a 3kDa cut off centrifugal filter (Amicon, Millipore) and washing multiple times. E64-DNA is then stored at 4°C till further use.

E64-DNA uptake. For E64-DNA trafficking to lysosome, TAMs were allowed to adhere to 8 well dishes, pulsed with TMR-Dextran (0.5mg/mL) in complete medium for 1h, washed with PBS, and cultured for 16h to allow TMR-Dextran to traffic to lysosomes. At this time, TAMs were treated with E64-DNA (100nM) for 30min, washed with PBS, and imaged 30min later using a Leica SP5 confocal microscope. Images were analyzed using ImageJ. For *in vitro* E64-DNA uptake by M2 BMDMs from *wt*, *Scarb1*-/-, *Msr1*-/-, or *Cd36*-/-mice, 100nM E64-DNA or other types of nucleic acids (D1-D2, D2, R1-R2, R2) was incubated with 0.2 million BMDMs for 30mins, washed with PBS, and uptake was assessed by flow cytometry. For the *in vitro* M1 and M2 macrophage uptake competition assay, M2 BMDMs were labeled with Hoechst dye 33342 (2μg/mL, ThermoFisher Scientific) in a tube for 10mins and washed with PBS twice. M1 and M2 BMDMs were co-incubated at 1:1 ratio (0.2 million cells total) with E64-DNA (100nM) for 15mins, washed with PBS, and E64-DNA uptake was assessed by flow cytometry. For *in vivo* E64-DNA uptake, 25μg of E64-DNA was injected intratumorally (i.t.) or intravenously (i.v.) by retro-orbital route into E0771 tumor-bearing mice. Tumors were isolated 7h after injection, digested, and E64-DNA uptake was assessed by flow cytometry.

dsDNA serum stability. 10uM dsDNA was added to 100% mouse serum obtained from 8-week-old C57/BL6 mice and incubated for various time points (0-24h) at 37ºC. DNA degradation was assessed using 18% polyacrylamide gels stained with SYBR™ Gold (ThermoFisher Scientific).

$CD8^+$ T cell isolation. Mouse splenocytes were isolated from OT-1 or pMel mice as previously described (Reardon et al., 2018). $CD8^+$ T cells were isolated using the $CD8^+$ T Cell Isolation Kit (Miltenyi Biotec) according to manufacturer's instructions, and purity and activation status were assessed by flow cytometry.

Antigen cross-presentation assays. For *in vitro* antigen cross-presentation, macrophages were seeded at density of 100,000 cells/well in tissue culture treated 96-well plates (Corning). For the OT-1 system, macrophages were incubated with $OVA_{257-264}$ peptide (10μg/mL) or ovalbumin protein (OVA, 2mg/mL) for 2h. For the pMel system, macrophages were incubated with $gp100_{25-33}$ peptide (10μM) or X-ray irradiated B16F10 cells (60Gy, 50,000 cells) for 2h. After two washes with PBS, CFSE-labeled $CD8^+$ T cells were added (100,000/well) and co-cultured with macrophages for 72hrs. For *ex vivo* antigen cross-presentation, TAMs were isolated from B16.OVA tumors, plated, and co-cultured with 10,000 CFSE-labeled $CD8^+$ T cells (isolated from OT-1 mice) at a 1:1 ratio for 72hrs. For allostimulation, $CD8^+$ T cells were co-cultured with TAMs that had not been pre-treated with antigens. Anti-CD3 (5μg/ml) and anti-CD28 (5μg/ml) antibodies were used as a positive control. **For $CD8^+$ T cell activation**, IFNγ production in the culture medium at 72 hours was quantified using a mouse IFN-γ ELISA kit (Invitrogen). In some cases, cells were treated with BD GolgiPlug for the final 6h of coculture to allow intracellular IFNγ accumulation. Cells were collected, washed in Stain Buffer (BD Biosciences) and stained for activation markers for 15 minutes in the dark at room temperature.

Cells were fixed with BD Cytofix Fixation Buffer (BD Biosciences) for 20mins at 4°C. Fixed cells were permeabilized with BD Perm/Wash Buffer (BD Biosciences) and stained with an anti-IFNγ antibody (Biolegend, clone: 4S.B3). The percent of IFNγ$^+$/CD44$^+$ CD8$^+$ T cells was quantified by flow cytometry. **For CD8$^+$ T cell proliferation**, cells were labeled with 5μM 5,6-carboxyfluorescein diacetate succinimidyl ester (CFSE, Invitrogen), according to the manufacturer's instructions. The number of proliferating cells (CFSE-diluted) was quantified using CountBright™ beads (Invitrogen). In some cases, proliferating cells were quantified by the Proliferation Platform Software (FlowJo v.10.4.1).

Tumor inoculation and treatment. For the TNBC model, E0771 cells ($0.5x10^6$) were injected into the 4th mammary fat pad of the right ventral side of C57BL/6 mice. For other models, LLC1 cells ($0.5x10^6$), B16F10 cells ($1x10^6$), or B16.OVA cells ($1x10^6$) were injected into the flank of C57BL/6 mice. Tumor volume was assessed by calipers, and experiments were terminated when tumor volume reached >1000mm^3. For *in vivo* treatments, 25μg/injection of E64-DNA or DNA every 4 days, or 50mg/kg/intraperitoneal injection of cyclophosphamide every other day for three doses, followed by a week rest and another three doses every other day (Sigma) was used.

CD8$^+$ T cell depletion. Anti-mouse CD8α (clone 2.43) or rat IgG2b (isotype control) were injected intraperitoneally (200μg/injection) 3 days before the first treatment, and once/week after the last treatment. CD8$^+$ T cell depletion was confirmed by flow cytometry.

TAMs depletion. Anti-mouse CSF1R (clone AFS98) or rat IgG2b (isotype control) were injected intraperitoneally (300μg/injection) every other day for three doses before the first treatment, and every three days after the last treatment to maintain depletion.

Statistics. Statistical significance was determined with the Student's two-tailed, unpaired *t*-test ($p<0.05$). Linear regression was performed using Prism v.7 software. For shotgun proteomics studies, significance was assessed by a combination of the *t*-test and *G*-test (Becker et al., 2010) with correction for false-discovery rate (<5%) using PepC software (Heinecke et al., 2010).

Results

M2-like TAMs are characterized by elevated lysosomal protein levels and activity.

In order to identify tumor-promoting pathways in M2 macrophages, I compare them to their antitumorigenic M1 counterparts. I prepared the whole cell lysate samples obtained from M2-activated (IL-4) and M1-activated (LPS/IFNγ) bone marrow-derived macrophages (BMDMs), and Dr. Tomas Vaisar performed the discovery-based shotgun proteomics. Statistical analysis with the *G*-test and *t*-test identified 337 and 413 proteins significantly elevated in M2 and M1 BMDMs respectively (FDR<5%), many of which have been previously described (eg. M2: ARG1, YM1; M1: NOS2, CD11a) (Becker et al., 2012) (**Figures 2.1a-b**).

Informatics analysis of proteins elevated in M2 BMDMs identified enrichments in mitochondria, electron transport, and lipid metabolism (**Figure 2.1c**), which are consistent with their reliance on oxidative phosphorylation (Odegaard et al., 2007; Rodríguez-Prados et al., 2010). Interestingly, informatics also identified an enrichment of 18 lysosomal proteins in M2 BMDMs including several proteases (**Figures 2.1c-d**), five of which were representatively validated by immunoblotting (**Figure 2.2a**). The elevated levels of lysosomal proteins in M2 BMDM were consistent with enhanced lysosomal degradation assessed by an ovalbumin degradation assay (DQ-OVA) (**Figures 2.1e**).

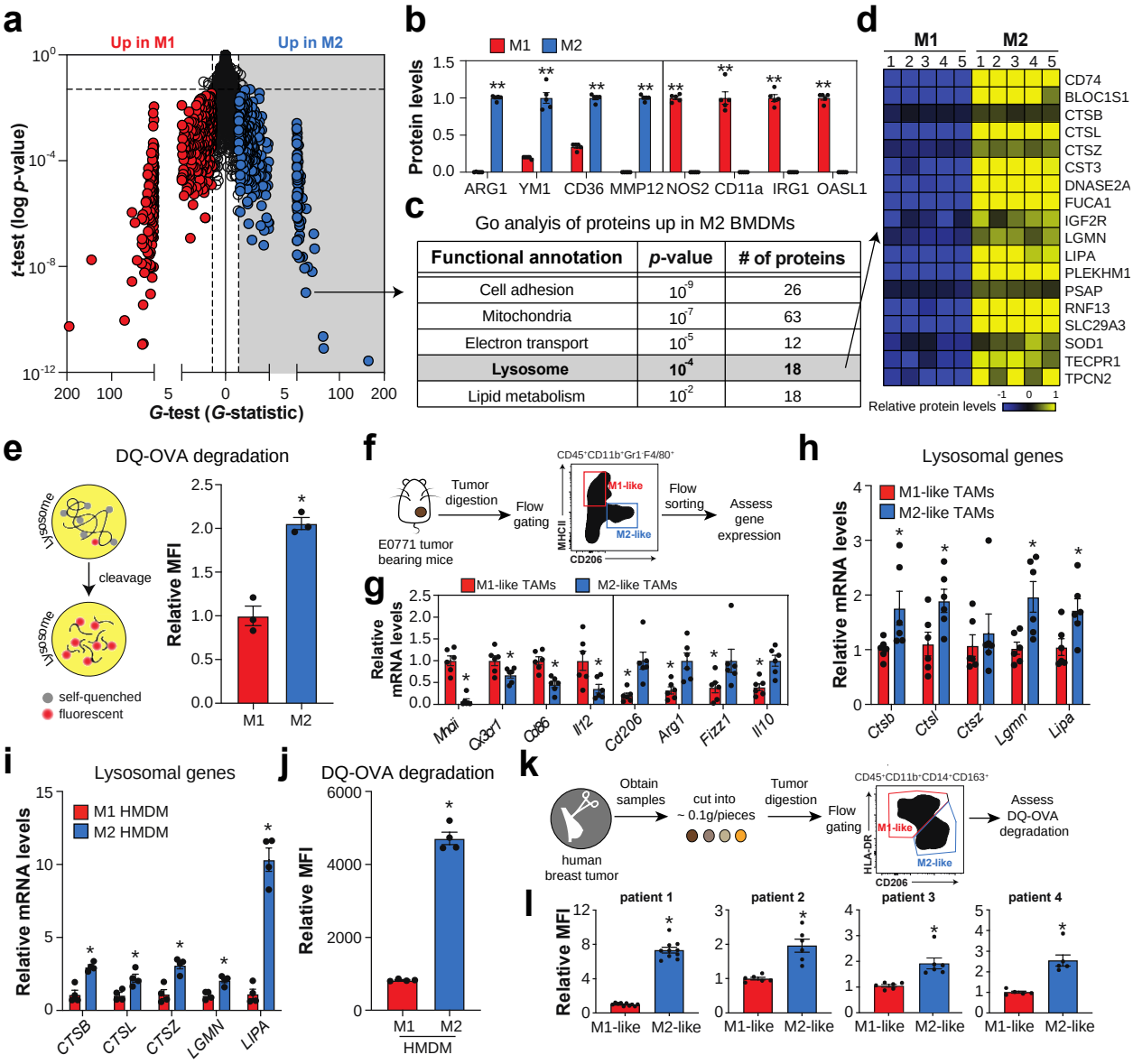

Figure 2.1. M2 macrophages have elevated lysosomal enzyme levels and activity. a, Shotgun proteomics analysis of whole cell lysates from M1 and M2 BMDMs. Differentially abundant proteins were identified by the *G*-test and *t*-test (FDR<5%). See also Table S1. n=5/group. **b**, Levels of known M1/M2-associated proteins from proteomics data. Proteins were quantified by spectral counting and standardized to the condition with highest abundance. n=5/group. **c**, Top five pathways from gene ontology (GO) analysis of proteins elevated in M2 BMDMs (p<0.05, Fisher's exact test with Benjamini-Hochberg correction). **d**, Heatmap of lysosomal protein levels in M1 and M2 BMDMs. Scale: $(M2\text{-}M1_{avg})/(M2+M1_{avg})$ or $(M1\text{-}M2_{avg})/(M1+M2_{avg})$. n=5/group. **e**, DQ-OVA degradation assays of M1 and M2 BMDMs. Assay scheme (*left*) and quantification (*right*). n=3/group. **f**, M1-like and M2-like TAMs were sorted from murine E0771 tumors. **g-h**, mRNA levels of M1- and M2-associated genes (**g**) and lysosomal genes (**h**) in sorted TAMs. n=6/group. **i-j**, Lysosomal gene expression (**i**) and DQ-OVA degradation (**j**) in M1 and M2

Figure 2.1 continued. HMDMs. n=4/group. **k**, M1-like and M2-like TAMs were sorted from human ER+ breast tumors. **l**, DQ-OVA degradation assays of sorted TAMs. n=5-10/patient. *, $p<0.05$ Student's *t*-test. **, FDR<5% *G*-test and *t*-test, error bars indicate the mean of independent experiments ± s.e.m. LC/MS is performed by Dr. Tomas Vaisar (University of Washington). Proteomic data (b) is analyzed by me, with the help of Dr. Lev Becker. Patient breast tumor samples were provided by Dr. Swati Kulkarni (Northwestern University).

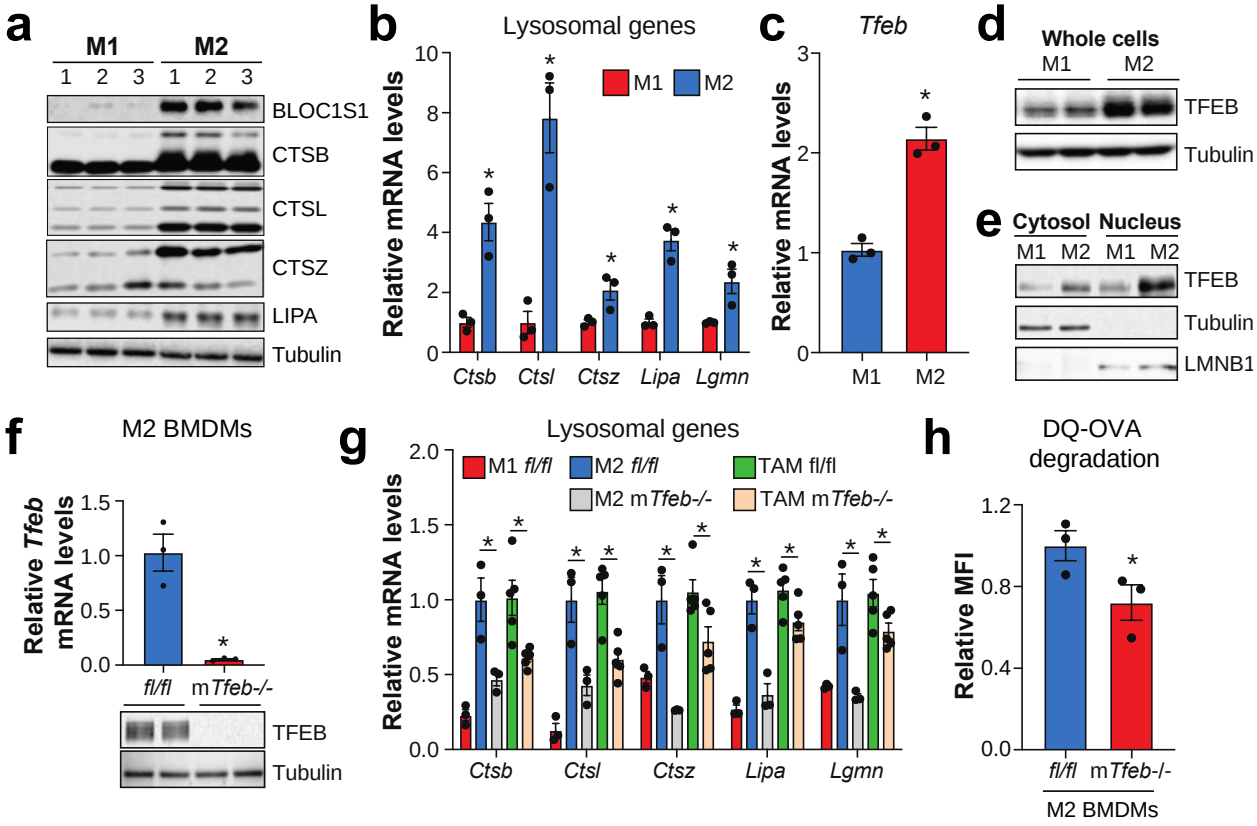

Figure 2.2. TFEB is responsible for elevated lysosomal enzymes in M2-like macrophages. a, Validation of lysosomal proteins elevated in M2 BMDMs by immunoblotting, related to Fig.1d. **b**, mRNA levels of lysosomal genes in M1 and M2 BMDMs. n=3/group. **c**, *Tfeb* mRNA levels in M1 and M2 BMDMs. n=3/group. **d**, TFEB protein levels in M1 and M2 BMDMs. **e**, Cytosolic and nuclear TFEB levels in M1 and M2 BMDMs. **f**, Validation of m*Tfeb*-/-. mRNA levels (top) n=3/group and protein levels (bottom). **g**, A comparison of lysosomal gene expression in M1 and M2 BMDMs from *fl/fl* mice versus M2 BMDMs from m*Tfeb*-/- mice, n=3/group; and a comparison of lysosomal gene expression in TAMs from *fl/fl* and m*Tfeb*-/- E0771 tumors, n=4/group. **h**, DQ-OVA degradation assays of *fl/fl* and m*Tfeb*-/- M2 BMDMs. n=3/group. *, $p<0.05$ Student's *t*-test, error bars indicate the mean of independent experiments ± s.e.m. Immunoblots (d, f) took the help of Anna Tang.

Although the M1/M2 system is a useful experimental model for *in vitro* studies, macrophages adopt more complex phenotypes *in vivo* (Geissmann et al., 2010). Hence, I used two approaches to corroborate our findings *in vivo*. First, I compared lysosomal gene expression in M2-like TAMs ($CD206^{high}MHCII^{low}$) and M1-like TAMs ($CD206^{low}MHCII^{high}$) sorted from E0771 tumors (**Figure 2.1f-g**). In comparison to M1-like TAMs, M2-like TAMs displayed elevated lysosomal enzyme levels including *Ctsb*, *Ctsl*, *Lgmn*, and *Lipa* (**Figure 2.1h**). Second, I purified total TAMs from E0771 tumors (~90-95% pure with minimal contamination with other myeloid cells, **Figure 2.3**) and compared them to mammary adipose tissue macrophages and thioglycolate-elicited peritoneal macrophages from tumor-free mice. Lysosomal enzyme levels and activity were elevated in TAMs relative to both types of macrophages (**Figure 2.4**).

I also studied the regulation of lysosomal enzyme levels and activity in human macrophages, which can sometimes exhibit distinct properties from murine macrophages (Schroder et al., 2012; Thomas and Mattila, 2014). In comparison to M1 polarized human monocyte-derived macrophages (HMDMs), M2 polarized HMDMs had increased lysosomal gene expression (*CTSB*, *CSTL*, *CTSZ*, *LGMN*, *LIPA*) and DQ-OVA degradation (**Figure 2.1i-j, 2.5**). Moreover, analysis of TAMs from human ER+ breast cancer patients revealed an increase in DQ-OVA degradation in M2-like ($CD206^{high}$HLA-DR^{low}) versus M1-like ($CD206^{low}$HLA-DR^{high}) TAMs (**Figure 2.1k-l**). Altogether, these studies demonstrate that lysosomal enzyme levels and/or activity are induced in M2 macrophages *in vitro* and M2-like TAMs *in vivo*, in both mice and humans.

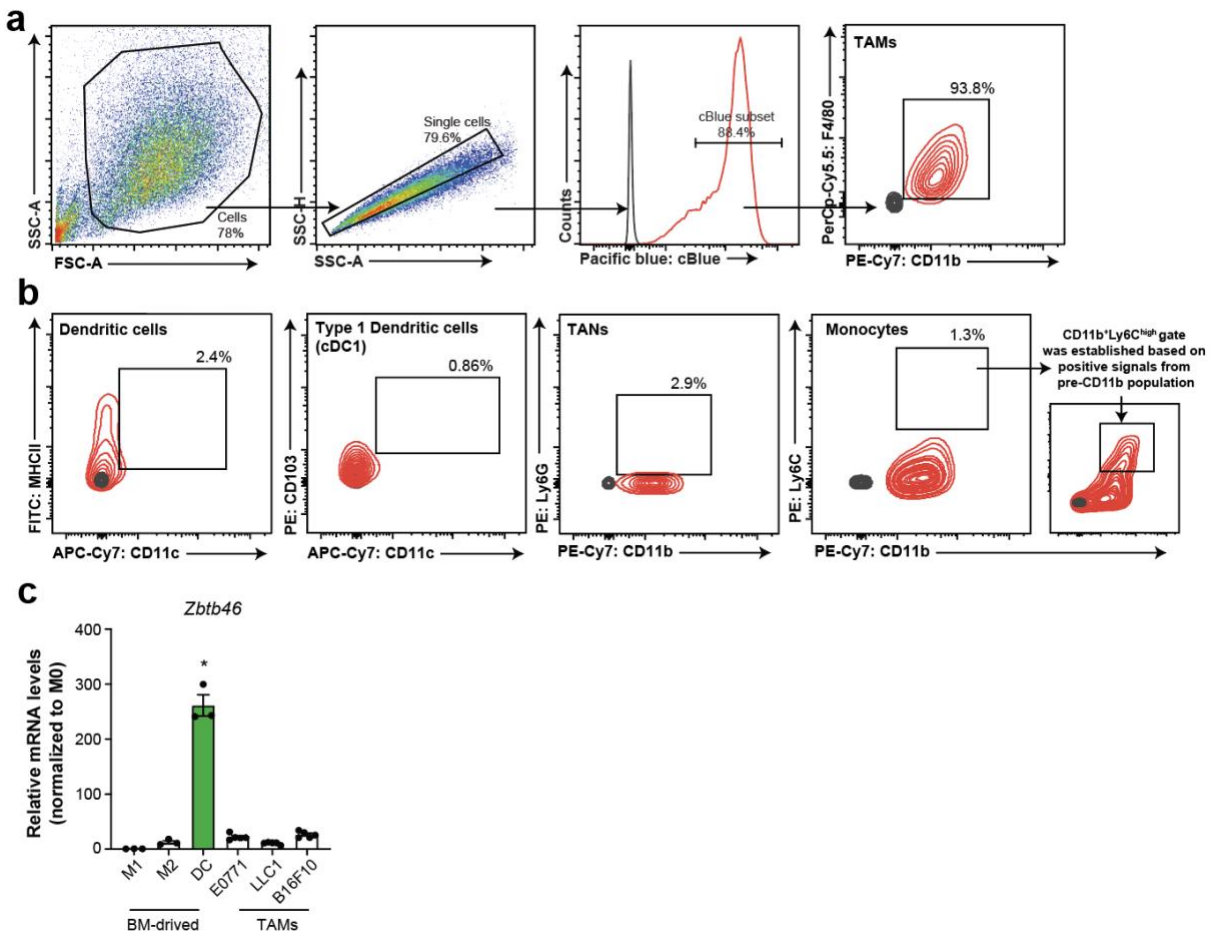

Figure 2.3 Validation of TAMs purity. a, Flow cytometry analysis of TAMs purified from E0771 tumors. **b**, Quantification of other types of myeloid cells in the purified TAM population. DC contamination was assessed by quantifying MHCII^{high}CD11c^{+} cells, and CD11c^{+}CD103^{+} (Type 1 dendritic cell subset). TAN and monocyte contamination were assessed by quantifying CD11b^{+}Ly6G^{+} and CD11b^{+}Ly6C^{high} cells respectively. **c**, mRNA expression levels of *Zbtb46*, a DC specific transcription factor, in TAMs isolated from E0771, LLC1, and B16 tumors, and bone marrow-derived M1/M2 macrophages and DCs. n=3/group. *, $p<0.05$ Student's *t*-test, error bars indicate the mean of independent experiments ± s.e.m.

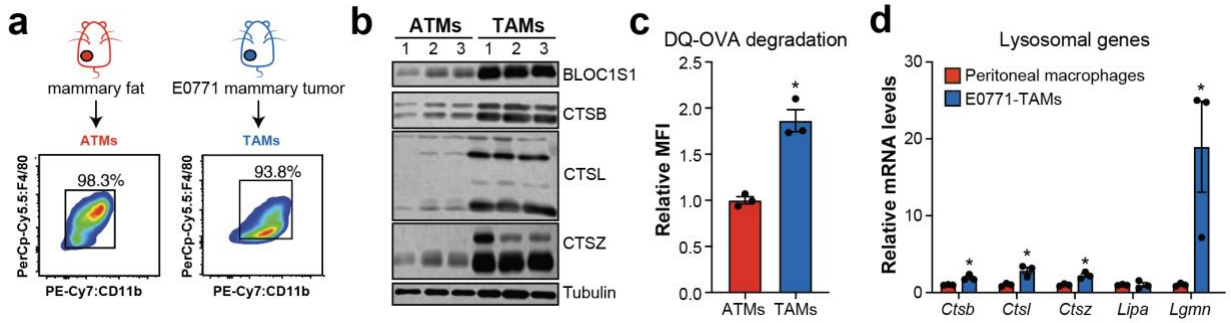

Figure 2.4. TAMs exhibit increased lysosomal enzyme levels and activity. a, Isolation of mammary ATMs from tumor-free mice and TAMs from E0771 mammary tumor-bearing mice. Purity of ATMs and TAMs was validated by flow cytometry. **b**, Immunoblot analysis of lysosomal protein levels in ATMs and TAMs. **c**, DQ-OVA degradation assays of ATMs and TAMs. n=3/group. **d**, mRNA expression of lysosomal genes in TAMs isolated from E0771 tumors and thioglycolate-elicited peritoneal macrophages from tumor-free mice. n=3/group. *, $p<0.05$ Student's *t*-test, error bars indicate the mean of independent experiments ± s.e.m.

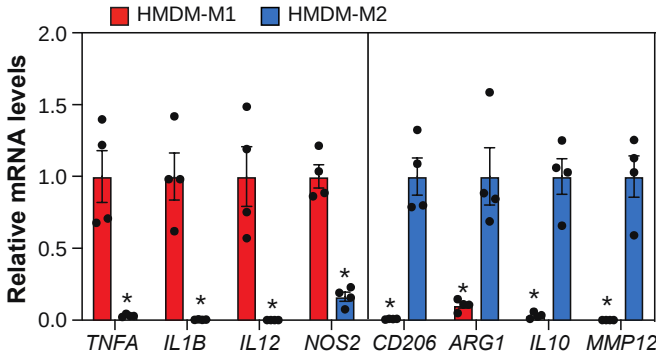

Figure 2.5. Validation of M1 and M2 activation of HMDMs. mRNA expression levels of M1- and M2-associated genes in HMDMs treated with LPS/IFNγ (M1) or IL10/IL4 (M2). Expression levels were normalized to the cell type with the highest expression of each gene. n=4/group. *, $p<0.05$ Student's *t*-test, error bars indicate the mean of independent experiments ± s.e.m. Blood is donated by myself and taken by Kristen Becker for me to isolate monocytes.

Reducing lysosomal activity in TAMs by genetic manipulation improves antitumor immunity.

I next explored the mechanism by which lysosomal proteins are elevated in M2 macrophages. Because many lysosomal proteins were induced, and this induction was also observed at the mRNA level (**Figure 2.2b**), I hypothesized that transcriptional control might be

involved. Previous studies identified transcription factor EB (TFEB) as a master regulator of the lysosome (Sardiello et al., 2009; Settembre et al., 2011). Three lines of evidence suggest that TFEB is responsible for the induction of lysosomal proteins in M2 macrophages. First, TFEB mRNA and protein levels were both elevated in M2 BMDMs (**Figures 2.2b-c**). Second, TFEB translocation to the nucleus was increased in M2 BMDMs (**Figure 2.2d**). Third, deleting *Tfeb* in myeloid cells (m*Tfeb*-/-) lowered lysosomal gene expression and DQ-OVA degradation in both M2 BMDMs and TAMs (**Figures 2.2f-h, 2.6a-d**). These findings indicate that M2 macrophages activate TFEB to promote lysosomal protein expression and enhance lysosomal degradation.

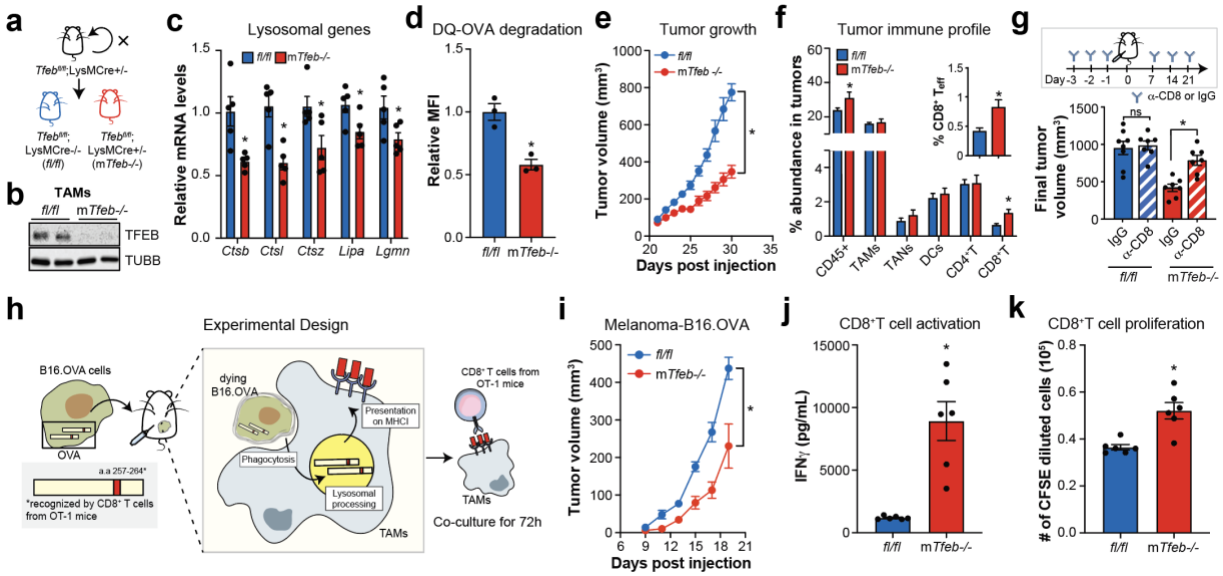

Figure 2.6. Deleting *Tfeb* in myeloid cells attenuates tumor growth through CD8$^+$ T cell. a, Breeding scheme of *fl/fl* and m*Tfeb*-/- mice. **b-g**, E0771 cells were injected into the 4th mammary fat pad of the right ventral side of *fl/fl* and m*Tfeb*-/- mice. **b**, TFEB protein levels in TAMs. **c**, mRNA levels of lysosomal genes in TAMs. n=5/group. **d,** DQ-OVA degradation assays of TAMs. n=3/group. **e**, E0771 tumor growth rates. n=11-12/group. **f**, Tumor immune cell composition. n=10-11/group. **g**, Final tumor volumes in mice treated with IgG or α-CD8 antibodies. Experimental design (*top*). Final tumor volume (*bottom*). n=7-8/group. **h**, Experimental design for antigen cross-presentation using the B16.OVA-OT-1 model. **i**, B16.OVA tumor growth rate in *fl/fl* and m*Tfeb*-/- mice. n=7/group. **j-k**, OT-1-CD8$^+$ T-cell activation (**j**) and proliferation (**k**) following co-culture with TAMs isolated from *fl/fl* and m*Tfeb*-/- B16.OVA tumors. n=6/group. *, $p<0.05$ Student's *t*-test. ns, not significant. CD8$^+$T$_{eff}$ = effector CD8$^+$ T cells, error bars indicate the mean of independent experiments ± s.e.m. *Tfeb*$^{fl/fl}$ mice is a gift from Dr. Andrea Ballabio (UNINA, Italy).

Notably, deleting *Tfeb* did not eliminate lysosomal gene expression or abolish lysosomal degradation in M2 macrophages, but rather attenuated them to levels observed in M1 macrophages (**Figure 2.2g**). This observation is consistent with the notion that TFEB does not regulate the basal level of lysosomal genes but rather modulates their induction in response to environmental cues (Napolitano and Ballabio, 2016). In addition, lysosomal number, lysosomal pH, and autophagy were all unaffected in TAMs from m*Tfeb-/-* mice (**Figure 2.7**). Thus, m*Tfeb-/-* mice enable one to reduce lysosomal proteins and proteolysis in M2-like TAMs while preserving basal lysosomal functions.

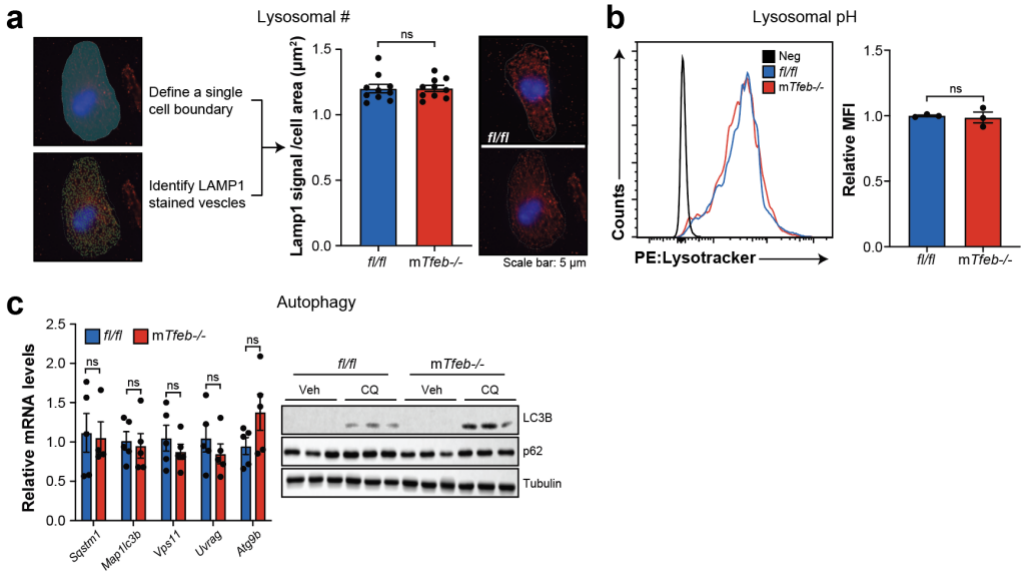

Figure 2.7. Characterization of mTfeb-/- TAMs. a, Quantification of lysosomes in *fl/fl* and m*Tfeb-/-* TAMs based on LAMP1 immunostaining. Schematic for quantification (*left*). Quantification of average LAMP1 signal/cell area (n=10/group) with an average of >40 cells/field (*middle*). Representative images (*right*). LAMP1 (red) and DAPI (blue). **b**, Quantification of lysosomal pH in *fl/fl* and m*Tfeb-/-* TAMs based on lysotracker staining. Representative flow cytometry image (*left*). Quantification of relative MFI of lysotracker signal (*right*). n=3/group. **c**, Autophagy gene expression in *fl/fl* and m*Tfeb-/-* TAMs (*left*, n=5). LC3B and p62 protein levels in *fl/fl* and m*Tfeb-/-* TAMs following treatment with vehicle (Veh) or chloroquine (CQ, 50µM) for 24h (*right*). Veh = H_2O. *, $p<0.05$ Student's *t*-test. TAMs were isolated from E0771 tumors. ns, not significant; error bars indicate the mean of independent experiments ± s.e.m. Quantification of lysosomal # was performed by Dr. Alex Hoffman and Blake McBeth.

To study how the elevation of the lysosomal activity in TAMs contribute to tumorigenesis, I injected m*Tfeb-/-* mice and *fl/fl* littermate controls with E0771 cells (triple-negative breast cancer, TNBC), B16F10 cells (melanoma), or LLC1 cells (lung cancer). Deleting *Tfeb* in myeloid cells attenuated tumor growth in all three models (**Figures 2.6e, 2.8a**), implying that hyperactive lysosomal activity in TAMs broadly influences tumorigenesis.

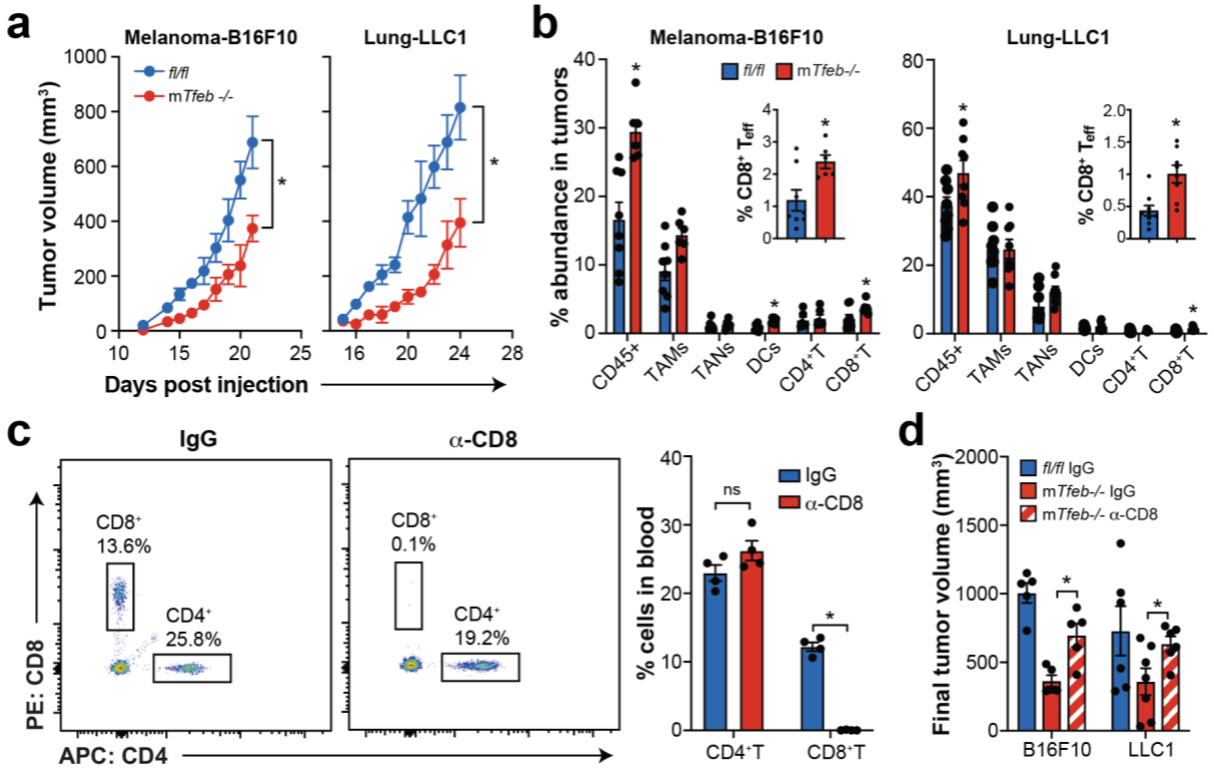

Figure 2.8. Deleting *Tfeb* in myeloid cells attenuates tumor growth through CD8⁺ T cells in B16F10 and LLC1 models. a, B16F10 and LLC1 tumor growth rates in *fl/fl* and m*Tfeb-/-* mice. n=8-14/group. **b**, Tumor immune cell composition in B16F10 and LLC1 tumor bearing *fl/fl* and m*Tfeb-/-* mice. n=6-10/group. **c**, Blood $CD8^+$ T cell levels in mice treated with α-CD8 or IgG antibodies. Representative flow cytometry data (*left*). Quantification of $CD8^+$ and $CD4^+$ T cells (*right*). **d**, Final tumor volume in B16F10 and LLC1 tumor bearing *fl/fl* and m*Tfeb-/-* mice treated with IgG or α-CD8 antibodies. n=5-7/group. *, $p<0.05$ Student's *t*-test; ns, not significant, error bars indicate the mean of independent experiments ± s.e.m. $CD8^+T_{eff}$ = effector $CD8^+$ T cells.

Because TAMs promote tumor growth, in part, by suppressing adaptive immunity (Mantovani et al., 2017; Noy and Pollard, 2014), I quantified tumor immune cells in m*Tfeb-/-*

and *fl/fl* control mice. I observed increases in total $CD8^+$ T cells ($CD3^+CD4^-CD8^+$) and effector $CD8^+$ T cells ($CD3^+CD4^-CD8^+CD62L^{low}CD44^{high}$) in all 3 models and these changes were specific since numbers of TAMs ($CD11b^+F4/80^+$), tumor-associated neutrophils (TANs, $CD11b^+Ly6G^+$), DCs ($CD11c^+$ $MHCII^{high}$), and $CD4^+$ T cells ($CD3^+CD4^+CD8^-$) were minimally affected (**Figures 2.6f, 2.8b**).

I next investigated whether the decreased tumor growth in m*Tfeb-/-* mice was reliant on $CD8^+$ T cell function. I injected m*Tfeb-/-* mice with an anti-CD8 antibody to deplete $CD8^+$ T cells or an IgG control antibody and evaluated effects on tumor growth. Depleting $CD8^+$ T cells in m*Tfeb-/-* mice restored tumor growth in all 3 tumor models (**Figures 2.6g, 2.8c-d**). In contrast, depleting $CD8^+$ T cells in *fl/fl* control mice had no impact on E0771 tumor growth (**Figure 2.6g**). These results suggest that deleting *Tfeb* in myeloid cells activates $CD8^+$ T cells to oppose tumorigenesis.

How does deleting *Tfeb* in myeloid cells activate $CD8^+$ T cells? One possibility is that *Tfeb-/-* impacts the M2-like phenotype of TAMs, which has been previously linked to immune suppression in cancer (Mantovani et al., 2017; Noy and Pollard, 2014). Arguing against this possibility, M2 markers (*Arg1*, *Il10*, *Fizz1*) and M1 markers (*Tnfa*, *Il1b*, *Nos2*) were minimally and inconsistently affected in TAMs from E0771, LLC1, and B16F10 tumors of m*Tfeb-/-* versus *fl/fl* mice (**Figure 2.9a**). For example, mRNA levels of *Arg1* were lower in TAMs isolated from E0771 and B16F10 tumors but increased in TAMs from LLC1 tumors.

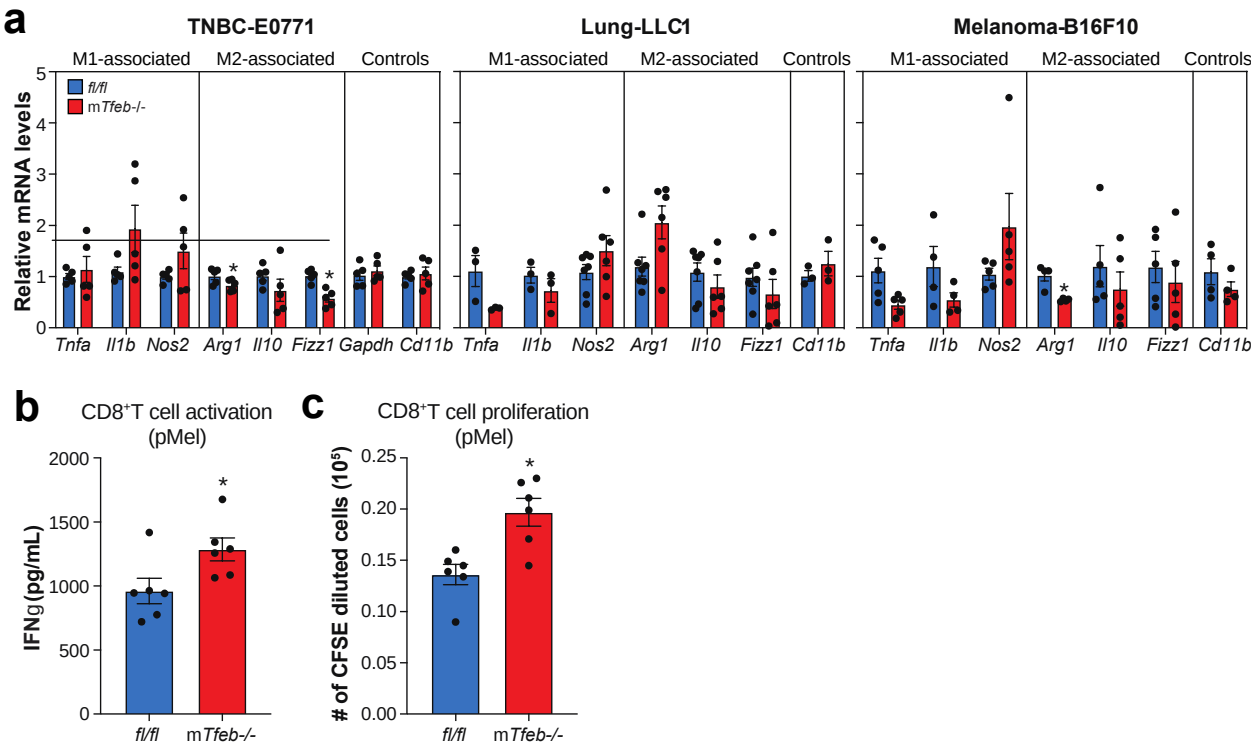

Figure 2.9. TAMs from m*Tfeb*-/- mice exhibit improved antigen cross-presentation with minimal phenotypic changes. a, M1- and M2-associated gene expression in TAMs from *fl/fl* and m*Tfeb*-/- E0771 tumors (*left*, n=5/group), LLC1 tumors (*middle*, n=5/group) and B16F10 tumors (*right*, n=4 group). **b-c**, Quantification of pMel-CD8$^+$ T cell activation (**b**) and proliferation (**c**) following co-culture with TAMs isolated from *fl/fl* and m*Tfeb*-/- B16.OVA tumors. n=6/group *, p<0.05 Student's *t*-test, error bars indicate the mean of independent experiments ± s.e.m.

TAMs can cross-present antigens to activate class I restricted T cells (Singhal et al., 2019). Moreover, in antigen presenting cells, lysosomal activity inversely correlates with their ability to present antigens (Delamarre et al., 2005; Trombetta and Mellman, 2005). I therefore reasoned that deleting *Tfeb* could activate CD8$^+$ T cells by enhancing antigen cross-presentation in TAMs. To test this possibility, I used the B16.OVA model to evaluate antigen cross-presentation *ex vivo* (Lund et al., 2012). B16.OVA cells are engineered to express ovalbumin (OVA) protein, which contains the antigenic $OVA_{257-264}$ peptide recognized by CD8$^+$ T cells from OT-1 mice. They also express gp100 which contains the endogenous antigenic $gp100_{25-33}$

peptide recognized by $CD8^+$ T cells from pMel mice. I subcutaneously injected B16.OVA cells in the flank to create a tumor. Isolated TAMs were subsequently co-cultured with $CD8^+$ T cells from OT-1 mice or pMel mice to evaluate their antigen cross-presentation capability *ex vivo* (**Figure 2.6h**).

As in other models, B16.OVA tumor growth was attenuated in m*Tfeb-/-* mice (**Figure 2.6i**). TAMs from m*Tfeb-/-* mice activated $CD8^+$ T cells purified from OT-1 mice or pMel mice more effectively, as evidenced by increased IFNγ production and proliferation (**Figures 2.6j-k, 2.9b-c**). This effect was not due to contamination of TAMs with tumor DCs, which was measured at <3% based on flow cytometric quantification of $CD11c^+MHCII^{high}$ and $CD11c^+CD103^+$ DCs, as well as expression levels of *Zbtb46*, a DC specific transcription factor (Satpathy et al., 2012) (**Figure 2.3**). Similarly, contamination with TANs and monocytes was insignificant (<3%) (**Figure 2.3**). Thus, genetically downregulating lysosomal activity selectively in myeloid cells (via m*Tfeb-/-*) attenuates tumors by promoting adaptive immunity.

A lysosome-targeted DNA nanodevice promotes antigen cross-presentation by TAMs.

Having found that broadly lowering lysosomal activity in TAMs improves their ability to cross-present antigens, Lev and I sought to identify a therapeutically actional target. Lev and I therefore analyzed 18 lysosomal proteins elevated in M2 BMDMs (see *Figure 2.1d*), which pinpointed an enrichment in cysteine protease and antigen presentation (**Figure 2.10a**). Indeed, Cysteine proteases were specifically elevated in M2 versus M1 BMDMs, while aspartic proteases were not (**Figures 10a-b**). Furthermore, previous studies showed that unlike aspartic proteases, cysteine proteases fail to generate antigenic peptides when incubated with OVA *in vitro* and can completely digest smaller OVA-derived antigenic peptides (Diment, 1990;

Rodriguez and Diment, 1995). Indeed, incubating gp100$_{25\text{-}33}$ with purified cysteine proteases (cathepsin B, CTSB and cathepsin L, CTSL) prior to delivering it to TAMs blocked their ability to activate CD8^{+} T cells, while incubation with purified aspartic proteases (cathepsin D, CTSD and cathepsin E, CTSE) had a negligible effect (**Figures 2.11a-b**).

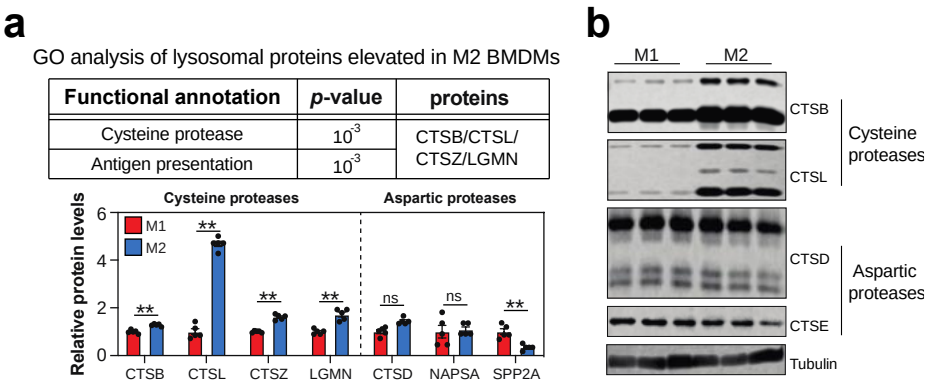

Figure 2.10. Cysteine proteases, not aspartic protease, are specifically upregulated in M2 BMDMs and affect antigen preservation. a, Top two pathways from GO analysis of up-regulated lysosomal proteins in M2 BMDMs (*top*, $p<0.05$, Fisher's exact test with Benjamini-Hochberg correction). Cysteine protease and aspartic protease levels in M1/M2 BMDMs quantified by spectral counting (*bottom*, n=5/group). **b**, Immunoblots of representative cysteine and aspartic protease in M1 and M2 BMDMs. **, FDR<5% *G*-test and *t*-test (from shotgun proteomics analyses, see also Fig 1a, Table S1); ns, not significant; error bars indicate the mean of independent experiments ± s.e.m. LC/MS is performed by Dr. Tomas Vaisar (University of Washington). Proteomic data (b) is analyzed by me, with the help of Dr. Lev Becker.

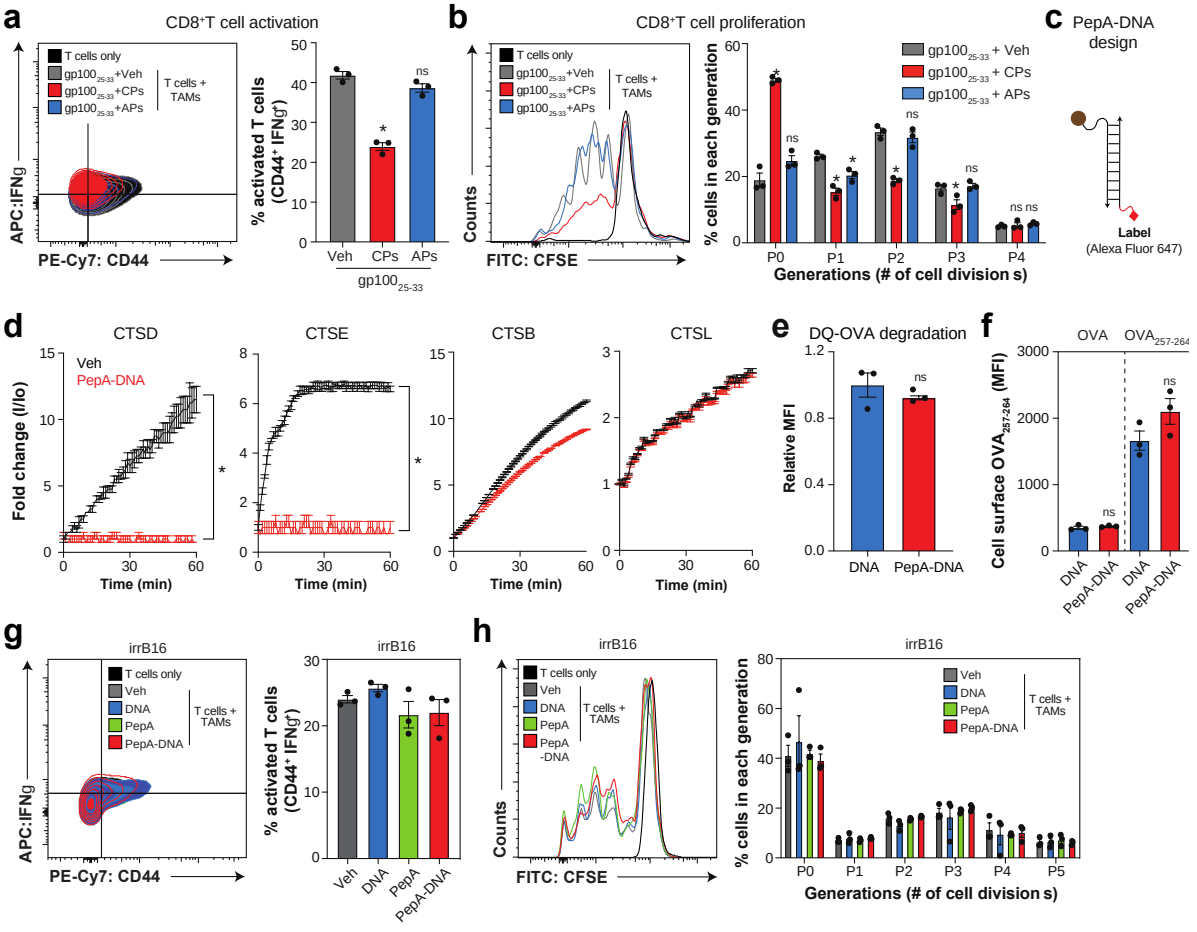

Figure 2.11. Inhibiting aspartic protease activity in the lysosome has minimal effect on antigen cross-presentation by macrophages. a-b, $gp100_{25\text{-}33}$ (1.5µg) was incubated with vehicle (Veh; PBS), cysteine proteases (CPs) (0.1µg CTSB and 0.1µg CTSL), or aspartic proteases (APs) (0.1µg CTSD and 0.1µg CTSE) in pH 5 sodium acetate buffer at 37°C for 3h. Degradation was stopped by adjusting to pH 7.4 with cell culture media (dilution to 10 µg/mL). Inhibition of CPs and APs was confirmed by activity assays and diluted solution was subsequently used for antigen cross-presentation assays. pMel-$CD8^+$ T cell activation (**a**) and proliferation (**b**) after 72h of co-culture with TAMs pre-stimulated with diluted $gp100_{25\text{-}33}$ digestion solution. n=3/group. **c**, PepA-DNA design: one strand is conjugated with PepA on its 5' end and the other with Alexa Fluor 647 to monitor uptake. **d**, Catalytic activity assays for lysosomal cysteine proteases (CTSB, CTSL; 5nM) or aspartic proteases (CTSD, CTSE; 5nM) in the presence of vehicle (Veh; PBS) or PepA-DNA (25nM). Results are plotted as fluorescence intensity at time *t*, relative to time 0 (I/Io). n=3/group. **e-h**, Peritoneal macrophages were isolated and treated with vehicle (Veh; PBS), DNA, PepA, or PepA-DNA (100nM) for the indicated times and various functional endpoints were measured. **e**, Effect of PepA-DNA (2h) on DQ-OVA degradation. n=3/group. **f**, Quantification of MHCI-bound $OVA_{257\text{-}264}$ on peritoneal macrophages 3h post treatment with OVA protein or $OVA_{257\text{-}264}$ peptide. n=3/group. **g-h**, pMel-$CD8^+$ T cell activation (**g**) and proliferation (**h**) after 72h of co-culture with peritoneal

Figure 2.11 continued. macrophages pre-stimulated with irradiated B16F10 cells (irrB16). n=3/group. *, $p<0.05$ Student's *t*-test, error bars indicate the mean of independent experiments ± s.e.m. ns, not significant. PepA-DNA was made by Dr. Kasturi Chakraborty for me.

Moving forward, I aimed to test whether the elevated cysteine protease activity in lysosomes of TAMs impeded their ability to cross-present antigens. Cysteine proteases predominantly function in endocytic pathway. Yet, many of their pro-tumorigenic functions are linked to extracellular cysteine protease activity in tumors (Mohamed and Sloane, 2006). Whether treating TAMs with E64 (Matsumoto et al., 1999), a small molecule that inhibits cysteine protease activity, would improve antigen cross-presentation was considered. E64 has difficulty penetrating cells and localizing to lysosomes (Powers et al., 2002), which could potentially limit its access to the pool of cysteine proteases in the lysosome. To overcome these challenges, our lab collaborated with Dr. Yamuna Krishnan's group and adopted their DNA-based lysosomal targeting nanotechnology (Chakraborty et al., 2016; Leung et al., 2019; Surana et al., 2011). DNA nanotechnology has provided effective ways to localize fluorescent molecules in lysosomes of phagocytes in nematodes or immune cells in culture (Surana et al., 2011; Veetil et al., 2017). One such delivery pathway utilizes double-stranded DNA (dsDNA) which is endocytosed via scavenger receptors that are highly expressed by macrophages (Leung et al., 2019). We reasoned that if E64 was conjugated to DNA, the DNA nanodevice could localize the E64 payload to the lysosome of TAMs (**Figure 2.12a**).

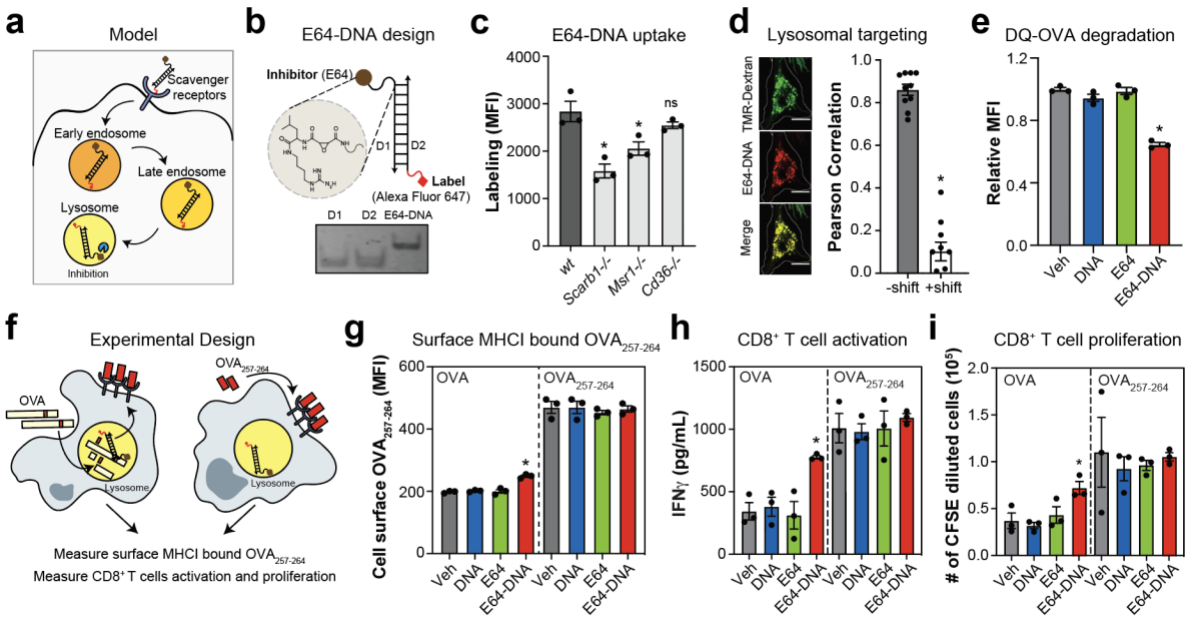

Figure 2.12. A lysosome-targeted DNA nanodevice (E64-DNA) promotes antigen cross-presentation by TAMs. a, Scheme of E64-DNA trafficking to lysosome. **b**, E64-DNA design: one strand (D1) is conjugated with E64 on its 5' end and the other (D2) with Alexa Fluor 647 to monitor uptake (*top*). E64-DNA purity and integrity were validated by native polyacrylamide gel electrophoresis (*bottom*). **c**, E64-DNA uptake by M2 BMDMs from *wt*, *Scarb1*-/-, *Msr1*-/-, or *Cd36*-/- mice. Uptake was quantified by flow cytometry; n=3/group. **d**, Representative images (*left*) and Pearson correlation (*right*) of co-localization of TMR-Dextran labeled lysosomes (green) with E64-DNA (red). Pearson correlation with and without a 20-pixel shift (~ lysosome diameter) of the green signal. n=10 cells/group. **e**, DQ-OVA degradation by TAMs treated with E64-DNA, DNA, or E64 (100nM) for 2h. n=3/group. **f**, Experimental design of antigen-cross presentation by TAMs treated with OVA or $OVA_{257-264}$. **g-i**, Effect of E64-DNA on antigen cross-presentation by TAMs pre-treated with E64-DNA, DNA, or E64 (100nM) for 2h, followed by treatment with OVA protein or $OVA_{257-264}$ peptide for 3h. Quantification of MHCI-bound $OVA_{257-264}$ on TAMs (**g**). OT-1 $CD8^+$ T-cell activation (**h**) and proliferation (**i**) after 72h of co-culture with TAMs. n=3/group. Vehicle (Veh) = phosphate-buffered saline. *, $p<0.05$ Student's *t*-test, error bars indicate the mean of independent experiments ± s.e.m. ns, not significant. TAMs were isolated from E0771 tumors. E64-DNA was made by Dr. Kasturi Chakraborty for the whole study. She also performed the imaging and quantification of the lysosomal targeting.

E64 was chemically conjugated to a 38-base pair DNA duplex to yield the nanodevice E64-DNA. In E64-DNA one strand is covalently attached to E64 at its 5' end through a C6 amine linker. It is hybridized to a complementary strand that displays an Alexa Fluor 647 label to monitor

cell-specific endocytic uptake, organelle localization, and temporal labeling efficacy (**Figure 2.12b**). In E64-DNA, the DNA scaffold serves two main purposes. First, it enables specific uptake of the nanodevice by macrophages via scavenger receptors; and thereafter the trafficking pathway leads to device accumulation in the lysosome. Second, it introduces Alexa Fluor 647 in a precise ratio with the functional molecule E64, to assay physiological effects of E64 while simultaneously quantitating uptake by various cell types in the tumor.

I found that E64-DNA localized specifically to lysosomes of TAMs. Uptake occurred through specific scavenger receptors because *Scarb1-/-* (scavenger receptor class B type 1) or *Msr1-/-* (macrophage scavenger receptor 1) reduced E64-DNA uptake by M2 BMDMs, while *Cd36-/-* (scavenger receptor class B, member 3) did not (**Figure 2.12c**). E64-DNA was localized specifically to lysosomes of TAMs and attenuated their capacity to degrade DQ-OVA (**Figures 2.12d-e**). Importantly, neither free E64 nor DNA alone had any such effect (**Figure 2.12e**).

In order to address the need for a duplex DNA-based assembly in achieving lysosomal targeting, differently structured variants of 38 nucleotides in length. ssDNA, dsDNA, ssRNA, and dsRNA tagged with Alexa 647 were generated. I found that internalization by M2 BMDMs required the presence of DNA, in either the single- or double-stranded form (**Figure 2.13a-b**). These findings suggest that nanodevice uptake is specific for the DNA backbone and not simply dependent on size or shape.

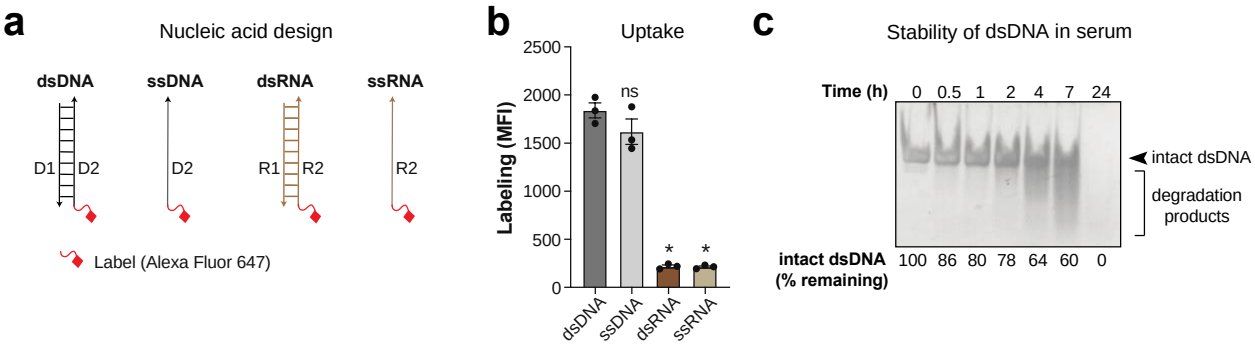

Figure 2.13. Uptake and stability of dsDNA. a, Schematic of various fluorescently labeled nucleic acid structures used for uptake studies in BMDMs. Each nucleic acid scaffold is either a single stranded or double stranded 38 mer DNA or RNA sequence. Each scaffold is labelled with an Alexa Fluor®647 fluorophore on the 5' end of one of the strands. **b**, Uptake of various types of nucleic acids by M2 BMDMs. n=3/group. **c**, Native polyacrylamide gel of dsDNA incubated in 100% mouse serum for various time points. Intact dsDNA was quantified by densitometry. *, $p<0.05$ Student's *t*-test, error bars indicate the mean of independent experiments ± s.e.m. ns, not significant. Various fluorescently labeled nucleic acid constructs were made by Dr. Kasturi Chakraborty.

From a series of experiments that evaluated the properties of E64-DNA, I found that E64-DNA retained its specificity for cysteine proteases, did not impact TAM viability, and did not affect lysosomal cysteine protease protein levels or autophagy gene expression (**Figures 2.13a-e**). Importantly, E64-DNA did not activate the STING pathway (Burdette and Vance, 2013) as it did not induce TBK1 and IRF3 phosphorylation in TAMs, nor did it elevate inflammatory cytokine expression (**Figures 2.14f-g**). More generally, E64-DNA did not alter the TAM phenotype as evidenced by the unchanged M1- and M2-asociated gene expression levels (**Figure 2.14g**). This reveals that E64-DNA offers an avenue to attenuate cysteine protease activity selectively in lysosomes, without significantly altering the TAM phenotype.

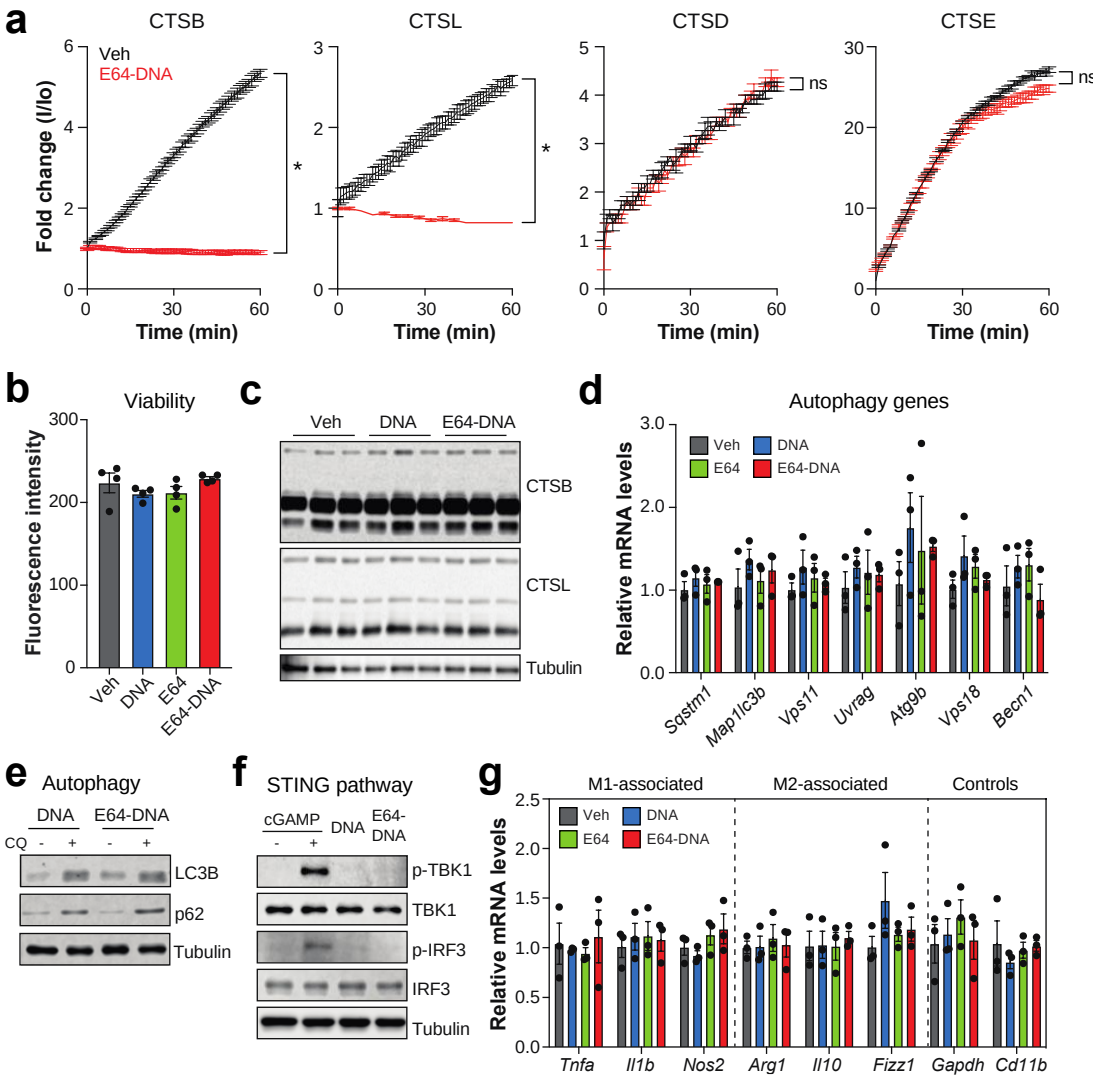

Figure 2.14. Effects of E64-DNA on the functional properties of TAMs. a, Catalytic activity assays for lysosomal cysteine proteases (CTSB, CTSL; 5nM) or aspartic proteases (CTSD, CTSE; 5nM) in the presence of vehicle (Veh; PBS) or E64-DNA (25nM). Results are plotted as fluorescence intensity at time *t*, relative to time 0 (I/Io). n=3/group. **b-d**, TAMs isolated from E0771 tumors were treated with vehicle (Veh; PBS), DNA, E64, or E64-DNA (100nM) to evaluate a variety of parameters. **b**, Cell viability (Calcein-AM) following a 72h exposure. n=4/group. **c**, CTSB and CTSL protein levels following a 24h exposure. **d**, Relative mRNA levels of autophagy genes following a 24h exposure. n=3/group. **e**, LC3B and p62 protein levels in DNA or E64-DNA (10uM) treated TAMs following a 24h treatment with vehicle (Veh; H_20) or chloroquine (CQ, 50μM). **f,** Effect of E64-DNA (2h) on TBK and IRF3 phosphorylation. TAMs treated with 3'3'-cGAMP (10μg/mL, 6h) were used as a positive control for STING activation. **g**, Effect of E64-DNA (24h) on M1- and M2-associated gene expression. n=3/group. *, $p<0.05$ Student's *t*-test, error bars indicate the mean of independent experiments ± s.e.m. ns, not significant. TAMs were isolated from E0771 tumors. Immunoblots (e) were run by Anna Tang.

Next, I evaluated if E64-DNA treatment affected antigen cross-presentation in TAMs. I used the OVA-OT-1 $CD8^+$ T cell system (**Figure 2.12f**). In this assay, TAMs are treated with OVA, which is processed in the lysosome to liberate an antigenic peptide ($OVA_{257-264}$) that if successfully presented on cell surface MHCI, will activate $CD8^+$ T cells from OT-1 mice. As a control, TAMs are treated with $OVA_{257-264}$, which circumvents the lysosome by directly binding cell surface MHCI. This control tests the importance of OVA cleavage in the lysosome for antigen presentation.

When TAMs were first treated with E64-DNA and then allowed to process OVA, they showed increased cell surface MHCI-associated $OVA_{257-264}$ as well as improved ability to induce $CD8^+$ T cell IFNγ production and proliferation (**Figures 2.12g-i**). In contrast, none of these parameters were affected when TAMs were treated with E64-DNA followed by the $OVA_{257-264}$ peptide (**Figures 2.12g-i**). This reveals the importance of OVA cleavage within the lysosome. Importantly, treatment with E64 or DNA alone did not enhance antigen cross-presentation (**Figures 2.12g-i**). This indicates that E64-DNA was required to localize the E64 inhibitor within the lysosome and attenuate lysosomal activity, which was supported by the DQ-OVA degradation assay (see Figure 2.12e). When TAMs were treated with E64-DNA *in the absence of antigen*, no activation or proliferation of $CD8^+$ T cell was observed (**Figures 2.15a-b**).

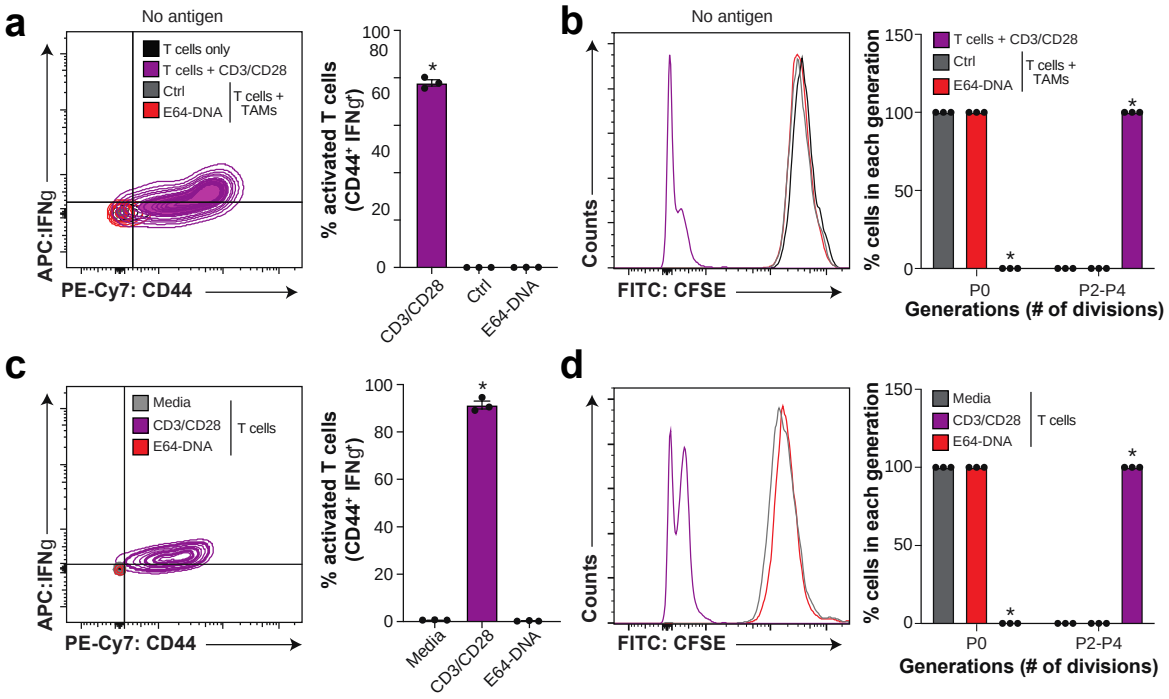

Figure 2.15. E64-DNA does not activate T cells through allostimulation or direct stimulation. **a-b**, Control for allostimulation. CD8$^+$ T cell activation (**a**) and proliferation (**b**) after 72h of co-culture with E64-DNA-treated (100nM) TAMs that had not been exposed to antigen. CD3/CD28 antibodies were included as a positive control for T cell activation. n=3/group. **c-d**, Control for direct effects of E64-DNA on T cells. CD8$^+$ T cell activation (**c**) and proliferation (**d**) after 72h of culturing in complete growth media (Media) in the presence/absence of E64-DNA (100nM). CD3/CD28 antibodies were included as a positive control for T cell activation. n=3/group. *, $p<0.05$ Student's *t*-test, error bars indicate the mean of independent experiments ± s.e.m.

Given that lysosomal degradative capacity is inversely correlated with antigen presentation (Delamarre et al., 2005; Trombetta and Mellman, 2005), and the lysosome has several classes of proteases, I tested whether antigen cross-presentation could be enhanced by inhibiting aspartic proteases in the lysosome. Kaz complexed the LAP inhibitor pepstatin A to DNA nanodevice to create PepA-DNA (**Figure 2.11c**). I found that although PepA-DNA specifically inhibited LAP activity *in vitro* (**Figure 2.11d**), it could not attenuate DQ-OVA degradation or improve antigen cross-presentation when delivered to macrophages (**Figures**

2.11e-h). These findings underscore a specific role played by the pool of cysteine protease in lysosome in restraining antigen cross-presentation by TAMs and M2 macrophages.

E64-DNA preferentially targets M2-like TAMs.

In *C. elegans*, exogenously introduced DNA nanodevices preferentially label phagocytic cells called coelomocytes that highly express scavenger receptors (Surana et al., 2011). Coelomocytes in nematodes are considered to be functionally similar to macrophages in vertebrates. Indeed, macrophages are also characterized by high scavenger receptor levels relative to other cell types (Canton et al., 2013). I therefore tested whether E64-DNA could preferentially target TAMs in mice by injecting it into E0771 tumors (intratumoral delivery; i.t.) and monitoring its uptake by various cell types (**Figure 2.16a**). I found that E64-DNA preferentially targeted TAMs and lowered their DQ-OVA degradation (**Figures 2.16b-c**). This indicates that the DNA nandevice was delivered to lysosomes, and moreover selectively to TAMs versus other cell types in tumors of mice.

Approximately 80% of TAMs were labeled by E64-DNA following intra-tumoral injection. To determine whether E64-DNA uptake was differentially distributed amongst distinct TAM subpopulations, I stratified TAMs according to their M2-like ($CD206^{high}$) and M1-like ($CD206^{low}$) phenotypes (Cassetta and Pollard, 2018) and found that E64-DNA was ~3-fold enriched in M2-like TAMs *in vivo* (**Figure 2.16d**).

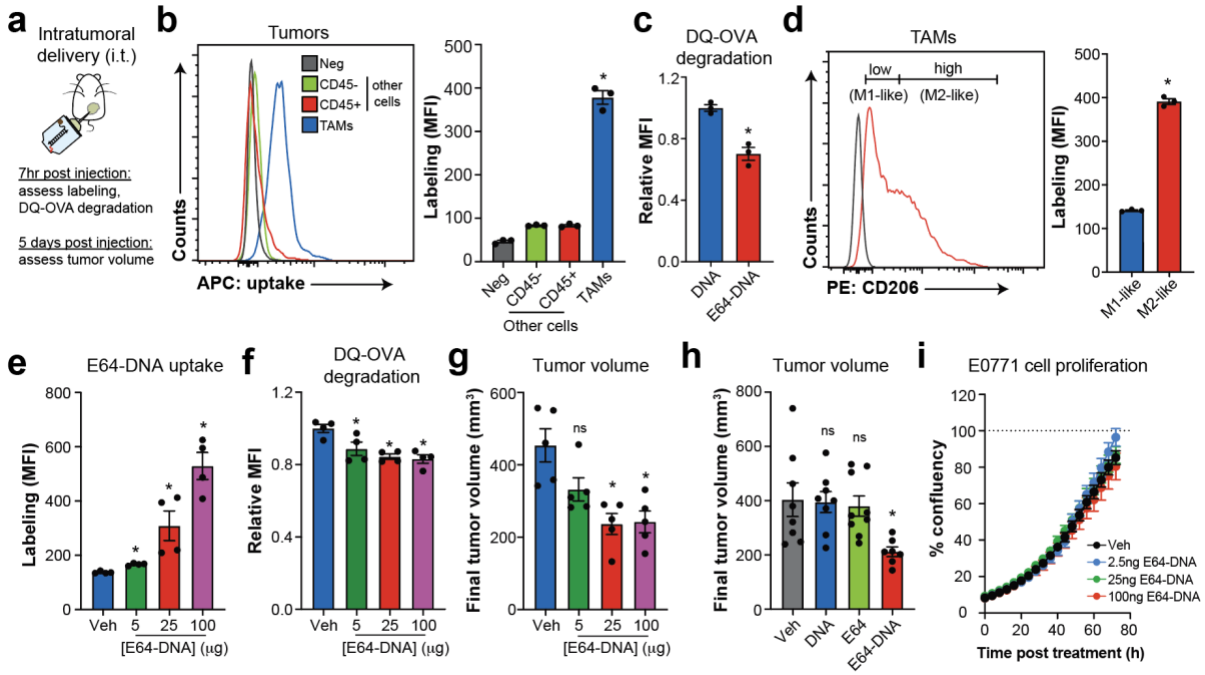

Figure 2.16 The E64-DNA nanodevice preferentially localizes in lysosomes of M2-like TAMs and lowers tumor growth. a, Experimental design of intratumoral delivery (i.t.). **b-d**, DNA or E64-DNA (25 μg) were injected intratumorally into E0771 tumors. **b**, Flow cytometry analysis of E64-DNA uptake by various tumor cell types 7h after injection. n=3/group. **c**, DQ-OVA degradation by TAMs isolated from tumors 7h after injection. n=3/group. **d**, Flow cytometry analysis of E64-DNA uptake by $CD206^{high}$ or $CD206^{low}$ TAMs 7h after injection. Representative flow images of CD206 gating (*left*) and quantification (*right*) are shown. n=3/group. **e-g**, E64-DNA (5μg, 25μg, 100μg) was injected intratumorally into E0771 tumors. Flow cytometry analysis of E64-DNA uptake (**e**) and DQ-OVA degradation (**f**) by TAMs 7h after injection. n=4/group. E0771 tumor volume 5 days after injection (**g**). n=5/group. **h**, E64, DNA, or E64-DNA (25 μg) were injected into E0771 tumors and tumor volume was assessed 5 days after injection. n=8-9/group. **i**, Effect of E64-DNA on E0771 cell proliferation *in vitro*. n=6/group. Vehicle (Veh) = phosphate-buffered saline. *, $p<0.05$ Student's *t*-test, error bars indicate the mean of independent experiments ± s.e.m. Neg = unlabeled negative control.

To test this in a more controlled system, I co-cultured M1 BMDMs and Hoescht-labeled M2 BMDMs (1:1 ratio) and exposed them to E64-DNA in a competition assay. A similar enrichment of E64-DNA labeling was observed in M2 BMDM over M1 BMDM (**Figure 2.17**). This correlates well with the elevated expression of scavenger receptors in M2 over M1 macrophages. (Canton et al., 2013).

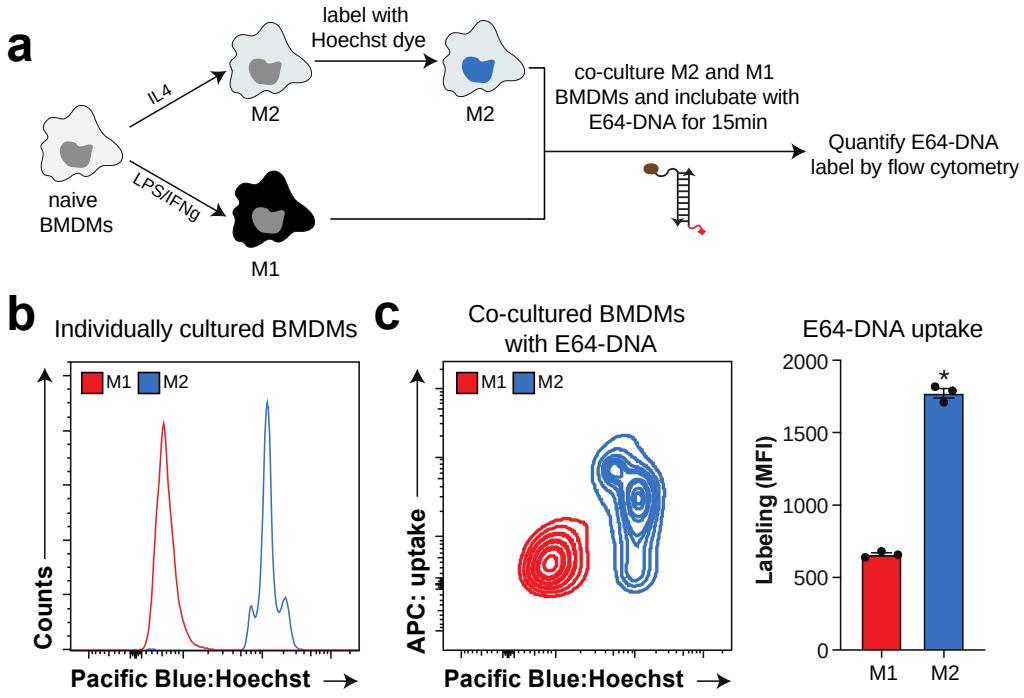

Figure 2.17. E64-DNA is preferentially internalized by M2 BMDMs *in vitro*. a, Schematic of an E64-DNA uptake competition assay in M1 and M2 BMDMs. **b**, Hoechst dye levels in individually cultured M1 and M2 BMDMs. **c**, E64-DNA uptake by co-cultured M1 and M2 BMDMs. Representative flow cytometry data (*left*) and quantification (*right*) are shown. n=3/group. *, $p<0.05$ Student's *t*-test, error bars indicate the mean of independent experiments ± s.e.m.

E64-DNA improves antigen cross-presentation by TAMs and attenuates tumor growth via CD8$^+$ T cells.

High cysteine protease levels in tumors are a poor prognostic marker for a wide range of solid tumors(Olson and Joyce, 2015), but the contribution of the population of cysteine protease localized in lysosomes is unknown. Activity-based probes have recently revealed that the majority of tumor cysteine protease activity is TAM-associated (Gocheva et al., 2010). Interestingly, high doses of E64 (1mg, daily) showed limited impact on tumor growth in murine cancer models (Gopinathan et al., 2012). One reason could be that E64 has a limited ability to cross cell membranes (Powers et al., 2002), which could limit its access to the pool of cysteine proteases in

the lysosome. Hence, I tested whether E64-DNA might produce a therapeutic response since it could overcome the cell-entry barriers encountered by the small molecule E64.

I injected E64-DNA at various doses (5-100 μg, single dose) into E0771 tumors and monitored effects on TAM uptake and lysosomal degradative capacity (7h post-delivery), as well as tumor growth (5 days post-delivery). TAMs internalized the drug in a non-saturable, dose-dependent manner (**Figure 2.16e**). E64-DNA treatment attenuated DQ-OVA degradation by TAMs and diminished tumor growth, with both effects saturating at the 25 μg dose (**Figures 2.16f-g**), while free DNA and free E64 showed no such effects (**Figure 2.16h**). Moreover, E64-DNA did not directly decrease E0771 proliferation *in vitro* (**Figure 2.16i**), indicating that its effects on tumor growth were not due to their action on cancer cells. Thus, these findings reveal that 25 μg of E64-DNA is sufficient to adequately inhibit lysosomal cysteine protease activity in TAMs and attenuate tumor growth.

I next evaluated whether similar effects could be obtained by intravenous (i.v.) administration. Intravenously delivered E64-DNA was preferentially internalized by TAMs (versus other cell types in the tumor) and attenuated their lysosomal activity as revealed by the DQ-OVA degradation assay (**Figures 2.18a-b**). The ability to detect TAM labeling 7h post injection was supported by our *in vitro* serum stability assay which showed that ~60% of DNA remained intact up to this time point (**Figure 2.13c**). Further, i.v. delivered E64-DNA attenuated E0771 tumor growth over a 5-day period (**Figure 2.18c**). It also increased $CD8^+$ effector T cells in tumors (**Figure 2.18d**). This effect was not due to the ability of E64-DNA to directly activate $CD8^+$ T cells *in vitro* (**Figures 2.15c-d**).

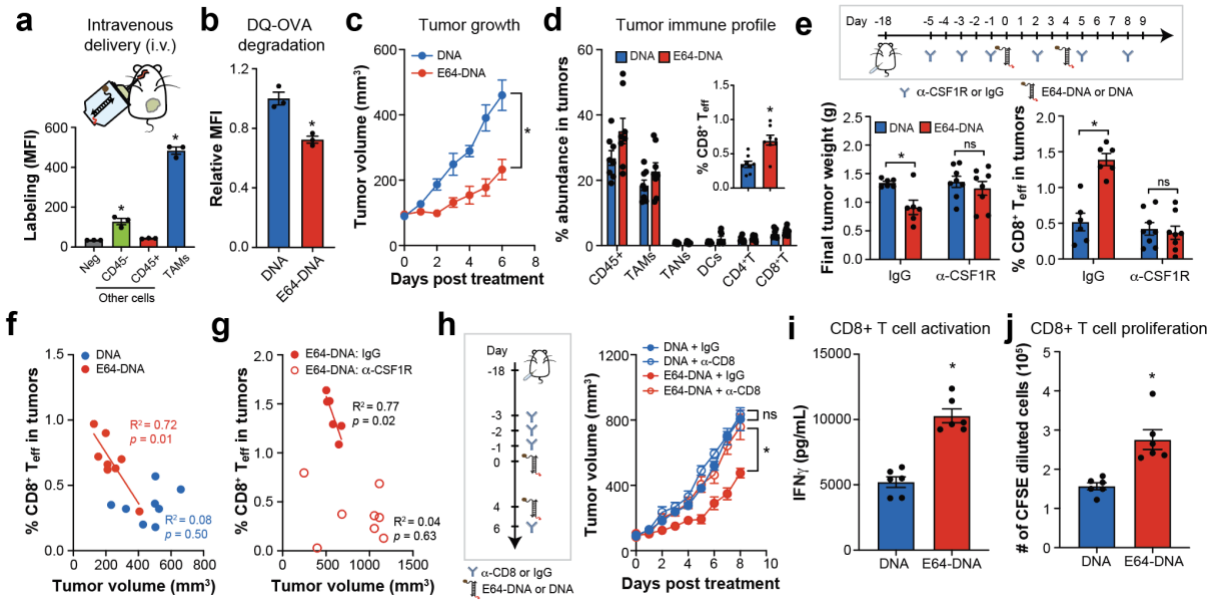

Figure 2.18. Intravenously delivered E64-DNA targets TAMs to activate CD8+ T cells and attenuate tumor growth. a-j, E64-DNA or DNA (25 μg) was intravenously delivered (i.v.; retro-orbital) into E0771 tumor-bearing mice. **a**, Flow cytometry analysis of E64-DNA uptake by various tumor cell types 7h after a single injection. n=3/group. **b**, DQ-OVA degradation by TAMs isolated from tumors 7h after a single injection. n=3/group. **c**, E0771 tumor growth over 5 days after a single injection. n=8/group. **d**, Immune cell composition of tumors 5 days after a single injection. n=8/group. **e**, Experimental design (*top*). Effect of IgG or α-CSF1R (300μg) on E0771 tumor growth (*bottom, left*) and $CD8^+$ effector T cells in tumors (*bottom, right*) in mice treated with E64-DNA or DNA. n=5-8/group. **f-g**, Linear regression of $\%CD8^+$ effector T cells in tumors vs. tumor volume in DNA or E64-DNA treated mice (**f**, n=8/group), and in E64-DNA treated mice treated with IgG or α-CSF1R antibodies (**g**, n=6-8/group). **h**, Experimental design (*left*). Effect of α-CD8 or IgG antibodies (200μg) on E0771 tumor growth in mice treated with E64-DNA or DNA (*right*). n=5/group. **i-j**, Antigen cross-presentation by TAMs from E0771 tumors of DNA or E64-DNA-treated mice. OT-1 $CD8^+$ T cell activation (**i**) and proliferation (**j**). n=6/group. *, $p<0.05$ Student's *t*-test; ns, not significant; error bars indicate the mean of independent experiments ± s.e.m. $CD8^+T_{eff}$ = effector $CD8^+$ T cells.

The demonstration that E64-DNA preferentially targets TAMs *in vivo* does not necessarily imply that TAMs are required for its efficacy. To directly test the importance of TAMs in E64-DNA-mediated antitumor activity, we used an anti-CSF1R antibody to deplete TAMs in the E0771 model. Effects of E64-DNA on tumor growth and $CD8^+$ effector T cells

were both abolished in TAM-depleted mice (**Figure 2.18e**). Moreover. the abundance of $CD8^+$ effector T cells inversely correlates with tumor volume in E64-DNA-treated mice (**Figure 2.18f**). And this correlation was absent in DNA-treated mice (**Figure 2.18f**) and in E64-DNA-treated mice depleted of TAMs (**Figure 2.18g**).

These findings suggest a model that the DNA nanodevice, E64-DNA, acts via TAMs to activate $CD8^+$ T cells in the E0771 model. To test this, I depleted $CD8^+$ T cells and monitored effects on E0771 tumor growth in mice. Depleting $CD8^+$ T cells restored tumor growth in E64-DNA-treated mice (i.v.) but had no impact on tumor growth in DNA-treated mice (**Figure 2.18h**). Effects on $CD8^+$ T cells were associated with improved cross-presentation by TAMs isolated from E64-DNA-treated mice, both in the E0771 model (**Figure 2.18i-j**) and the B16.OVA model, where E64-DNA (i.v.) also attenuated tumor growth (**Figure 2.19**). Taken together, these results suggest that blocking cysteine protease activity in lysosomes of TAMs activates $CD8^+$ T cells to attenuate tumor growth.

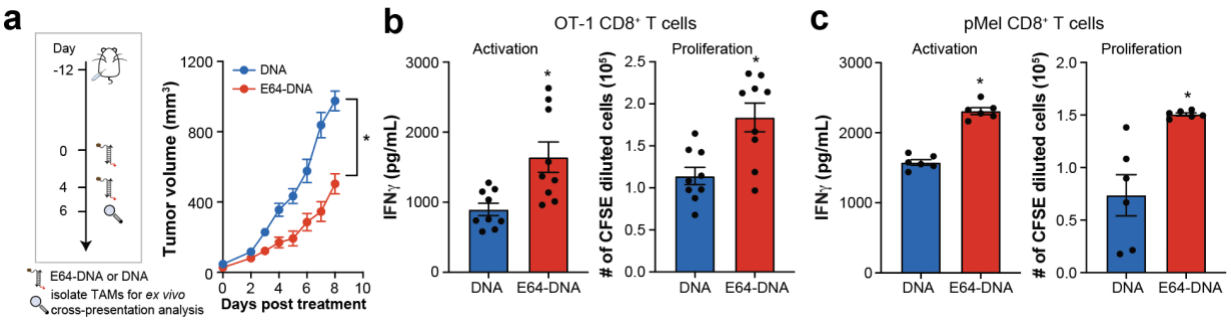

Figure 2.19. E64-DNA attenuates B16.OVA tumor growth and improves antigen cross-presentation by TAMs. a, Experimental design (*left*). Effect of E64-DNA (25µg, i.v.) on B16.OVA tumor growth (*right*). n=8/group. **b**, OT-1-$CD8^+$ T cell activation (*left*) and proliferation after 72h of co-culture with TAM isolated from DNA or E64-DNA (i.v.) treated B16.OVA tumors. n=6/group. **c**, pMel-$CD8^+$ T cell activation (*left*) and proliferation (*right*) after 72h of co-culture with TAMs isolated from DNA or E64-DNA (i.v.) treated B16.OVA tumors. n=6/group.*, $p<0.05$ Student's *t*-test, error bars indicate the mean of independent experiments ± s.e.m.

E64-DNA-cyclophsophamide combination therapy results in sustained tumor regression.

Although E64-DNA treatment attenuates tumors, it does not lead to sustained tumor regression as a monotherapy. Since E64-DNA enables TAMs to better utilize tumor antigens to activate $CD8^+$ T cells, we considered whether enhancing antigen supply by increasing the number of dead cancer cells in proximity of TAMs could improve its antitumor efficacy. I therefore tested the efficiency of cyclophosphamide (CTX), an alkylating agent used as a frontline treatment for TNBC and many other malignancies, in combination with E64-DNA. CTX was delivered at metronomic doses (50 mg/kg/mice) to induce cancer cell killing and maintain antitumor immunity (Kerbel and Kamen, 2004; Sistigu et al., 2011). I found that combining E64-DNA (i.v.) with CTX led to sustained tumor regression in the E0771 model, an effect that could not be replicated by either treatment alone (**Figure 2.20**).

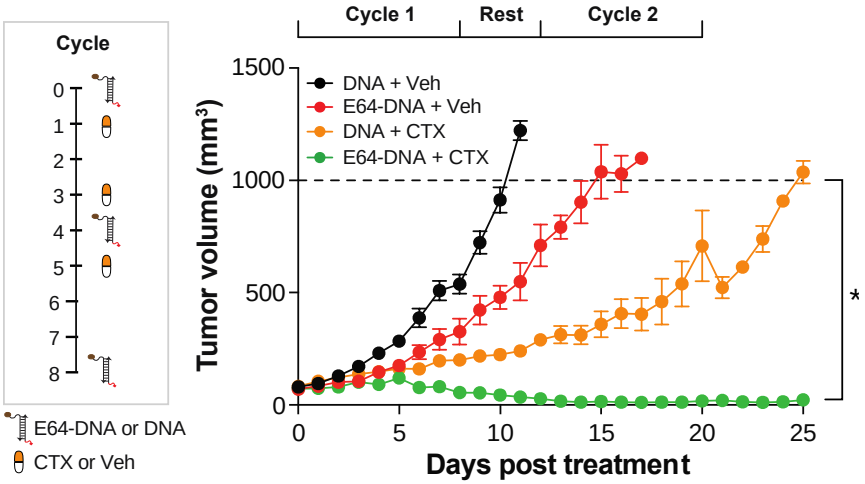

Figure 2.20. E64-DNA synergizes with low-dose cyclophosphamide in the E0771 model. Experimental design (*left*). Effect of E64-DNA and cyclophosphamide (CTX, 50mg/kg), alone or in combination, on E0771 tumor growth (*right*). n=6/group.

E64-DNA attenuates tumor progression in C3(1)-TAg GEM model

I investigated whether E64-DNA could show efficacy either alone or in combination with cyclophosphamide in a genetically engineered mouse (GEM) model, where tumors

spontaneously and independently arise at multiple sites. I used the C3(1)-TAg GEM model of TNBC, which shares many features with human TNBC patients, including early atypia of mammary ductal epithelium (~8 weeks of age), progressing to intraepithelial neoplasia (~12 weeks of age), and culminating in the independent development of genetically similar tumors in multiple mammary glands (~16-24 weeks). I started two cycles of treatment after the appearance of the first palpable tumor (week 16-17) and monitored the effects until 5 weeks after the initial treatment (21-22 weeks). Consistent with our findings in syngeneic models, E64-DNA attenuated tumor growth alone, and further showed better efficacy in combination with cyclophosphamide (**Figure 2.21**).

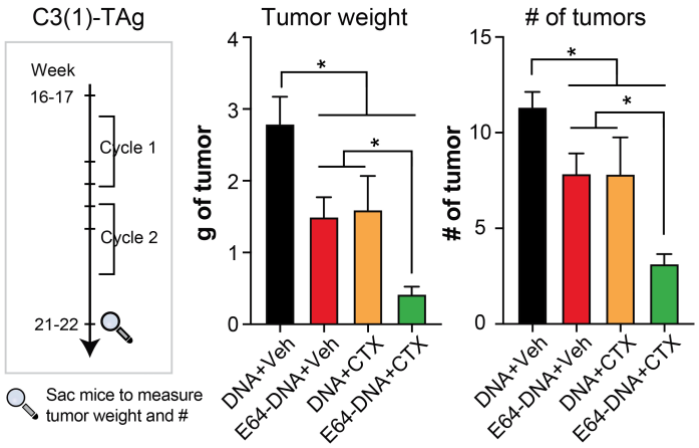

Figure 2.21. The combination of E64-DNA with CTX provides better efficacy in attenuating C3(1)-Tag tumors. Experimental design (*left*). Effect of E64-DNA and cyclophosphamide (CTX, 50mg/kg), alone or in combination, on C3(1)-Tag total tumor weight (*middle*) and the number (#) of tumors (*right*). n=6-9/group.

Discussion

Although the pro-tumorigenic functions of TAMs have been well characterized, TAMs can also perform antitumor functions (Mantovani et al., 2017; Singhal et al., 2019). Our limited understanding of the underlying mechanisms has stymied the development of therapeutics that leverage their antitumor capabilities. Here, combining discovery-based proteomics with genetic

(m*Tfeb-/-*) and therapeutic (E64-DNA) interventions, my studies identify elevated cysteine protease activity in lysosomes of TAMs as a targetable mechanism that impedes the antitumorigenic function of TAMs. My findings support a model (**Figure 2.22**) wherein elevated lysosomal cysteine protease activity in TAMs destroys antigens, resulting in attenuated antigen cross-presentation and $CD8^+$ T cell activation in tumors. I posit that the contribution of this pathway to adaptive immune suppression would be governed by the abundance of M2-like TAMs in a tumor, which is associated with poor prognosis across many cancers (Gentles et al., 2015; Mantovani et al., 2017; Takeya and Komohara, 2016).

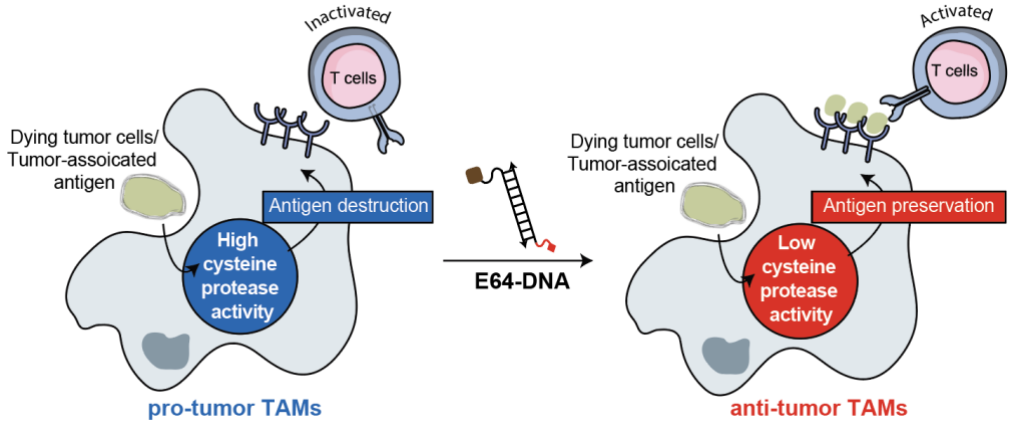

Figure 2.22. The proposed models.

Antigen cross-presentation is a function classically ascribed to DCs. However, macrophages are also capable of performing this function, albeit less efficiently (Cruz-Leal et al., 2018; Embgenbroich and Burgdorf, 2018; Shen et al., 2004). Further, human TAMs isolated from the early stage of lung cancer also have this capability (Singhal et al., 2019). Because TAMs are far more abundant and phagocytic than tumoral DCs, I propose that their overdegradation of tumor-associated antigens and failure to instruct $CD8^+$ T cells represents a blockade in antitumor immunity.

The importance of antigen cross-presentation by TAMs is underscored by my studies in the E0771 model (TNBC). While $CD8^+$ T cells are present in E0771 tumors, they do not oppose tumor development; their levels do not correlate with tumor size, and their depletion has no impact on tumor growth. However, following E64-DNA treatment $CD8^+$ T cells are increased, inversely correlated with tumor size, and their depletion increases tumor growth. Importantly, these E64-DNA-mediated effects depend on the presence of TAMs and are independent of changes to their pro-tumorigenic M2-like phenotype or their expression of immunosuppressive genes such as *Arg1* and *Il10*. Thus, re-engaging antigen cross-presentation by TAMs facilitates adaptive immune activation even in the context of an immunosuppressive environment.

Efficient antigen presentation requires optimal lysosomal activity since hypoactivity would limit the generation of antigenic peptides while hyperactivity would destroy them (Delamarre et al., 2005; Trombetta and Mellman, 2005). My studies reveal that M2-like TAMs harbor heightened lysosomal cysteine protease activity that limits antigen cross-presentation. These findings reinforce the importance of lysosomal processing to antigen presentation and extend our understanding in two critical ways.

First, I demonstrate that the lysosomal degradative capacity of macrophages is regulated by their phenotypic state. I show that lysosomal protein levels and activity are elevated in M2 versus M1 macrophages and identify TFEB as the mechanism. Differences in lysosomal proteolysis between M1 and M2 macrophages may be well suited to their diverse functional requirements *in vivo* (Gordon and Taylor, 2005). M1 macrophages predominate during infection, where they phagocytose and clear pathogens. In this context, limited lysosomal proteolysis may help preserve antigens and activate adaptive immunity to protect the host from infection. On the other hand, M2 macrophages help to clear dead host cells during wound repair. In this setting,

enhanced lysosomal proteolysis may help destroy antigens, limit adaptive immune activation, and protect the host from potential autoimmune responses. However, my studies demonstrate that this antigen destructive property of M2-like macrophages is detrimental in tumors as it blocks adaptive immune participation in the antitumor response.

Second, I demonstrate that the lysosomal degrative capacity of M2-like TAMs and its impact on cross-presentation is predominantly determined by cysteine proteases, not aspartic proteases. I show that cysteine proteases are induced in M2 relative to M1 macrophages, and that inhibiting cysteine protease activity in TAMs attenuates DQ-OVA degradation and improves antigen cross-presentation. In contrast, aspartic proteases were not up-regulated in M2 macrophages, and inhibition of this class of enzymes had minimal effects on DQ-OVA degradation and antigen cross-presentation. Consistent with these findings, my studies and others (Diment, 1990; Rodriguez and Diment, 1995) show that incubating antigenic peptides with purified lysosomal cysteine protease s *in vitro* inhibits the ability of macrophages to present them to T cells, while incubation with purified aspartic proteases has minimal impact.

The requirement of optimal lysosomal processing and the specificity of generating MHCI-restricted antigenic peptide to cysteine proteases further provide a rationale for using E64, the specific cysteine protease inhibitors, over general lysosomal inhibitors, such as chloroquine. Inhibiting a broad class of lysosomal enzyme activities or other aspects of lysosomal function, such as autophagy, may lead to a non-optimal level of antigen preservation as well as dysfunction in the phagocytosis pathway that is required to deliver antigen sources into the lysosome.

Pre-clinical studies indicate several potential mechanisms by which cysteine proteases promote tumorigenesis, including cell intrinsic activity in multiple tumor cell types and

extracellular activity that facilitates metastasis (Olson and Joyce, 2015). My studies reveal that suppressing the activity of the population of cysteine proteases localized inside lysosomes of TAMs results in tumor attenuation. To achieve this, our lab adopted the nanotechnology provided by Dr. Krishnan's group: linking a small molecule inhibitor of cysteine proteases, E64, to a DNA nanodevice as a lysosomal delivery agent in mice. Not only does this strategy overcome the cell-permeability problems of E64, but the DNA scaffold is also selectively taken up by TAMs over other cell-types in the tumor and localizes in lysosomes of those cells, thereby conferring therapeutic properties at doses of E64 that are otherwise ineffective.

My studies with E64-DNA have several important implications for implementing DNA nanodevices in therapeutics development. First, in contrast to aptamers, where DNA is the therapeutic (Pastor et al., 2011), our approach uses DNA as a *carrier* to specifically deliver the therapeutic to macrophages over other cell types in the tumor. This specificity arises from the recognition of duplex DNA by scavenger receptors on macrophages, including MSR1 and SCARB1, which were shown to be required for E64-DNA uptake. Second, our approach does not eliminate the target cell. Instead, it reprograms it to acquire a new property that is therapeutically beneficial. It is therefore distinct from other DNA nanostructures that deliver therapeutics such as doxorubicin, siRNA, or thrombin, that cause the death of the targeted cells (Cho et al., 2014; Lee et al., 2012; Li et al., 2018b, 2016; Zhang et al., 2016). Finally, our approach facilitates intracellular delivery of a therapeutic to lysosomes of a specific cell type, i.e., macrophages. Polymer-based or liposome-based nanoparticles, which are internalized by phagocytosis, can also target the lysosome. However, it has proven challenging for nanoparticles to get enriched specifically in macrophages over other phagocytes.

Although improving antigen cross-presentation by TAMs attenuates tumor growth, it does not eliminate tumors as a monotherapy. One explanation is that the basal rate of cancer cell death is insufficient to provide TAMs with enough antigen to fully capitalize on their improved cross-presentation. Indeed, combining E64-DNA with metronomic doses of cyclophosphamide results in sustained tumor regression in the E0771 model. Metronomic chemotherapy has been proposed as a new treatment paradigm for patients, and clinical trials are underway. In this approach, chemotherapy is administered more frequently at lower doses to elicit multi-factorial benefits (cancer cell killing, inhibition of angiogenesis, preservation of immunity) and diminish side effects (Maiti, 2014). My findings raise the possibility of synergistically combining this approach with E64-DNA, which preferentially targets TAMs and improves their ability to activate adaptive immunity. Given that chemotherapy is a frontline treatment for many solid tumors, most of which are characterized by a preponderance of TAMs, we envision that this approach may have broad therapeutic implications.

In summary, I demonstrate the therapeutic value of targeting a DNA nanodevice with organelle-level precision in TAMs within murine tumors. Successful localization of the nanodevice in lysosomes of the target cells does not kill them, but instead reprograms them to improve their ability to present antigens, which in turn activates the adaptive immune response. The new-found capability of organelle-targeted DNA nanodevices to modulate macrophage behavior in tumors suggests a broader possibility to manipulate macrophage function in other diseases, as every organ harbors tissue-specific macrophages of variable phenotype.

CHAPTER THREE: HYPOXIA-INDUCED LACTATE PRODUCTION BY TUMOR-ASSOCIATED MACROPHAGES PROMOTES TUMORIGENESIS

Introduction

Tumor-associated macrophages (TAMs) are the most prevalent immune cell in the tumor microenvironment (Cassetta and Pollard, 2018). TAMs predominantly adopt an anti-inflammatory M2-like phenotype characterized by increased levels of proteins (e.g., ARG1, VEGF, MMPs, IL10) that promote angiogenesis, attenuate anti-cancer immune response, and facilitate metastatic dissemination (Cassetta and Pollard, 2018; Mantovani et al., 2017; Noy and Pollard, 2014). Studies have shown that depleting TAMs in pre-clinical models attenuated tumor growth and metastasis (Cotechini et al., 2015; Poh and Ernst, 2018), and high TAM abundance correlates with poor survival in patients across many cancer types (Gentles et al., 2015; Mantovani et al., 2017; Takeya and Komohara, 2016). For these reasons, M2-like TAMs are an emerging target for anti-cancer therapy development (Cassetta and Pollard, 2018; DeNardo and Ruffell, 2019; Mantovani et al., 2017; Poh and Ernst, 2018; Vitale et al., 2019).

While M2-like TAMs contribute to many cancers, mechanisms producing their M2-like phenotype and its prevalence across different tumor types are poorly understood. This knowledge is required to target TAMs therapeutically and to identify patients that would benefit from such therapies. One potential pathway to influence macrophage polarization is via metabolic reprogramming. Previous studies showed that glycolysis supports a pro-inflammatory M1 phenotype in macrophages, while mitochondrial respiration is required for the M2 phenotype. In collaboration with Dr. Yingming Zhao's group, our previous work directly challenged this paradigm (Zhang et al., 2019).

We showed that treating macrophages with LPS or bacteria (conditions that support M1 polarization) induces lactate production, which in turn promotes a late phase switch to an M2-like phenotype. The mechanism underlying this surprising observation involves a novel lactate-stimulated epigenetic modification termed histone lysine lactylation (Kla) that marks promoters of genes associated with the M2-phenotype (e.g., Arg1) and directly promotes transcription. Lowering macrophage lactate production by deleting lactate dehydrogenase A (*Ldha*-/-) reduced histone Kla marks at the Arg1 promoter and Arg1 expression without altering pro-inflammatory cytokine expression during M1 polarization (Zhang et al., 2019). Together, our studies support a model wherein the switch to aerobic glycolysis that occurs during M1 polarization starts a "lactate timer" that uses an epigenetic mechanism to induce M2-like characteristics in the later phase (**Figure 3.1a**). From a physiological standpoint, this perhaps assists in repairing collateral damage incurred by the host during infection. In preliminary studies, we further showed that Kla modification is also present in human macrophages. This is associated with higher glycolysis in macrophages, as evidence by the acidification of media (**Figure 3.1b**).

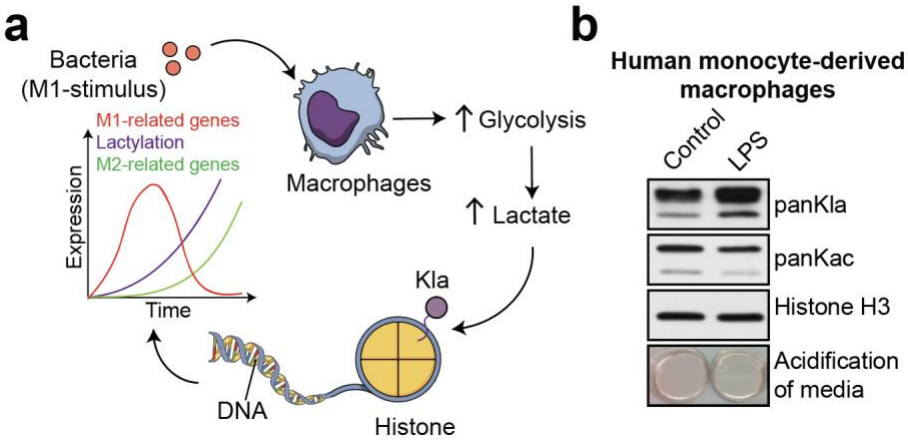

Figure 3.1. Histone Kla in macrophages drives an M1 to M2 phenotypic switch. a, Graphical summary of Zhang et al., Nature, 2019. **b**, HMDMs were treated or without LPS for 24hr. Immunoblot of histone lactylation (panKla), acetylation (panKac), and photos of HMDM-cultured media were shown. Western blot and media acidification photo were provided by Dr. Di Zhang.

Such transition to an M2-like phenotype during infection also resembles the pattern seen in cancer where TAMs transition towards an M2-like phenotype during tumor progression. Studies have shown that hypoxia, a key environmental stimulus in tumors, can induce lactate production. In this study, I aimed to examine if hypoxia-induced lactate production by TAMs metabolically reprograms them to promote the Kla-M2 pathway to promote tumorigenesis. I showed that hypoxia-induced lactate production by macrophages elevates the expression of M2-like genes, marked by Kla at their promotes. I further demonstrated the spatial and quantitative relationship between hypoxia, Kla, and an M2-like phenotype within a single tumor (GEM model & human tumors) and across tumors with variable hypoxia (syngeneic models). Moreover, inhibiting endogenous lactate production by TAMs (via *Ldha* deletion) reduces tumor growth, attenuates the M2-like phenotype of TAMs, and increases $CD8^+$ T cells in tumor with high hypoxia, but not low hypoxia. Importantly, lactate level in the TME is independent of tumor hypoxia or macrophage LDHA status, suggesting that this epigenetic pathway is primarily driven by endogenous lactate production by TAM rather than exogenous lactate in TME. Collectively, my studies demonstrated an important role for a "hypoxia-induced lactate-Kla-M2 pathway" in TAMs to promote tumorigenesis.

Materials and Methods

Regulatory. Animal studies were approved by the Institutional Animal Care and Use Committee (ACUP #72209, #72504) at the University of Chicago. Cancer cell lines were approved by the Institutional Biosafety Committee (IBC #1503).

Mouse models. 6-7-week-old C57BL/6 female mice, LysM-Cre knock in mice, $Ldha^{fl/fl}$, and C3(1)-TAg mice were purchased from The Jackson Laboratory. Myeloid cell specific *Ldha*-

/- mice (m*Ldha*-/-) and their littermate controls (*fl/fl*) were generated by crossing *Ldha*$^{fl/fl}$ mice with LysM-Cre$^{+/-}$ mice. Mouse genotype was confirmed by PCR using the following primers: *Ldha*$^{fl/fl}$ forward, CTGAGCACACCCATGTGAGA; reverse, AGCAACACTCCAAGTCAGGA; LysM common, CCCAGAAATGCCAGATTACG; LysM WT: TTACAGTCGGCCAGGCTGAC; LysM-Cre: CCCAGAAATGCCAGATTACG. Mice were housed in the specific pathogen free animal facility at the Gordon Center for Integrative Science building at the University of Chicago.

Cell Lines. E0771 and Py8119 cells were a gift from Dr. Marsha Rosner, University of Chicago. LLC1 cells were purchased from ATTC (CRL-1642^{TM}). B16F10 cells were a gift from Dr. Thomas Gajewski, University of Chicago. B16.OVA cells were a gift from Dr. Jeffrey Hubbell, University of Chicago. Cells were cultured in Dubecco's Modified Eagles Medium (DMEM; HyClone) containing 10% heat-inactivated FBS (Gemini Bio Products) and 1% penicillin/streptomycin (Gibco).

Bone marrow-derived macrophage (BMDM) isolation and activation. BMDMs were differentiated from bone marrow stem cells with L-cell conditioned media for six days as previously described (Kratz et al., 2014). For M1 activation, BMDMs were treated with LPS (5ng/mL) and IFNγ (12ng/mL) for 24hrs. For M2 activation, BMDMs were treated with IL-4 (20ng/mL, R&D Systems) for 48hrs.

Murine tumor processing. Tumors were digested with Type 4 Collagenase (Worthington, 3mg/mL) and hyaluronidases (Sigma, 1.5mg/mL) at 37ºC with horizontal shaking at 200rpm for 45 mins (E0771) or 30 mins (LLC1 and B16F10). The digested tumor was filtered through a 100μm cell strainer, incubated in RBC lysis buffer for 5 min, and passed through a 40μm cell strainer. **For tumor immune cell analyses**, cells were labeled with various antibodies

and analyzed by flow cytometry. **For sorting**, cells were resuspended in isolation buffer (0.1% BSA/PBS, 2mM EDTA), layered onto Ficoll-Paque^{TM} PLUS (GE Healthcare), and centrifuged at 450xg for 30mins. Mononuclear cells were obtained by collecting the middle white layer. Enriched mononuclear cells were stained with antibodies, and M1-like and M2-like tumor-associated macrophages (TAMs) were sorted using a BD FACS Aria Fusion cell sorter. **For isolation of pooled TAMs**, TAMs were isolated using CD11b microbeads (Miltenyi Biotec) according to the manufacturer's instruction, and purity was assessed by flow cytometry. **Antibodies used include**: CD45 (47-0451), CD11b (25-0112), MHCII (11-5321), Ly6C (12-5932), CD4 (17-0041), CD8 (12-0081), CD44 (25-0441) from ThermoFisher Scientific; CD3 (560527), CD62L (561917), CD11c (561241), Gr1(553129) from BD Biosciences, and Ly6G (127614), CD103 (121415), CD206 (141706) from BioLegend. Viability was assessed by calcein blue AM (BD Biosciences). Flow data were quantified by FlowJo v.10.4.1.

Isolation and activation of human peripheral blood monocyte-derived macrophage (HMDM). Monocytes were purified from the buffy coat using CD14 microbeads (MiltenylBiotec) and differentiated into HMDMs using human M-CSF (125ng/mL, R&D Systems) for 7 days as previously described (Kratz et al., 2014). For M1 activation, HMDMs were treated with LPS (100ng/mL, Sigma) and IFNγ (1ng/mL, R&D Systems) for 48hrs. For M2 activation, HMDMs were treated with IL-4 (10ng/mL, R&D Systems) and IL-10 (10ng/mL), R&D Systems for 48hrs.

Human breast tumor tissue processing and immune analysis. Human breast tumor tissue was cut into ~100mg pieces, each of which was digested in HBSS $Ca2^{+}$/$Mg2^{+}$ buffer containing TL (14U/ml) and DL (28U/ml) (Roche) and DNAse I (15mg/mL) at 37ºC with horizontal shaking at 200rpm for 45mins, adapted from previously described (Cassetta et al.,

2019). Digested tumors were filtered through a 100μm cell strainer, incubated in RBC lysis buffer for 5 min, passed through a 40μm cell strainer, and resultant cells were resuspended in isolation buffer (0.1% BSA/PBS, 2mM EDTA). For DQ-OVA degradation assays, cells were incubated with DQ-ovalbumin, and DQ-OVA fluorescence was quantified in $CD45^+CD11b^+CD14^+CD163^+$ TAMs. Antibodies used include: CD11b (17-0118-41) from ThermoFisher Scientific; CD45 (557748), CD163 (563887), CD14 (347497), CD206 (321120), HLA-DR (560651) from BD Biosciences. Flow data were quantified by FlowJo v.10.4.1.

Tumor spatial analysis of Kla and hypoxia in macrophages by microscopy. Tumors were isolated and fixed in 4% paraformaldehyde in PBS for 24h, embedded in paraffin blocks, and sectioned (5μm). Slides were stained with CD206 (for murine: AF2353; for human: AF2536, R&D systems), Kla (PTM-1401, PTM BIO), HIF1α (NB100-105, Novus Biologicals). For murine tumors to be stained with hypoxyprobe (HP1-200Kit, Pimnoidazole HCl/hypoxyprobe-1), mice were injected with hypoxyprobe (60mg/kg) intraperitoneally 1 hour prior to sacrifice. Cell nuclei were labeled with DAPI (ThermoFisher Scientific). Images were obtained with a Nikon Eclipse Ti2 microscope and analyzed using NIS-Elements software.

Collecting tumor interstitial fluid (TIF). Mice were euthanized by cervical dislocation. Tumors were immediately isolated, rinse with PBS, and were placed on top of a 40μm nylon mesh filter on top of a tube. The tube was centrifuged at 106 x*g* for 10 minutes at 4 °C. Transfer the fluid to a fresh Eppendorf tube, followed by another centrifugation at 3000 rpm for 15 minutes at 4 °C. The supernatant was subjected to GC/LC-MS analysis.

Tumor hypoxia and Kla analysis by flow cytometry. Digested tumor cells were labeled with fluorophore attached antibodies for cell type identification before fixed in 4% paraformaldehyde in PBS for 15mins, followed by 20min PBST (0.2%Triton X). Fixed cells

were blocked in 5%BSA/PBST for 30mins, washed, and incubated with antibodies to Kla (PTM-1401, PTM BIO) or HIF1α (NB100-105, Novus Biologicals) for an hour. Corresponding secondary antibodies (P10994, Invitrogen; ab150113, Abcam) were applied for another hour before analyzing using flow cytometry.

Lactate addition and measurement. Intracellular lactate was measured using a lactate colorimetric assay kit (K607, BioVision) according to the manufacturer's instruction. Exogenous lactic acid (L6402, Sigma) was added to TAMs at various doses.

Shotgun proteomics. Whole cell lysates of TAMs from E0771 or B16F10 models were collected in 4% sodium deoxycholate (SDC) in 10mM Tris, 1 mM EDTA, pH 7.4 for trypsin digestion. Samples were denatured by heating at 56ºC and reduced with 5mM dithiothreitol (DTT) for 1h, alkylated with 15mM iodoacetamide for 30 min at room temperature in the dark, and excess iodoacetamide was quenched with an additional 5mM DTT. Samples were digested with trypsin (Promega, Madison, WI) at 1:20 w/w ratio overnight at 37°C with mixing. After digestion, SDC was precipitated by addition of 1% trifluoroacetic acid and insoluble material was removed by centrifugation at 14,000x*g* for 10min. Samples were then desalted by solid phase extraction using Oasis HLB 96-well μElution Plate, dried down, stored at -80°C, and reconstituted with 0.1% formic acid in 5% acetonitrile to a peptide concentration of 0.1μg/μL for LC-MS analysis.

LC/MS analyses. Digested peptides were injected onto a trap column (40x0.1mm, Reprosil C18, 5μm, Dr. Maisch, Germany), desalted for 5 min at a flow of 4μL/min, and separated on a pulled tip analytical column (300 x 0.075 mm, Reprosil C18, 1.9 μm, Dr. Maisch, Germany) with a 3 segment linear gradient of acetonitrile, 0.1%FA (B) in water, 0.1%FA (A) as follows: 0-2 min 1-5%B, 2-150 min 5-25%B, 150-180 min 25-35%B followed by column wash

at 80% B and re-equilibration at a flow rate 0.4μL/min (Waters NanoACQUITY UPLC). Tandem MS/MS spectra were acquired on Orbitrap Fusion Lumos (Thermo Scientific) operated in data-dependent mode on charge states 2-4 with 2s cycle time, dynamic exclusion of 30s, HCD fragmentation (NCE 30%), and MS/MS acquisition in the Orbitrap. MS spectra were acquired at a resolution 120,000 and MS/MS spectra (precursor selection window 1.6Da) at a resolution of 30,000 (for PMN media) or 15,000 (in-gel digests, recombinant peptides). Peptides and proteins were identified using the Comet search engine[4] with PeptideProphet and ProteinProphet validation. Search criteria included a 20ppm tolerance window for precursors and products, fixed Cys alkylation, and variable Met oxidation.

Western blot analyses. Cells were lysed with 1% SDS containing protease and phosphatase inhibitors (Sigma), and protein was quantified with the BCA Protein Assay Kit (Pierce). Proteins (10-20μg) were resolved on 10%, 12.5%, or 15% SDS-PAGE gels depending on the target protein, transferred to PVDF membranes (Millipore), blocked with 5% BSA (Sigma) in 0.1% TBS/Tween-20 at RT for 2hrs, stained with primary and secondary antibodies, and visualized using the ECL detection kit (Biorad) and an LI-COR imager.

Antibodies – Antibodies against panKac (PT-101, PTM-BIO), panKla (PTM-1401, PTM-BIO), H3k18la (PTM-1406, PTM-BIO), Tubulin (2125, CST), LDHA (2012S, CST).

RNA-seq. Total RNA was extracted from BMDM cells activated as indicated using an RNeasy Plus Mini Kit (74134, Qiagen). 2-4ug of total RNA was used as starting material to prepare libraries using Illumina TruSeq Stranded mRNA Library Prep Kit Set A (RS-122-2101, Illumina). The size of the libraries was selected by using the Agencourt AMPure XP beads (A63882, Beckman Coulter), with an average size of 400 bp. The libraries were sequenced using Illumina HiSeq 4000 (pair end 50 bp). Bioinformatic analysis of RNA-seq data: sequencing

quality was evaluated by FastQC v.0.11.4. All reads were mapped to the reference genome of Illumina iGenomes UCSC mm10 using HISAT2 v.2.1.021. Differential expression analysis was implemented using edgeR v.3.16.522, after retaining only genes for which counts per million (cpm) was larger than one in four samples and normalizing the library sizes across samples using the TMM method of the edgeR package. Hierarchical clustering was performed, and heat maps were generated using Perseus v.1.6.1.1 (http://www.coxdocs.org/doku.php?id=perseus:start). The log2-transformed gene expression values (RPKM) were normalized by subtracting the mean in every row, and hierarchically clustered with a Pearson correlation algorithm. Gene Ontology analysis (GOTERM_BP_DIRECT) was carried out using DAVID bioinformatics resources 6.8 (Huang et al., 2009a, 2009b)

ChIP–seq. Native ChIP was carried out following the published protocol (Cuddapah et al., 2009) with spike-in for normalization purposes. Spike-in was carried out according to vendor protocols (61686, Active Motif). In brief, 50 ng of Spike-in chromatin (53083, Active Motif) was added to 25 μg of BMDM chromatin to incubate with 2 μg Spike-in antibody (61686, Active Motif) together with 4 μg of anti-H3K18la antibodies. After 4 h of incubation at 4 °C, Protein A Sepharose (17-5280-01, GE Healthcare Life Sciences) was added and incubated for another 2 h, followed by sequential wash with buffer TSE I (0.1% SDS, 1% Triton X-100, 2 mM EDTA, 20 mM Tris-HCl pH 8.0, 150 mM NaCl), TSE II (0.1% SDS, 1% Triton X-100, 2 mM EDTA, 20 mM Tris-HCl pH 8.0, 500 mM NaCl), buffer III (0.25 M LiCl, 1% NP-40, 1% deoxycholate, 1 mM EDTA, 10 mM Tris-HCl pH 8.0), and TE buffer (1 mM EDTA, 10 mM Tris-HCl pH 8.0). Chromatin DNA was finally eluted with buffer containing 1% SDS and 0.1 M NaHCO3. The eluates were digested with RNase A (12091021, Thermo Fisher Scientific) and proteinase K (AM2546, Thermo Fisher Scientific). DNA was recovered using the QIAquick PCR purification

kit (28106, Qiagen) according to the manufacturer's instructions. ChIP–seq libraries were constructed with an Accel-NGS 2S Plus DNA Library Kit (Swift Biosciences) according to the manufacturer's protocol. The libraries were then amplified and assessed for fragment size using TapeStation (Agilent) and quantified using a Qubit dsDNA HS AssayKit (Thermo Fisher Scientific). The indexed libraries were pooled and sequenced on a Hiseq4000 Sequencer (Illumina) using the 50-nucleotide single-read configuration. Bioinformatics analysis of ChIP–seq data: sequencing quality was evaluated by FastQC v.0.11.4. All reads were mapped to the reference genome of Illumina iGenomes UCSC mm10 using Bowtie v.2.2.626,27, and only uniquely mapped reads were retained. Then SAMtools v.0.1.1928 was used to convert files to bam format, sort, and remove PCR duplicates. Peaks were called using MACS v.2.2.129 under q = 0.01. To quantify and directly compare H3K18la or H3K18ac in different samples (M0 and M1 macrophages), the uniquely mapped H3K18la or H3K18ac reads in promoter regions (Å} 2 kb around transcriptional start sites) of each gene were counted by featureCounts v.1.5.0-p130, and then normalized by Spike-in ChIP read counts of the corresponding condition (M0 macrophages treated with or without 24hr 1% hypoxia). The overlap genes in ChIP–seq and RNA–seq data were used for all subsequent analysis. Gene Ontology analysis (GOTERM_BP_DIRECT) was carried out using DAVID Bioinformatics Resources 6.823,24.

Measurement of gene expression by qRT-PCR. Cell pellets were lysed in RLT buffer. Total RNA was isolated using the RNAeasy kit (Qiagen) with on-the-column DNAse digestion (Qiagen), converted to cDNA using reverse transcription kit (Qiagen), and amplified using QuantiTect SYBR Green PCR Kits (Qiagen). The following murine primers were used:
18s forward: GCCGCTAGAGGTGAAATTCTT, reverse: CGTCTTCGAACCTCCGACT.
Mhcii forward: AGCCCCATCACTGTGGAGT, reverse: GATGCCGCTCAACATCTTGC.
Nos2 forward: GCTCCTCTTCCAAGGTGCTT, reverse: TTCCATGCTAATGCGAAAGG.

Ym1 forward: GCCCACCAGGAAAGTACACA, reverse: TGTTGTCCTTGAGCCACTGA.

Il12 forward: GGAGCACTCCCCATTCCTACT, reverse: GAACGCACCTTTCTGGTTACAC.

Cd86 forward: TGTTTCCGTGGAGACGCAAG, reverse: TTGAGCCTTTGTAAATGGGCA.

Cd206 forward: GGGCTTACGGTGAACCAAAT, reverse: GCTCCTCTTCCAAGGTGCTT.

Arg1 forward: CTCCAAGCCAAAGTCCTTAGAG, reverse: AGGAGCTGTCATTAGGGACATC.

Vegfα forward: CAGGCTGCTGTAACGATGAAG, reverse: CTATGTGCTGGCTTTGGTGA.

Mmp9 forward: GGACCCGAAGCGGACATTG, reverse: CGTCGTCGAAATGGGCATCT.

Mmp10 forward: CCCAGCTAACTTCCACCTTTC, reverse: AATTCAGGCTCGGGATTCCAA.

Mmp12 forward: GCCTGTGGGGCTGCTCCCATG, reverse: GTTGCCCAGTTGCTTCTAGCCC.

Mmp13 forward: CTATCCCTTGATGCCATTACCAG, reverse: ATCCACATGGTTGGGAAGTTC.

Mmp28 forward: TGCCATCACTGTAGGGAGTTA, reverse: GGACGAGGCTCTACAGTGATG.

Klf4 forward: AGGAACTCTCTCACATGAAGCG, reverse: GGTCGTTGAACTCCTCGGTC.

Sirt6 forward: CAGGGTTGTCGCCTTACGCGG, reverse: ACCACGCTGGAGGACTGCCAC.

The following human primers were used:

18S forward: CCCAACTTCTTAGAGGGACAAG, reverse: CATCTAAGGGCATCACAGACC.

ARG1 forward: GGCAAGGTGATGGAAGAAAC, reverse: AGTCCGAAACAAGCCAAGGT.

VEGFA forward: AGGGCAGAATCATCACGAAGT, reverse: AGGGTCTCGATTGGATGGCA.

IL10 forward: GGGAGAACCTGAAGACCCTC, reverse: ATAGAGTCGCCACCCTGATG.

MMP12 forward: CATGAACCGTGAGGATGTTGA, reverse: GCATGGGCTAGGATTCCACC.

Tumor inoculation and treatment. For the TNBC model, E0771 or Py8119 cells ($0.5x10^6$) were injected into the 4th mammary fat pad of the right ventral side of C57BL/6 mice. For the melanoma model, B16F10 cells ($1x10^6$) were injected into the flank of C57BL/6 mice. Tumor volume was assessed by calipers, and experiments were terminated when tumor volume reached >1000mm^3.

Statistics. Statistical significance was determined with the Student's two-tailed, unpaired *t*-test ($p<0.05$). Linear regression was performed using Prism v.7 software. For shotgun proteomics studies, significance was assessed by a combination of the *t*-test and *G*-test (Becker et al., 2010) with correction for false-discovery rate (<5%) using PepC software (Heinecke et al., 2010).

Results

Hypoxia induces histone Kla and M2 phenotype in murine and human macrophages

Our previous discovery of the role of lactate in driving the M2-like phenotype via histone Kla in the context of powerful M1 stimuli suggests that any condition that increases lactate production by TAMs might trigger a similar mechanism to promote their M2-like phenotype. Hypoxia, a key environmental stimulus in tumors (Eales et al., 2016; Henze and Mazzone, 2016; Petrova et al., 2018), promotes lactate production and M2-associated gene expression in macrophages (Dengler et al., 2014; Eales et al., 2016). I therefore hypothesized that hypoxia promotes the histone Kla modification at promoters of M2-like genes.

To test this, I cultured bone marrow-derived macrophages (BMDMs) in 21% O_2 (normoxia) and 1% O_2 (hypoxia) conditions. Hypoxia enhanced lactate production by BMDMs, which is associated with the increased total and site-specific histone Kla modification (**Figures 3.2a-b**). RNA/ChIPseq with anti-H3K18la identified many M2-like genes whose mRNA levels were induced >2-fold and whose promoters were marked by increased H3K18la by more than 2-fold (blue numbers) (**Figure 3.2c**). These included pro-tumorigenic genes expressed by M2-like macrophages (*Arg1*, *Vegfa*, *Mmp's*), and genes required for M2 polarization (*Klf4*, *Sirt6*). Consistent with our observations in BMDMs, hypoxia exposed human monocyte-derived

macrophages (HMDMs) also showed elevated intracellular lactate production, increased Kla levels, and induced M2-like gene expression compared to those in normoxic conditions (**Figure 3.2d-f**).

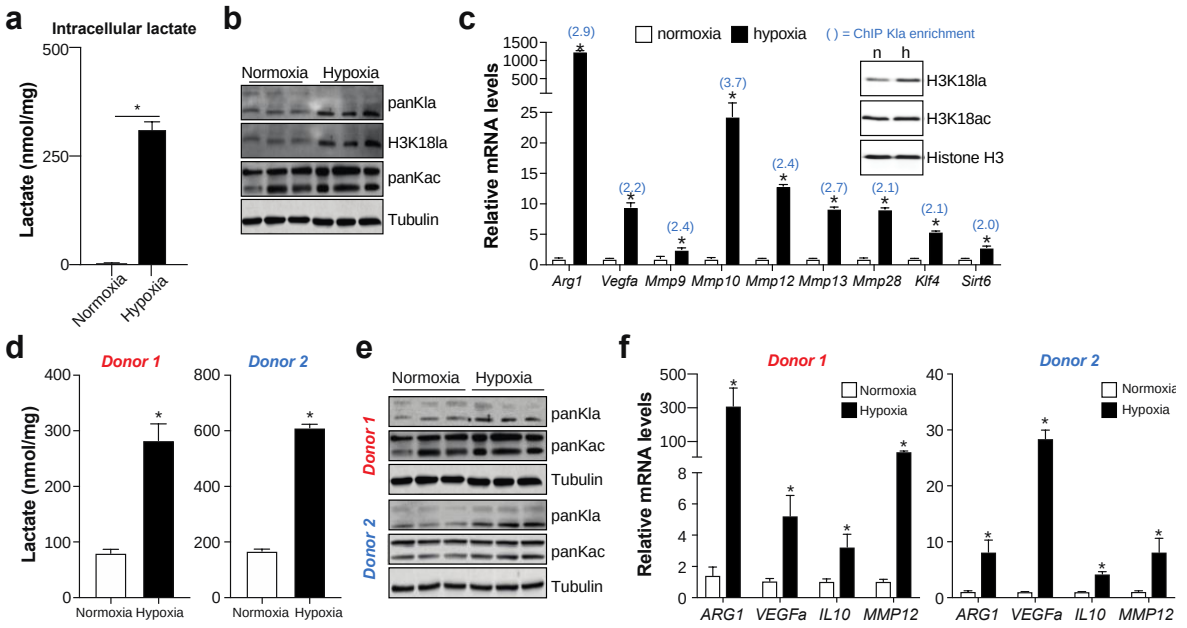

Figure 3.2. Hypoxia promotes histone lactylation & an M2-like macrophage phenotype. a-c, BMDMs were cultured in normoxia (n, 21% O_2) or hypoxia (h, 1% O_2) conditions. **a**, Intracellular lactate level at 48hrs. n=4/group. **b**, PanKla, H3K18la, and panKac (as control) protein levels at 48hrs. **c**, RNA/ChIPseq with anti-H3K18la identified elevated M2-like genes, with enriched Kla at their promoters (enriched in blue) at 24hrs. *, $p<0.05$, paired *t-test*. FDR<1%. *Inset*: H3K18la and h3K18ac levels. **d-f**, HMDMs from two healthy donors were cultured in normoxia (21% O_2) or hypoxia (1% O_2) conditions for 48hrs. **d**, Intracellular lactate level. n=4/group. **e**, PanKla and panKac (as control) protein levels. **f**, Representative M2-like gene expression. n=4/group *, $p<0.05$ Student's *t*-test, error bars indicate the mean of independent experiments ± s.e.m. Paired RNA/ChIPseq was performed by Dr. Yingming Zhao's lab. Blood was donated by me and Dr. Alex Hoffman, and taken by Kristen Becker for me to isolate monocytes.

Histone Kla associates with M2-like phenotype and hypoxia in murine and human tumors.

Although BMDMs and HMDMs are a useful experimental model for *in vitro* studies, macrophages adopt more complex phenotypes *in vivo* (Geissmann et al., 2010). Hence, in order to corroborate our findings *in vivo*, I started with the C3(1)-TAg genetic engineered mouse

(GEM) model of triple-negative breast cancer (TNBC), which shares many features with human TNBC tumors (Green et al., 2000). The C3(1)-TAg mice show early atypia of mammary ductal epithelium around 8 weeks of age, progress to intraepithelial neoplasia around 12 weeks of age, and develop tumors in multiple mammary glands between 16-22 weeks of age.

To first determine if histone Kla is present in TAMs in C3(1)-TAg tumors, I injected mice that had developed at least one tumor > $100mm^3$ with hypoxyprobe (allows for hypoxia assessment) 1h prior to sacrifice. Immunofluorescence analysis of purified TAMs showed Kla positive signal in the nucleus with variability in its intensity across TAMs (**Figure 3.3a**). Flow cytometry further revealed that Kla^{high} TAMs had elevated levels of hypoxyprobe and HIF1α relative to Kla^{low} TAMs (**Figure 3.3b**). Admittedly, HIF1α may not always correlate with tissue hypoxia status. Hence, the utilization of both hypoxyprobe and HIF1α, as well as hypoxia-associated genes (see below in TAMs, measured by proteomic) would strengthen the hypoxia assessment. Notably, Kla^{high} TAMs showed elevated CD206 levels, an indication of the M2-phenotype (**Figure 3.3c**). Flow sorting of the TAM population further validated that $CD206^{high}MHCII^{low}$ (M2-like TAMs) had increased expression of M2 like-genes, Kla, and intracellular lactate level compared to $CD206^{low}MHCII^{high}$ (M1-like TAMs) (**Figures 3.3d-g**). Moreover, Kaz and I developed an approach to study the spatial relationship between TAM Kla and hypoxia in individual tumors (**Figures 3.3h-i**). Results showed that TAMs that reside in higher hypoxia zones exhibit higher Kla levels compared to those in lower hypoxia zones (**Figures 3.3 h-i**).

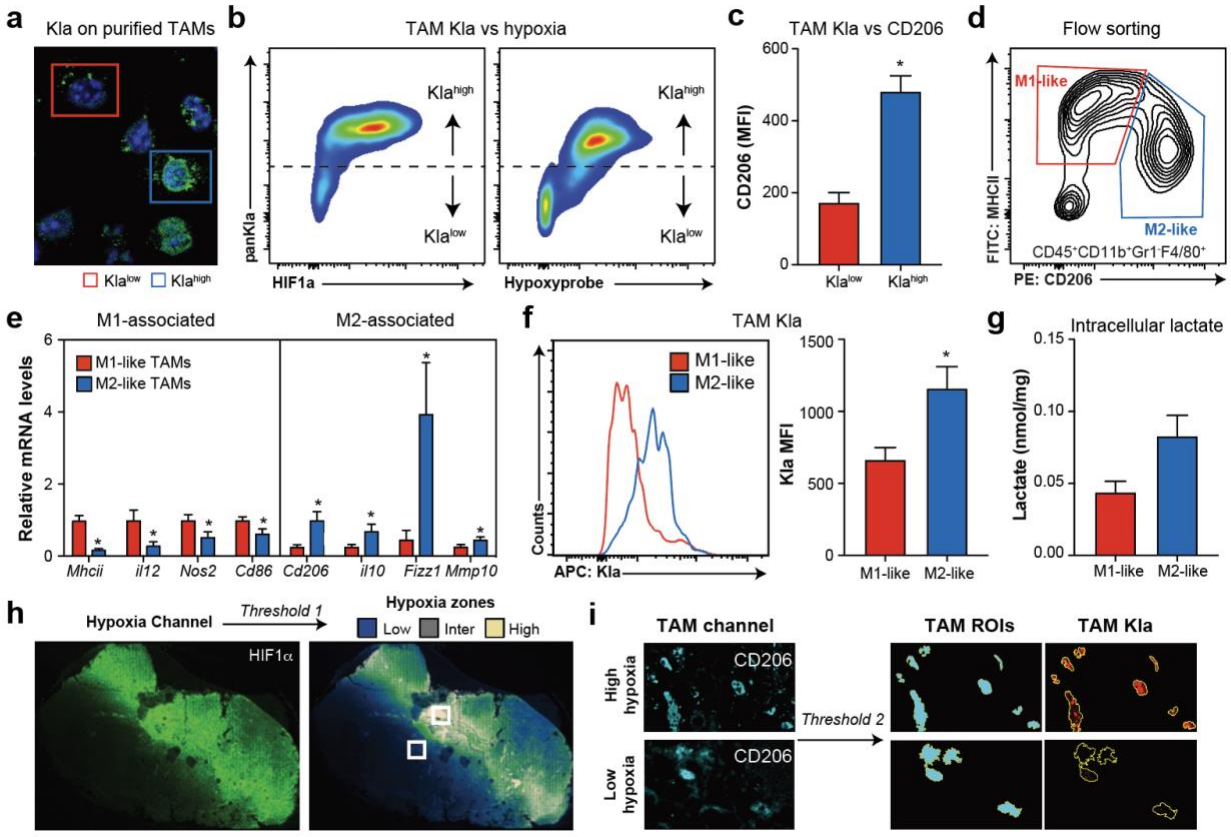

Figure 3.3. TAM Kla associates with hypoxia and M2-phenotype in C3(1)-TAg GEM model. a, Immunofluorescence staining of purified TAMs with anti-panKla (green) and DAPI (blue). **b-c**, Flow cytometry analysis of gated TAMs from digested tumors with anti-panKla, anti-HIF1α, hypoxyprobe Mab1, and anti-CD206. Representative plot of panKla versus HIF1α and hypoxyprobe (**b**). Quantification of CD206 MFI in Kla^{low} versus Kla^{high} TAMs (**c**). **d-g**, M1-like and M2-like TAMs from C3(1)TAg tumors were flow sorted based on CD206 and MHCII level. **d**, Experimental design. **e**, mRNA levels. n=5/group. **f**, Representative flow cytometry data of Kla level (*left*). Quantification (*right*). n=3/group. **g**, Intracellular lactate measurement. n=3/group. **h**, Intensity of HIF1α staining is used to identify zones of low, intermediate (inter), and high hypoxia. Areas (white box) in each zone will be applied to the TAM channel. **g**, CD206 was used to identify TAM-associated regions of interest (TAM ROI). Kla intensity is then quantified in TAMs ROIs. Image J analysis will be performed to finalize quantification. *, $p<0.05$ Student's *t*-test, error bars indicate the mean of independent experiments ± s.e.m. Spatially analysis (h-i) was performed by Dr. Kasturi Chakraborty.

Having interrogated the quantitative and spatial association of hypoxia-Kla-M2-like pathway in TAMs in C3(1)-TAg model of breast cancer, we began to investigate this pathway in human tumors. I performed similar studies on tumors obtained from ER^+ breast cancer patients.

After gating for TAMs ($CD45^+CD11b^+CD14^+CD163^+$), I stratified them as Kla^{high} and Kla^{low}, and found that Kla^{high} TAMs had elevated levels of HIF1α and CD206 (**Figures 3.4a-c**). For the spatial relationship between TAM Kla and hypoxia, a similar threshold analysis on formalin-fixed, paraffin-embedded tumor section were applied. Results showed that Kla^{high} TAMs localized to high hypoxia zones while Kla^{low} TAMs localized to low hypoxia zones of the tumors (**Figures 3.4d-e**).

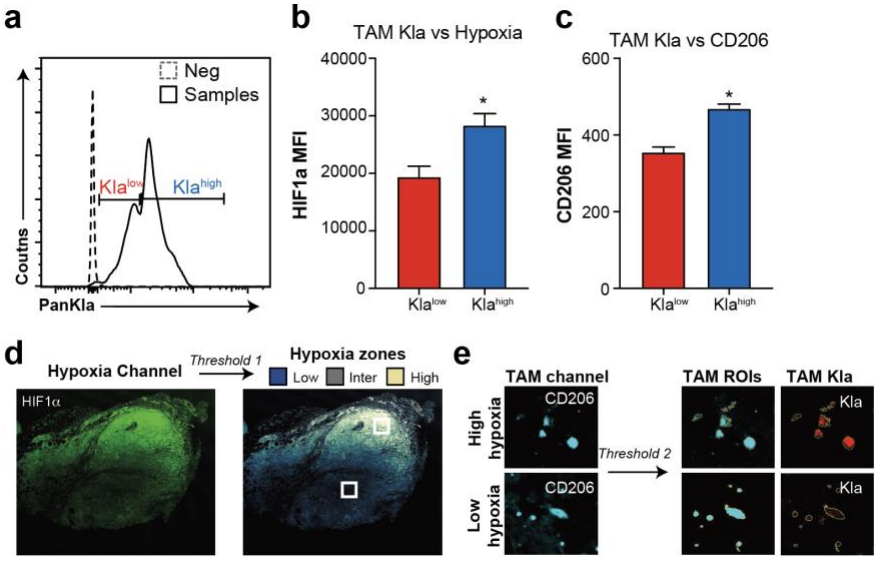

Figure 3.4. TAM Kla associates with HIF1a and CD206 in human breast cancer tumors. a-c, Flow cytometry analysis on gated TAMs from digested tumors. Stratification of TAMs based on Kla levels (a). HIF1α (**b**) and CD206 levels (**c**) in Kla^{high} and Kla^{low} TAMs. **d**, Intensity of HIF1α staining is used to identify zones of low, intermediate (inter), and high hypoxia. Areas (white box) in each zone will be applied to the TAM channel. **e**, CD206 was used to identify TAM-associated regions of interest (TAM ROI). Kla intensity is then quantified in TAMs ROIs. *, $p<0.05$ Student's *t*-test, error bars indicate the mean of independent experiments ± s.e.m. Spatially analysis (d-e) was performed by Dr. Kasturi Chakraborty. Patient breast tumor samples were provided by Dr. Swati Kulkarni (Northwestern University).

Lowering lactate production by deleting *Ldha* attenuates M2-like genes only in macrophages under hypoxia conditions.

Having presented the observational association between hypoxia and the lactate-Kla-M2 pathway in macrophages both *in vitro* and *in vivo*, we aimed to further investigate the role of

lactate in driving M2-like gene expression during hypoxia. I generated myeloid cell-specific *Ldha* deficient mice (m*Ldha*-/-) by crossing *Ldha*$^{fl/fl}$ mice with *LysM*-Cre$^{+/-}$ mice (**Figure 3.5a**). m*Ldha*-/- attenuated intracellular lactate levels and *Arg1* expression in BMDMs under hypoxic conditions when lactate is elevated, but not under normoxic conditions (**Figures 3.5b-d**). Similar results were also observed in TAMs (data not shown). These findings suggest that LDHA controls M2-like genes in the context of hypoxia-induced lactate overproduction but not under basal normoxia conditions, where lactate levels are low.

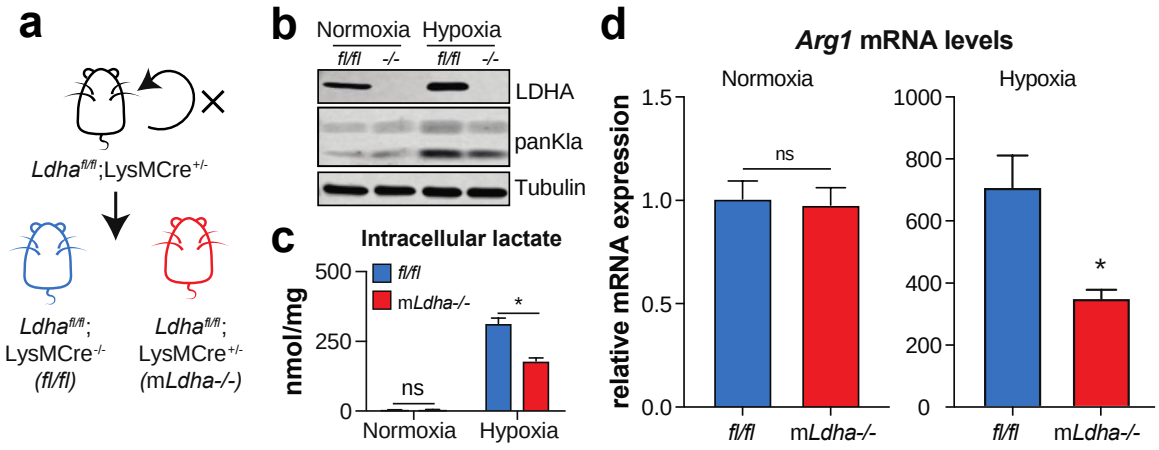

Figure 3.5 m*Ldha*-/- lowers lactate production and M2 gene expression in macrophages under hypoxia condition. a, The breeding scheme of *fl/fl* and m*Ldha*-/- mice. **b-d**, *fl/fl* (control) and m*Ldha*-/- BMDMs were cultured in 21%O2 (normoxia) or 1% O2 (hypoxia) for 24h. **b**, LDHA and panKla protein level. **c**, Intracellular lactate level. **d**, Arg1 mRNA levels. n=4/group. *, $p<0.05$ Student's t-test, error bars indicate the mean of independent experiments ± s.e.m. Genotyping of m*Ldha*-/- was done by Anna Tang, and breeding was facilitated by Kelly Schoenfelt.

m*Ldha*-/- decreases the M2-Kla pathway in TAMs and attenuates tumor growth only in models with a high degree of hypoxia.

What are the effects of lowering lactate production by TAMs *in vivo*? Because hypoxia is required for m*Ldha*-/- to lower M2-like gene expression, we first sought to identify tumor models with hypoxia. We characterized the degree of hypoxia in two models: E0771 tumors, a

syngeneic TNBC model, and B16F10, a syngeneic melanoma model. HIF1α staining on similarly sized tumors revealed that B16F10 tumors had significantly more hypoxic regions relative to E0771 tumors (**Figure 3.6a)**. Based on this result, we predicted that the Kla-M2 pathway might be elevated in B16F10 compared to E0771 tumors. We further predicted that blocking lactate production by deleting *Ldha* would only attenuate M2-associated gene expressions and tumor growth in B16F10 but not E0771 tumors.

Indeed, as evidenced by increased intracellular lactate levels, H3K18la modification, and M2-like protein abundance, the Kla-M2 pathway was higher in TAMs from B16F10 rather than E0771 tumors (**Figures 3.6b-d)**. These results were also supported by elevated levels of proteins involved in the 'glycolytic process' and 'response to hypoxia' in TAMs as well as increased basal glycolysis and glycolytic capacity of TAMs from B16F10 versus E0771 tumors (**Figures 3.6e-f**). Hence, the hypoxia-lactate-Kla-M2 pathway was highly operative in B16F10 TAMs but minimally detected in TAMs from E0771 tumors. This striking difference further predicted the effect of blocking lactate production by TAMs. I found that deleting *Ldha* decreased M2-like genes in TAMs from B16F10 but not E0771 tumors (**Figure 3.6g**). Because M2-like TAMs are known to support immunosuppressive tumor microenvironment and inhibit cytotoxic T cell activation (Dannenmann et al., 2013; Munn et al., 1999; Rodriguez et al., 2003, 2004; Saio et al., 2001), I monitored tumor growth and assessed tumor immune composition between *fl/fl* and m*Ldha*-/- mice. Consistent with a decreased M2-phenotype in m*Ldha*-/- TAMs, deleting *Ldha* attenuated tumor growth and elevated $CD8^+$ T cell and $CD8^+$ effector T cells ($CD8^+T_{eff}$) in B16F10 tumors, but not E0771 tumors (**Figures 3.6h-i)**. I further extended this phenotype to Py8119, another syngeneic TNBC model, and found that hypoxia induces lactate, Kla, and M2 signatures in TAMs, and deleting *Ldha* alleviates these inductions (data not shown).

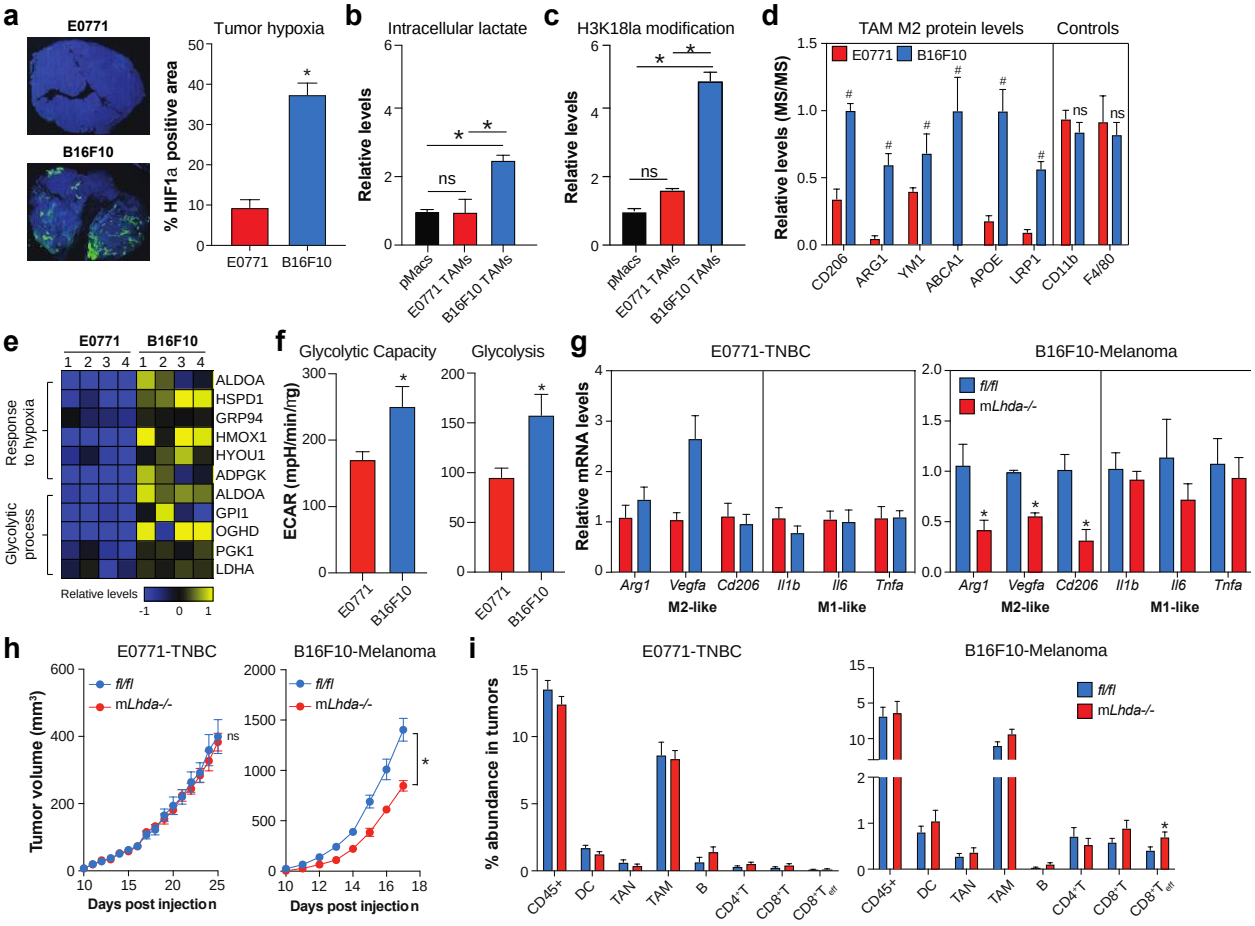

Figure 3.6 Hypoxia-lactate-Kla-M2 pathway is operative in B16F10 tumors but not in E0771 tumors. a, Representative image of HIF1a (green) and DAPI (blue) staining of E0771 and B16F10 tumors (left). Quantification of % HIF1α + area (right). n=16-23/group. b-g, TAMs purified from E0771 and B16F10 tumors. **b**, Intracellular lactate level of thioglycolate-elicited peritoneal macrophages (pMacs, used here as a none-hypoxia source comparison) and TAMs. n=5-7/group. **c**, Immunoblot quantification by densitometry (expressed relative to pMacs) of H3K18la modification of pMacs and TAMs. n=5/group. **d**, Proteomics analysis of TAMs. protein levels were standardized to the most abundant condition. n=4/group. **e**, Heatmap depicts differences in levels of proteins involved in response to hypoxia and glycolysis process in TAMs. Proteins were quantified by proteomics. blue = low, Yellow = high abundance. n=4/group. **f**, Glycolytic capacity and glycolysis of purified TAMs, measured by Seahorse assay. n=8-10/group. **g**, mRNA level of M1 and M2-like genes in purified TAMs. **h**, Tumor growth curves of E0771 and B16F10 models. n=8-14/group. **i**, Immune composition of tumors isolated from E0771 and B16F10 models. n=8-14/group. *, $p<0.05$ Student's *t*-test, ns, not significant; error bars indicate the mean of independent experiments ± s.e.m. HIF1α quantification was performed by Dr. Kasturi Chakraborty. Proteomic quantification was performed by Dr. Lev Becker.

Endogenous lactate production rather than exogenous lactate in the tumor microenvironment is the driver of the Kla-M2 TAM pathway.

Differential lactate levels in TAMs could be due to differences in exogenous lactate levels in the TME (largely determined by cancer cells) and/or differences in endogenous lactate production due to hypoxia-stimulated glycolysis in TAMs. We have three pieces of evidence indicating it was the endogenous lactate production by TAMs that matters. First, in collaboration with Dr. Alexander Muir's group, we quantified tumor interstitial fluid (TIF) by mass spectrometry using a previously established protocol (Sullivan et al., 2019). TIF lactate levels were not significantly different between E0771 and B16F10 tumors (**Figure 3.7a**), despite large differences in histone Kla and M2-like proteins in TAMs (**Figure 3.6d)**. Second, treating TAMs with 'TIF-appropriate' lactate levels (1-10mM, black bars) had minor effects on M2-like gene expression (**Figure 3.7b**). Third, although TAMs from m*Ldha*-/- tumor exhibited decreased M2-like genes (**Figure 3.6g**), there is no significant difference in lactate levels in TIF between *fl/fl* and m*Ldha*-/- tumors or in their hypoxia status (**Figures 3.7c-d**). These results illustrated that it was the endogenous lactate production rather than an exogenous source that predominately contribute to the Kla-M2 pathway in TAMs.

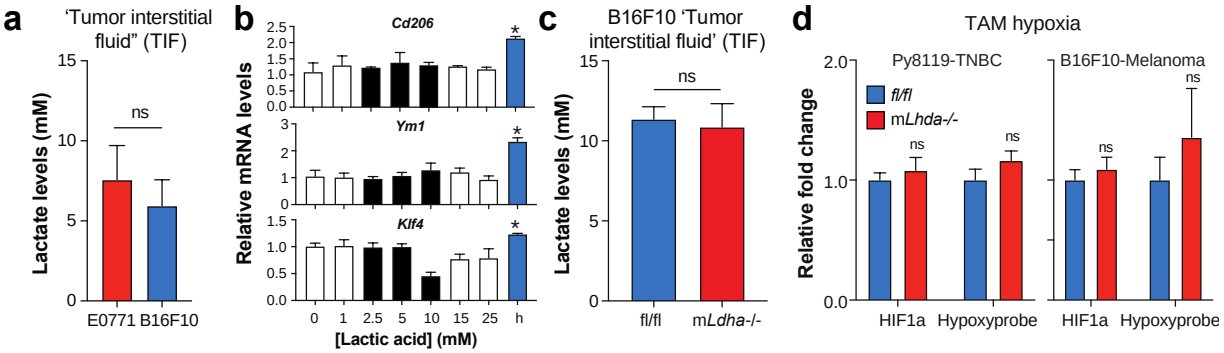

Figure 3.7. Exogenous lactate levels do not correlate with M2-like TAMs across tumors. a, Lactate levels in TIF from E0771 and B16F10 tumors quantified by mass spectrometry. n=8/group. **b**, Effects of different lactic acid concentration on M2-like gene expression in TAMs. TIF appropriate level (black color). h=1%O_2 hypoxia condition (blue color). n=3/group. **c**,

Figure 3.7 continued. Lactate levels in TIF from *fl/fl* or m*Ldha*-/- B16F10 tumors quantified by mass spectrometry. n=5/group. **d**, TAM Kla staining vs HIF1α and hypoxyprobe. n=7-11/group. *, $p<0.05$ Student's *t*-test, ns, not significant; error bars indicate the mean of independent experiments ± s.e.m. After I isolated tumor and collected TIF, lactate level in TIF was measured by Dr. Alexander Muir's group.

Discussion

Although the stimuli that induce the M2-like phenotype of macrophages *in vitro* have been well established in BMDMs, the understanding of how TAMs acquire an M2-like phenotype *in vivo* remains limited. Studies have shown that tumor hypoxia induces cellular glycolysis and lactate production, and TAMs adopt an M2-like phenotype during tumor progression (Dengler et al., 2014; Eales et al., 2016). Because our previous study demonstrated that lactate production by macrophages in an infection setting modifies histone Kla to induce an M1-to M2-like phenotypic switch, we thought to explore whether lactate-induced Kla modification could be applied in the setting of cancer to produce M2-like TAMs. Here, I first established that hypoxia induces lactate production, driving Kla modification and M2-like gene expression in both murine and human primary macrophages. We further explored the spatial and quantitative relationship between hypoxia, Kla, and M2-like phenotype not only within a tumor but also across different tumors. Importantly, I provided preliminary evidence suggesting that targeting LDHA in TAMs represents a promising therapeutic target to attenuate this "hypoxia-induced lactate-Kla-M2 pathway" in TAMs (**Figure 3.8**). Collectively, my studies demonstrated a metabolic pathway to promote an M2-like phenotype in TAMs through a novel epigenetic mechanism.

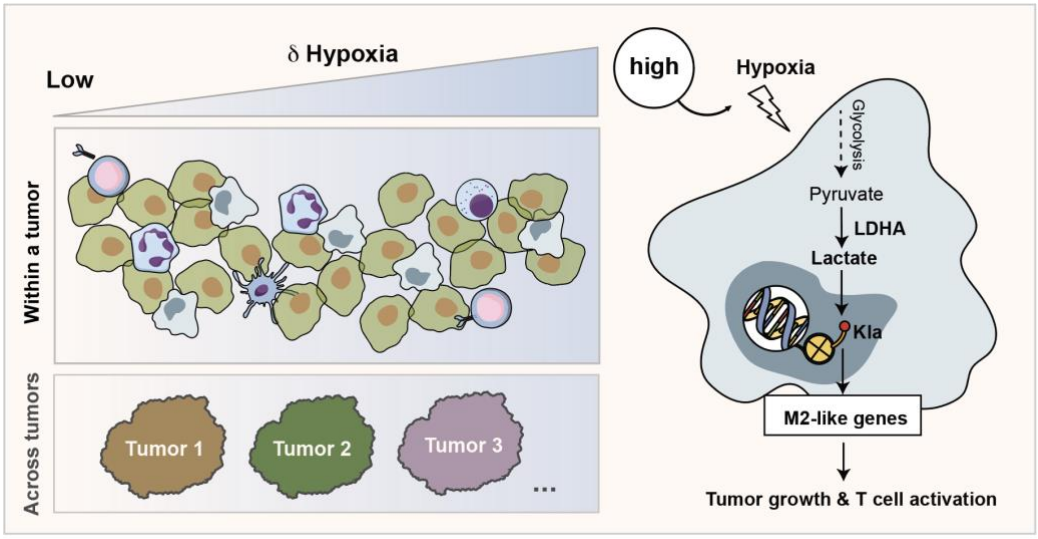

Figure 3.8. The proposed model.

Metabolic reprogramming has been an emerging concept in many cellular systems (Faubert et al., 2020; Kelly and O'Neill, 2015). In cancer, one of the most common features is the Warburg effect, depicting that cancer cells utilize the glycolysis pathway even when oxygen is available, i.e., aerobic glycolysis (Faubert et al., 2020; Ward and Thompson, 2012). Such active metabolic reprogramming allows them to utilize a variety of metabolites as unconventional nutrient sources for survival and invasion. This concept has been further extended to many immune cells in the TME. For instance, numerous studies have shown that lactate, a byproduct of glycolysis, can regulate the functions of many cell types, including dendritic cells, natural killer cells, regulatory T cells, and macrophages (Certo et al., 2020). In tumors, hypoxia has been regarded as the main environmental stimulus to upregulate cellular glycolysis and subsequent lactate production (Corbet and Feron, 2017). Previous studies have shown that exposing macrophages to exogenous lactate acid *in vitro* promotes glycolysis and induces M2-like gene expression phenotype (Colegio et al., 2014). But its importance for TAM polarization *in vivo* has not been demonstrated. My studies provide a mechanistic understanding of how lactate affects the M2-like phenotype in TAMs in three ways.

First, my studies provide a novel epigenetic mechanism by which hypoxia-induced lactate production could modify histones to directly regulate the expressions of many M2-associated genes in TAMs. Beyond *in vitro* validation using both murine (BMDMs) and human (HMDMs) systems, I used a GEM model and human patient breast tumor samples to demonstrate that Kla^{high} TAMs mostly reside in hypoxic areas and present an M2-like phenotype. Moreover, lowering TAMs' lactate production by deleting *Ldha* illustrated that TAMs from tumors with higher hypoxic signature (B16F10, Py8119) have elevated lactate, Kla, and M2-like phenotype compared to those from tumors with fewer hypoxic regions (E0771). Notably, the lower degree of hypoxia in the E0771 model does not represent for TNBC tumors in general. The purpose of using this model here was simply to provide a system that can be manipulated genetically to compare with models that have a higher degree of hypoxia. These findings establish a mechanism underlying the M2-like phenotype of TAMs and its variability within and across tumors, open questions that have not yet been answered. Nevertheless, future studies aim to identify the potential histone lactyltransferases that modify histone Kla to regulate M2-associated genes are warranted.

Second, my studies provide a clarification of the lactate source that affects the Kla-M2 pathways in TAMs. Admittedly, exogenously delivered lactic acid can induce an M2-like phenotype in macrophages *in vitro*, and TAMs in hypoxic regions are bathed in a lactate rich environment contributed by highly glycolytic cancer cells (Colegio et al., 2014; Corbet and Feron, 2017). Yet, macrophages need not be reliant on exogenous lactate, as they can generate their own via metabolic reprogramming. During infection, the metabolic shift of macrophages to glycolysis results in significant cell-autonomous lactate production, which mimics many components of the Warburg effect in cancer cells (O'Neill and Hardie, 2013). So how about in

TAMs? Is lactate from cancer cells or endogenous lactate production by TAMs the key source to induce the Kla-M2 pathways? Our study showed that lactate concentration in TIF is comparable regardless of the hypoxia status or macrophage LDHA status in the tumor. The striking difference in the phenotype of TAMs across high vs. low hypoxic models as well as the *fl/fl* vs. m*Ldha*-/- mice could not be explained by cancer cell-derived lactic acid in the TME. Moreover, exogenously delivered lactate within physiological concentration does not induce M2-associated genes in TAMs to the same level as when TAMs are exposed to hypoxia. Collectively, these results suggested that it is the endogenous lactate production independent of cancer cell-produced lactate that acts as a trigger for the Kla-M2 pathway in TAMs.

Third, my studies provide a mechanistic explanation to reconcile the tumor hypoxia-induced metabolic shift from an M1-like phenotype to an M2-like phenotype in TAMs. Previous studies have shown that exposing macrophages to hypoxia *in vitro* promotes glycolysis and induces an M2-like phenotype, mediated in part by HIF1α activation (Henze and Mazzone, 2016). Nevertheless, HIF1α and glycolytic metabolites are generally considered to promote inflammation and hence are associated with the pro-inflammatory M1-like phenotype (Lin and Simon, 2016). For example, glycolysis is thought to support pro-inflammatory cytokine expression in M1 macrophages treated with LPS/IFNγ (Murray, 2017). This seemingly conflicting phenomenon raises an interesting idea that perhaps lactate has homeostatic functions that counterbalance the otherwise inflammatory effects of HIF1α and glycolytic metabolites (Ivashkiv, 2020). However, the underlying mechanism is unclear. Extending from our previous findings (Zhang et al., 2019), our identification of the novel epigenetic pathway triggered by macrophage lactate production reconciles these differences and has important implications for the interplay among tumor hypoxia, TAM polarization, and tumor development.

Finally, although many LDHA inhibitors have been developed and shown pre-clinical efficacy, their main purpose is to modify metabolisms in cancer cells (Feng et al., 2018; Miao et al., 2013). Yet, the cell types that take up those inhibitors and ultimately lessened the tumor growth *in vivo* are unclear. Our understanding of how endogenous lactate alters the phenotype of TAMs provide not only an additional mechanism by which LDHA inhibitors might work, but also provides opportunities to repurpose them as TAM targeting therapeutics. Because my work also demonstrated that LDHA activity in TAMs contributes to adaptive immune suppression, one future direction would be to test whether LDHA inhibitors and checkpoint blockade (e.g., PD-L1) show synergy in tumors using the lactate-Kla-M2-TAM pathway as a biomarker. Altogether, my study would have important implications for epigenetic, metabolic, and immune therapies being developed or administrated clinically.

CHAPTER FOUR: GENERAL DISCUSSION AND FUTURE DIRECTIONS

Summary

Cancer is a collection of diseases driven by a large variety of genetic mutations that cause uncontrolled cell growth and spread to distant sites. Typically, those accumulated mutations in cancer cells will inevitably leave footprints, i.e., tumor antigens, that can be picked up by antigen-presenting cells to inform our adaptive immunity further to eliminate cancer cells (***top*, Figure 4.1**). However, cancer cells often create an immunosuppressive environment that evolves with their growth, consequently hindering the detection of their footprints. One of the most abundant immune cells in almost all tumor types is tumor-associated macrophages. Unfortunately, TAMs adopt a pro-tumorigenic M2-like phenotype that supports tumor growth and metastasis through multiple mechanisms. Clinical data has further shown that high TAM infiltration, especially those with an M2-like phenotype, is strongly correlated with poor patients' outcomes in many cancers. Therefore, targeting M2-like TAMs represents a promising therapeutic strategy.

This dissertation presents two distinct perspectives that conceptually broaden our understanding of how to interrogate TAM's role during cancer development and further provides two mechanisms that have the potential for developing effective TAM-targeting therapeutics. Chapter 2 describes the identification of lysosomal cysteine protease activity in TAMs that is critical in regulating the antigen cross-presentation ability of TAMs to oppose tumorigenesis. By analogy, M2-like TAMs behave like a drain that shifts the equilibrium of tumor antigens towards destruction, which dampens APCs' chance to alert the adaptive antitumor immune response. Attenuating lysosomal cysteine protease activity is likely to allow TAMs to preserve tumor

antigens for effective presentation and activation of the adaptive antitumor immune response (***red arrow*, Figure 4.1**). Practically, my studies also provide DNA nanotechnology that can preferentially deliver therapeutics to TAMs. Chapter 3 describes a hypoxia-induced lactate production by TAMs as a novel pathway to drive their immunosuppressive phenotypes via histone Kla modification. Lowering lactate production by TAMs decreased their M2-like phenotype and subsequently attenuated tumor growth in preclinical models where hypoxia is present (***green arrow*, Figure 4.1**). Because anti-VEGF antibodies have been shown to induce hypoxia (Shi et al., 2017), I envision that Kla modification in TAMs could potentially be used as a biomarker to predict the efficacy of combining anti-VEGF antibody and LDHA inhibitors in the clinics.

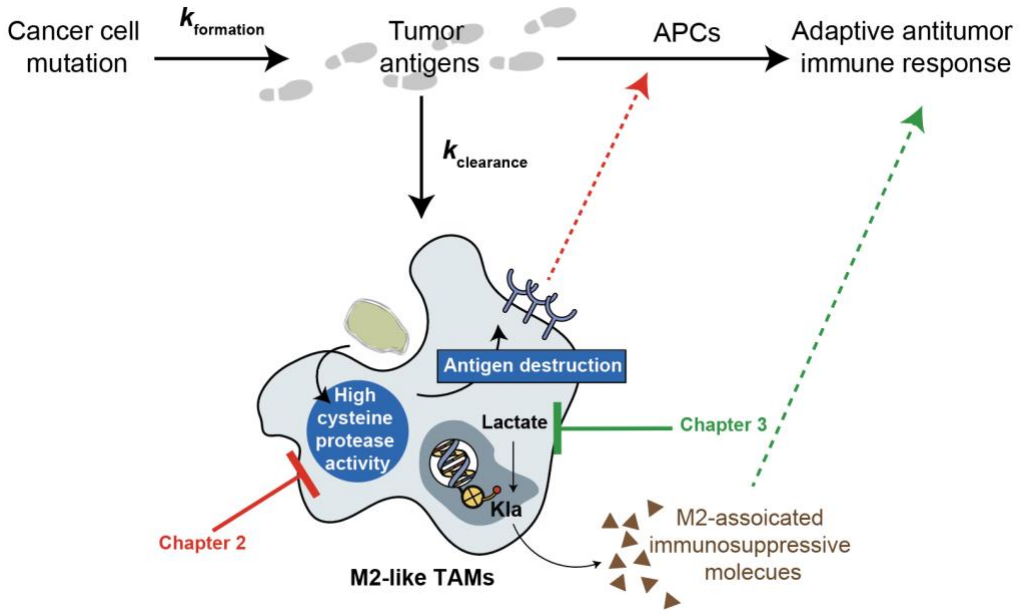

Figure 4.1. Proposed model summarizing studies in this thesis.

The broad potential implications for both my studies are *no coincidence* for the following three reasons: 1) TAMs are notably associated with almost all solid tumors; 2) our preliminary work mostly comes from a pattern obtained from unbiased proteomics across tumors or the

established M1/M2 model system instead of a single pathway in a single cancer type; 3) The phenotypic observations were extensively validated *in vitro* and *in vivo* in mice and humans before proceeding to mechanistic studies. Collectively, my studies provide new mechanistic understandings on the targetable M2 pathway and the M2-phenotype-producing pathway, serve as examples to illustrate how to exploit TAMs therapeutically from both approaches, and described a DNA-based nanotechnology platform to target TAMs *in vivo* specifically.

Extended results and discussion

The role of lysosomal cysteine protease in MHCII-restricted antigen presentation

My study showed that lowering lysosomal cysteine protease activity in TAMs improves their antigen cross-presentation capability. Because lysosomal cysteine proteases are also known to closely participate in MHCII-restricted presentation, which is essential for $CD4^+$ T cell activation, one question remains is whether E64-DNA affects presentation via MHCII in TAMs. There are two convergent processes involved in MHCII-restricted presentation. The first is to process the internalized antigens, and the second is to degrade invariant chains that block MHCII molecules to bind to the processed peptide (Mizuochi et al., 1994; Villadangos et al., 1999). Both processes are regulated by differential expression of lysosomal cysteine protease (Roche and Furuta, 2015). Although inhibition of any single type of protease in most cases does not significantly block MHCII presentation, presumably because of their redundancy (Nakagawa and Rudensky, 1999), diminishing overall lysosomal cysteine protease activity in TAMs has not yet been explored.

To test this, I used $CD4^+$T cells from OT-2 and TRP-1 mice, which recognize $OVA_{323-339}$ (fragment of OVA) or $TRP1_{113-126}$ (fragment of pMel from B16F10 melanoma cells) respectively

(Gerner et al., 2008; Haabeth et al., 2018). Results showed that treating TAMs with E64-DNA did not improve MHCII-restricted antigen presentation derived from OVA or irradiated B16 cells (irrB16), nor did it made any differences when TAMs were exposed to peptides ($OVA_{323-339}$ or $TRP1_{113-126}$) that directly bind cell surface MHCII molecules (**Figure 4.2**). These results suggested that E64-DNA did not affect antigen presentation via MHCII molecules by TAMs.

The observation that attenuation of lysosomal cysteine protease activity in TAMs only affects antigen cross-presentation but not MHCII-restricted presentation is not surprising. Because peptides presented on class I molecules are shorter and precise in length, while those on class II molecules are longer and variable in length (Roche and Furuta, 2015). This difference might affect the sensitivity of antigen loading. Admittedly, lysosomal activity in DCs is a critical factor in determining the balance between these two pathways in DC; increasing lysosomal proteolysis decreases the MHCI pathway but improves the MHCII pathway (Samie and Cresswell, 2015; Trombetta et al., 2003). However, macrophages have a much higher lysosomal degradative capacity and are efficient in presenting via MHCII molecules (in contrast to their poor efficiency in performing cross-presentation). Lowering their lysosomal cysteine protease activity by E64-DNA might not have much influence on MHCII-restricted II presentation. In addition, E64-DNA serves as a lysosomal attenuator instead of a killer -- genetically knocking out specific lysosomal protease genes (*Ctsb*-/-, *Ctsl*-/-, *Ctss*-/-) in mice. Therefore, the attenuated lysosomal cysteine protease activity could still be sufficient to generate peptides that fit in the MHCII groove and to degrade the invariant chain for peptide loading.

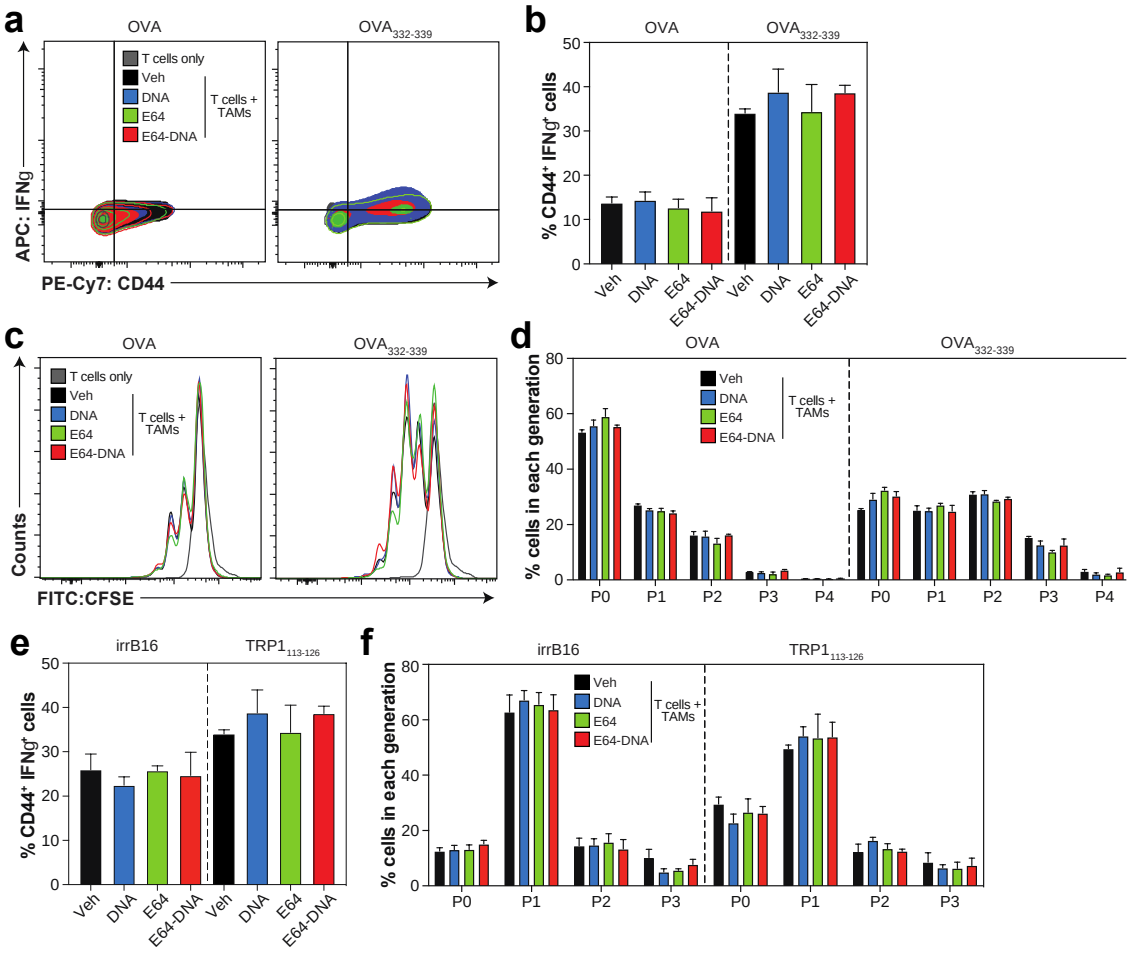

Figure 4.2. E64-DNA does not improve MHCII-restricted antigen presentation by TAMs. TAMs isolated from E0771 tumors were treated with vehicle (Veh), DNA, E64, or E64-DNA (100nM) for 2h. **a-d**, OT-2 $CD8^+$ T-cell activation (a-b) and proliferation (c-d) after 72h of co-culture with TAMs pre-stimulated with OVA protein or $OVA_{323-339}$ peptide. **e-f**, Trp1-$CD8^+$ T-cell activation (e) and proliferation (f) after 72h of co-culture with TAMs pre-stimulated with $Trp1_{113-126}$ or irradiated B16 cells. n=3/group. *, $p<0.05$ Student's *t*-test.

Optimal lysosomal processing during antigen-cross presentation.

The goal of our study described in Chapter 2 is to understand the mechanisms that limit antigen cross-presentation by TAMs and leverage it for therapeutic interventions. The intent was not to compare the cross-presentation capability of TAMs with that of DCs. DCs were used simply used as a reference for illustrating the importance of this study, i.e., considering that the % of total DC population in tumors is less than 3% (the cDC1 that has been reported to have

antigen cross-presentation would be even smaller) and TAMs are so abundant, harnessing TAMs capability for cross-present would be advantageous. Yet, because DCs are the most potent antigen cross-presenting cells (Embgenbroich and Burgdorf, 2018; Wculek et al., 2020), it is tempting to compare DC's lysosomal cysteine protease level and activity with TAMs and to examine how E64-DNA could affect antigen cross-presentation capability in DCs.

Proteomics data showed that lysosomal cysteine protease levels in DCs (bone marrow-derived DCs/BMDCs) are comparable to those in M1 and lower than M2 BMDMs (**Figure 4.3a**). Lysosomal protease levels are also reflected in their lysosomal degradative capability by DQ-OVA degradation assay (**Figure 4.3b**). Interestingly, E64-DNA inhibited rather than improved DC's cross-presentation capability (**Figures 4.3c-d**). Moreover, E64-DNA also inhibited MHCII-restricted presentation in DCs (data not shown).

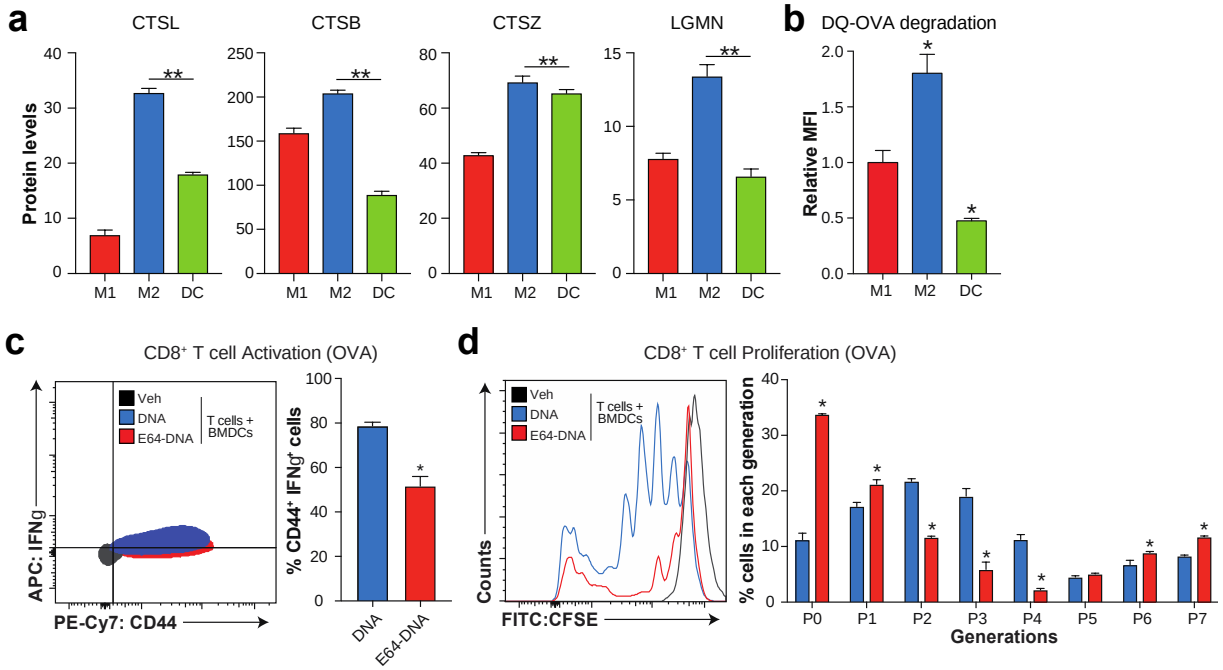

Figure 4.3. Characterizing the lysosomal cysteine protease level and activity in DCs and the effect of E64-DNA on their antigen cross-presentation capability. a, Spectral counts based on proteomics data. **b**, DQ-OVA degradation. **c-d**, OT-1-CD8$^+$ T cell activation (c) and proliferation (d) after co-culture with E64-DNA treated BMDCs. n=3/group. *, $p<0.05$ Student's t-test. **, FDR<5% G-test and t-test. LC/MS is performed by Dr. Tomas Vaisar (University of Washington). Proteomic data (b) is analyzed by me, with the help of Dr. Lev Becker.

Upon reasonable deduction, a model with MHCI-mediated cross-presentation and MHCII-restricted presentation with E64-DNA treatment is proposed to explain the above results (**Figure 4.4**). In this model, the optimal window for MHCI-mediated antigen cross-presentation is narrow. Thus, attenuating DCs' lysosomal cysteine protease activity, which is already around the optimal range, may be harmful to their cross-presentation capability. In contrast, the high lysosomal cysteine protease activity in TAMs diminished their cross-presentation capability; attenuating it improves their ability to cross-present. The optimal level for MHCII-restricted antigen presentation is much broader, and thus E64-DNA did not affect TAMs presentation capability despite attenuating lysosomal cysteine protease activity. In contrast, due to the lower level of lysosomal cysteine protease activity, DCs cannot afford to attenuate lysosomal cysteine protease activity while maintaining their presentation capability via MHCII.

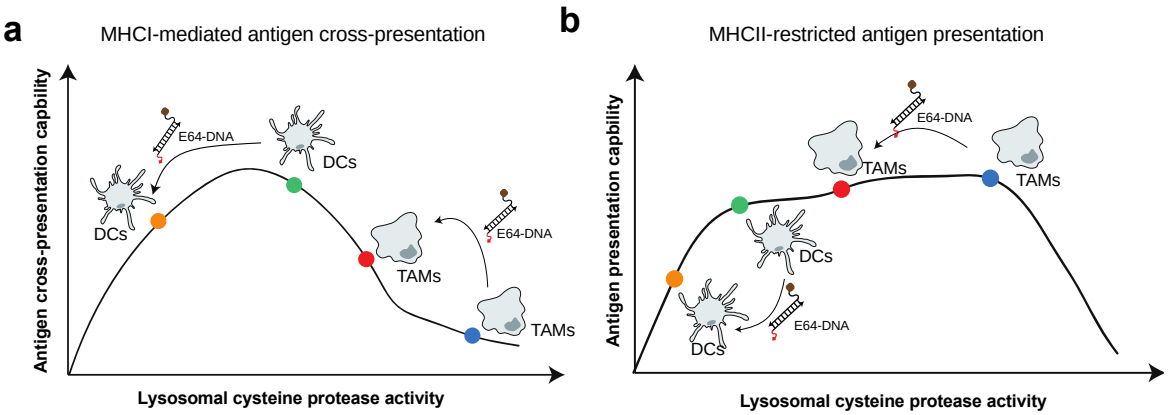

Figure 4.4. The proposed model of the relationship between lysosomal cysteine protease activity and antigen presentation capability with E64-DNA treatment. a, MHCI-mediated antigen cross-presentation. **b**, MHCII-restricted antigen presentation.

Future Directions

The role of proteasome-mediated antigen cross-presentation in TAMs.

The presentation of internalized extracellular antigens on MHCI molecules is a process termed antigen cross-presentation, critical in stimulating cytotoxic $CD8^+$ T cells response against

tumors (Fehres et al., 2014; Kurts et al., 2010; Sigal et al., 1999). In general, there are two main pathways of antigen cross-presentation: the vacuolar pathways and the endosome-to-cytosol pathways (Embgenbroich and Burgdorf, 2018). In vacuolar pathways, antigens are degraded/processed by lysosomal proteases and directly loaded on MHCI within the lysosomal compartment. The most studied player in this pathway is the involvement of cathepsin S for MHCI loading in DC (Shen et al., 2004). The other pathways involve transporting the internalized antigens from the endosomal compartment to the cytosol, where the proteasome degrades them for subsequently transported by TAP (transporter associated with antigen processing) for MHCI loading (Embgenbroich and Burgdorf, 2018). Our work only explored the vacuolar presentation pathway, and how much the cytosolic pathways contributed to antigen cross-presentation in TAMs remains unclear.

To explored this, I treated TAMs isolated from E0771 tumors with epoxomicin (EPM), a selective proteasome inhibitor, followed by addition of OVA or $OVA_{257-264}$. Flow cytometry was used to examine the $OVA_{257-264}$ on the cell surface. EPM didn't affect the ability of TAMs to display ready-to-present $OVA_{257-264}$, nor did it affect TAM's ability to process and present OVA proteins (**Figure 4.5**). This result suggests that TAMs mostly rely on the vacuolar pathways instead of endosome-to-cytosol pathways to present OVA proteins. Yet, previous studies using BMDC showed that the antigen type could also affect the pathways cells use for cross-presentation (Shen et al., 2004). Thus, how these two pathways in TAMs are dynamically "communicating" when encountering different types of antigens would be interesting to explore. Future studies also plan to examine whether TAMs at different activation states may prefer one pathway over the other.

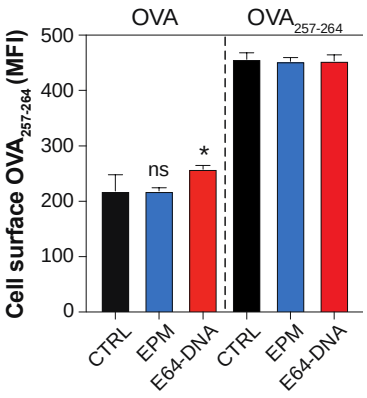

Figure 4.5. Inhibition of proteasome function does not affect OVA antigen presentation by TAMs. TAMs isolated from E0771 tumors were pre-treated with 100nM epoxomicin for 3h before addition of OVA or $OVA_{257-264}$. Cell surface MHCI bound $OVA_{257-264}$ was measured by flow cytometry. n=3/group. *, $p<0.05$ Student's *t*-test.

CD8+ T cell activation by E64-DNA treated TAMs: *in situ* vs. tumor-draining lymphoid nodes; naïve activation vs. restimulating activation.

A critical step for successfully activating $CD8^+$ T cells is cross-priming, which could either occur at the tumor sites or in tumor training lymphoid nodes (TdLN). Almost all studies on this subject stem from work done with DCs, the most efficient antigen cross-presentation cells. They found that DCs can both directly prime T cells at tumor sites (Broz et al., 2014) and traffic to tumor TdLN to activate T cells (Roberts et al., 2016). In contrast, evidence on how TAMs activate T cells in tumors remains unclear, despite some experimental results suggesting that TAMs do not migrate to TdLN, and that $CD169^+$ macrophages in TdLN phagocytose dead tumor cells and are transported via lymphatic flow and subsequently cross-present tumor antigens to $CD8^+$ T cells (Asano et al., 2011; Roberts et al., 2016). The little attention to exploring TAM-T-cell priming is partially due to the poor ability of TAMs to cross-present and the lack of an efficient method to stimulate them to activate T cells. However, considering their abundance and plasticity in tumors, the route for TAM-T-cells priming is an interesting and important question

to answer from both biological and therapeutic perspectives. The E64-DNA developed here might serve as a useful tool to explore this aspect.

I thought to first examine if E64-DNA treated TAMs have the ability to migrate to tumor TdLN. I isolate TAMs from CD45.1 mice, treated them with E64-DNA *ex vivo*, and injected them into tumors in CD45.2 mice (**Figure 4.6a**). My preliminary data showed that on 3 days post-injection, E64-DNA treated CD45.1 TAMs, but not DNA treated CD45.1 TAMs, were observed in TdLN, suggesting that following E64-DNA treatment TAMs gained the ability to migrate to TdLN (**Figure 4.6b**). Admittedly, this is an artificial system and may not represent the *in vivo* natural scarious. Indeed, TdLN of E64-DNA treated E0771 tumor-bearing mice did not show a significant increase in the macrophage populations on Day 3, arguing against the possibility that TAMs migrate to TdLN to activate $CD8^+$ T cells (**Figure 4.6c**). Yet, two possibilities could result in this negative observation. One is the timing of the measurement. I should include additional time points considering Day 3 may be too late or early for lymph node TAM migration. Second, I should increase the number of mice in each group since the % increase could be small and require higher n in each group to reach statistic power.

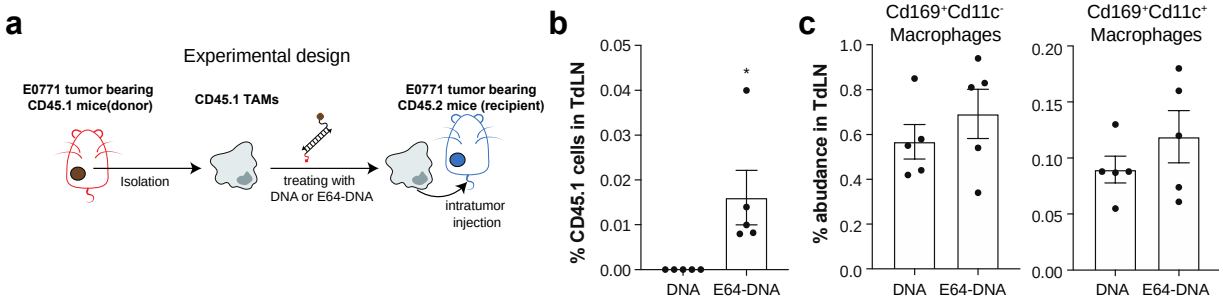

Figure 4.6 The ability of E64-DNA treated TAMs migrating to TdLN. a, Experimental design for b. **b**, Quantification by flow cytometry of % of CD45.1 population in TdLN 3 days post intratumor injection of DNA or E64-DNA treated TAM. n=5/group. **c**, Quantification by flow cytometry of the two different macrophage populations in TdLN 3 days post DNA or E64-DNA (25μg, i.t) treatment in E0771 tumor-bearing mice. n=5/group. *, $p<0.05$ Student's *t*-test.

Hence, in my future study, I plan to create a tumor in Kaede transgenic mice that express a photoconvertible fluorescence protein (Tomura et al., 2008) to explore this point further. In brief, when tumors reach 50-100 mm^3, they will be exposed to ultraviolet light to induce photoconversion to only labeled cells in tumors in red. I will then analyze TAMs in the tumor and TdLN at 7h, day 1, day, day3, and day 5 post E64-DNA administration. If we do not observe any photoconverted TAMs in the TdLN, it would be unlikely that TAMs traffic out of tumors to activate T cells.

Another remaining question is whether TAMs prime naïve T cells or restimulate activated T cells in tumors. My study used naïve T cells for *in vitro* or *ex vivo* antigen cross-presentation assay as a surrogate to measure TAMs' cross-presentation ability. My intention was not to decipher whether TAMs activate resident $CD8^+$ T cells in tumors. To test if E64-DNA treated TAMs could restimulate activated T cells in tumors, I will adopt the method used in a previous study (Broz et al., 2014) to coculture TAMs from E64-DNA treated B16.OVA tumors with activated $CD8^+$ T cells from OT-1 mice. Splenocytes will be stimulated with $OVA_{257-264}$ for 30 mins and expanded up to 4 days after stimulation, followed by purification of $CD8^+$ T cells.

LDHA inhibitor attenuates the M2 phenotype in TAMs.

Having demonstrated the importance of the hypoxia-induced lactate-Kla-M2 pathway in tumorigenesis in high hypoxia tumors, I sought to explore the therapeutic potential of LDHA inhibitors. Treating macrophages with the LDHA-specific inhibitor GNE attenuated the expression of many M2-like genes in BMDMs and TAMs, which were previously shown to be upregulated upon Kla induction (**Figure 4.7**).

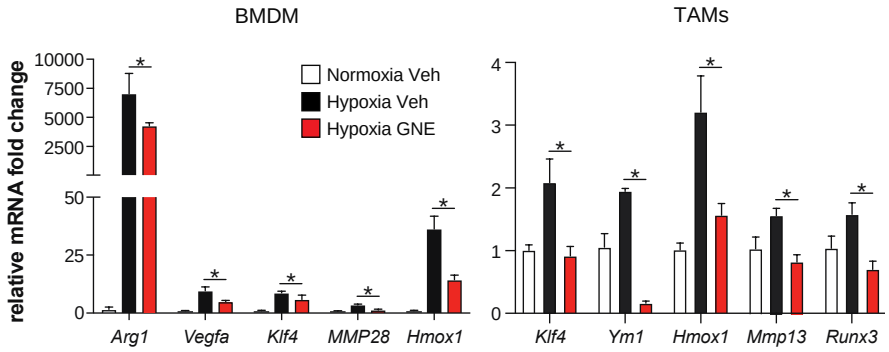

Figure 4.7 GNE attenuated M2-associated genes in macrophages. BMDMs or TAMs isolated from E0771 tumors cultured in normoxic or hypoxic condition with or without 5uM of GNE for 24hr. RNA was collected for gene assessment. mRNA levels of BMDM were measured by Anna Tang.

This result provides preliminary confidence that GNE could be used to lower lactate production by TAMs *in vivo*. For *in vivo* delivery, I will try intratumorally delivery first and then systemic delivery (intravenously or intraperitoneally). Because GNE is a small molecule and unlikely to be preferentially taken up by TAMs, I plan to conjugate it with our DNA nanodevice to achieve TAMs specific delivery. This conjugation will also allow us to distinguish the efficacy of lowering lactate levels in TAMs from cancer cells.

Leveraging DNA nanodevice as TAM/macrophage targeting platform (e.g., E64-GNE-DNA).

Another substantial merit of our studies is to provide a strategy that selectively targets provide strategy to selectively target TAMs. Admittedly, several carrier technologies have been developed for preferentially targeting macrophages. These include nanoparticles such as liposomes and microspheres and antibody-drug conjugates (ADCs). Nanoparticles can target macrophages passively via their high phagocytic potential or actively by decorating them with mannose (binds CD206 on macrophages) or galactose-type lectin I (binds asialoglycoprotein

receptor on macrophages) (Howard et al., 2016; Napoletano et al., 2012). However, nanoparticle-based systems interact with other innate immune cells beyond macrophages and thus have poor selectivity. ADCs using anti-CD206 (binds CD206 on macrophages) or Fc (binds Fcγ receptor on macrophages) have also been employed. While these approaches have improved selectivity, problems associated with the low efficiency of drug internalization have been reported. Moreover, these approaches are challenged by difficulties in obtaining defined conjugation ratios and in delivering multiple drugs in combination. Therefore, there is a need for new systems to selectively deliver drugs to macrophages within the body.

I have adopted a DNA-based nanodevice that has been shown to preferentially target macrophages *in vivo* (data for targeting adipose tissue macrophages by intraperitoneal injection and lung macrophages by intratracheal injection are not shown). The DNA-based nanodevice can comprise two or three modules: *i)* a macrophage targeting module (e.g., polyanionic DNA), which enables preferential uptake of the nanodevice by macrophages, *ii)* a therapeutic module (comprising one or more drugs, also referred to as a therapeutic load module) which enables targeting of the specific pathway(s) in macrophages, and (optionally) *iii)* a labeling module (e.g., a molecule that allows the measurement and/or quantification of nanodevice uptakes, such as a fluorophore or other detectable molecule (**Figure 4.8a**). This labeling module can also be substituted with another therapeutic target, resulting in a double target upon delivery.

Because attenuating lysosomal cysteine activity improves antigen cross-presentation ability by TAMs and lowering lactate production by TAMs attenuates their M2-phenotypes, I propose to leverage the DNA-based nanodevice by combining benefits. I plan to create an E64-GNE-DNA nanodevice (**Figure 4.8b**) where one strand of DNA conjugates with E64 and the other GNE. The DNA backbone is degraded in the lysosome, thereby liberating both molecules.

E64 will take action in the lysosome, and GNE, which is a membrane-soluble drug, will release from lysosome and inactivate LDH in the cytosol.

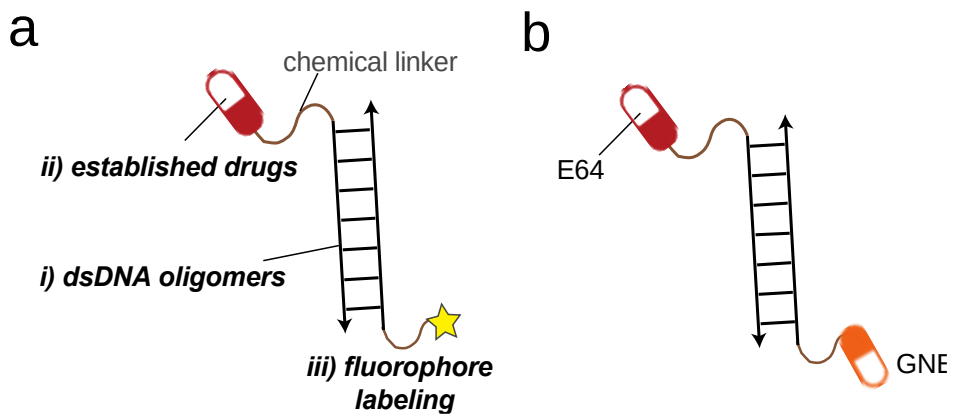

Figure 4.8 Illustration of DNA-based nanodevice. a, illustrations of the potential three modules of the DNA-based nanodevice. **b,** the configuration of the E64-GNE-DNA.

E64-GNE-DNA just one example of how to leverage this DNA-based nanotechnology platform. Considering the specificity, modularity, and trackability of this DNA-based nanodevice, many additional targets could be applied to *i*) target macrophages preferentially in multiple tissues, *ii*) allow for delivery of drugs that target lysosomal and cytosolic proteins, and *iii*) enables manipulation of macrophage functions.

There are eight categories I could examine as DNA-based platform targets since they have been identified to affect macrophage phenotypes. The *first* one is nuclear receptors. There are 48 nuclear receptors in the human genome, of which 28 has been shown to associated with macrophage and their phenotypes (Leopold Wager et al., 2019). The *second* aspect is the metabolic target (Penny et al., 2016, Geeraerts et al., 2017; Wenes et al., 2016). The *third* is epigenetic targets. Most work has been done to understand the epigenetic regulation of macrophages in the setting of infection and chronic diseases, yet not much on TAMs (de Groot

and Pienta, 2018). The *Fourth* category is TLR and stimulator of interferon genes (STING) pathways. Current practice mostly applies intratumoral injection of STING or/and TLR9 agonist combined with radiotherapy or chemotherapy or immune checkpoint inhibitors to create both local and systemic antitumor immunity. Although both pathways use IRF3 and NFκB to predominately control proinflammatory gene induction, STING and TLR9 pathways have evolved to sense different types of DNA species (Barber, 2015). The *fifth* target is the redox signaling pathway. Macrophages are the dominant producers of reactive oxygen species, such as nitric oxide and hydrogen peroxide. Those molecules are not only prone to oxidatively modify proteins or lipids, but also exhibit signaling properties that regulate macrophage polarization (Weigert et al., 2018). There are multiple redox targets, including transcription factors (e.g., Nrf2, PPARγ) that can transform redox signals. The *sixth* target is kinase signaling. This category includes the well-recognized PI3K/Akt pathway, which regulates macrophage survival, migration, and proliferation, and also their response to different metabolic and inflammatory signals (Vergadi et al., 2017). Importantly, AKT1 and AKT2 seem to have the opposite effect (Murray, 2017). I also include BTK and SRC, which have traditionally been targeted to cancer cells, but recent evidence has pointed out their role in macrophage phenotypes. The *last* category refers to reprogramming molecules, such as anti-CSF1R, CD40, CD47-SIRPa axis, since it includes many clinical testing drugs (Gholamin et al., 2017; Li et al., 2018a; Liu et al., 2015, 2017, Coussens et al., 2013; Palucka and Coussens, 2016; Vitale et al., 2019, Beatty et al., 2011; Hoves et al., 2018; Perry et al., 2018; Vonderheide, 2018).

REFERENCES

Adams, S. (2009). Toll-like receptor agonists in cancer therapy. Immunotherapy *1*, 949–964.

Adams, S., Kozhaya, L., Martiniuk, F., Meng, T.-C., Chiriboga, L., Liebes, L., Hochman, T., Shuman, N., Axelrod, D., Speyer, J., et al. (2012). Topical TLR7 agonist imiquimod can induce immune-mediated rejection of skin metastases in patients with breast cancer. Clin. Cancer Res. *18*, 6748–6757.

Afik, R., Zigmond, E., Vugman, M., Klepfish, M., Shimshoni, E., Pasmanik-Chor, M., Shenoy, A., Bassat, E., Halpern, Z., Geiger, T., et al. (2016). Tumor macrophages are pivotal constructors of tumor collagenous matrix. J. Exp. Med. *213*, 2315–2331.

Agrawal, S. (2008). Antitumor activity of IMO-2055, an agonist of TLR9, in combination with erlotinib and bevacizumab in non-small cell lung cancer xenografts in mice. Cancer Res. *68*, 2078–2078.

Ambrose, C.T. (2006). The Osler slide, a demonstration of phagocytosis from 1876 Reports of phagocytosis before Metchnikoff's 1880 paper. Cell Immunol. *240*, 1–4.

Anderson, S.E., Bautista, S., and Remington, J.S. (1976). Induction of resistance to Toxoplasma gondii in human macrophages by soluble lymphocyte products. J. Immunol. *117*, 381–387.

Arkan, M.C., Hevener, A.L., Greten, F.R., Maeda, S., Li, Z.-W., Long, J.M., Wynshaw-Boris, A., Poli, G., Olefsky, J., and Karin, M. (2005). IKK-beta links inflammation to obesity-induced insulin resistance. Nat. Med. *11*, 191–198.

Arwert, E.N., Harney, A.S., Entenberg, D., Wang, Y., Sahai, E., Pollard, J.W., and Condeelis, J.S. (2018). A Unidirectional Transition from Migratory to Perivascular Macrophage Is Required for Tumor Cell Intravasation. Cell Rep. *23*, 1239–1248.

Asano, K., Nabeyama, A., Miyake, Y., Qiu, C.-H., Kurita, A., Tomura, M., Kanagawa, O., Fujii, S., and Tanaka, M. (2011). CD169-positive macrophages dominate antitumor immunity by crosspresenting dead cell-associated antigens. Immunity *34*, 85–95.

Baer, C., Squadrito, M.L., Laoui, D., Thompson, D., Hansen, S.K., Kiialainen, A., Hoves, S., Ries, C.H., Ooi, C.-H., and De Palma, M. (2016). Suppression of microRNA activity amplifies IFN-γ-induced macrophage activation and promotes anti-tumour immunity. Nat. Cell Biol. *18*, 790–802.

Bain, C.C., and Mowat, A.M. (2014). Macrophages in intestinal homeostasis and inflammation. Immunol. Rev. *260*, 102–117.

Barber, G.N. (2015). STING: infection, inflammation and cancer. Nat. Rev. Immunol. *15*, 760–770.

Barclay, A.N., and Van den Berg, T.K. (2014). The interaction between signal regulatory protein

alpha (SIRPα) and CD47: structure, function, and therapeutic target. Annu. Rev. Immunol. *32*, 25–50.

Barrett, J.P., Henry, R.J., Villapol, S., Stoica, B.A., Kumar, A., Burns, M.P., Faden, A.I., and Loane, D.J. (2017). NOX2 deficiency alters macrophage phenotype through an IL-10/STAT3 dependent mechanism: implications for traumatic brain injury. J. Neuroinflammation *14*, 65.

Beatty, G.L., Chiorean, E.G., Fishman, M.P., Saboury, B., Teitelbaum, U.R., Sun, W., Huhn, R.D., Song, W., Li, D., Sharp, L.L., et al. (2011). CD40 agonists alter tumor stroma and show efficacy against pancreatic carcinoma in mice and humans. Science *331*, 1612–1616.

Becker, L., Gharib, S.A., Irwin, A.D., Wijsman, E., Vaisar, T., Oram, J.F., and Heinecke, J.W. (2010). A macrophage sterol-responsive network linked to atherogenesis. Cell Metab. *11*, 125–135.

Becker, L., Liu, N.-C., Averill, M.M., Yuan, W., Pamir, N., Peng, Y., Irwin, A.D., Fu, X., Bornfeldt, K.E., and Heinecke, J.W. (2012). Unique proteomic signatures distinguish macrophages and dendritic cells. PLoS One *7*, e33297.

Beckman, J.A., Creager, M.A., and Libby, P. (2002). Diabetes and atherosclerosis: epidemiology, pathophysiology, and management. JAMA *287*, 2570–2581.

Benjamin, D., Robay, D., Hindupur, S.K., Pohlmann, J., Colombi, M., El-Shemerly, M.Y., Maira, S.-M., Moroni, C., Lane, H.A., and Hall, M.N. (2018). Dual Inhibition of the Lactate Transporters MCT1 and MCT4 Is Synthetic Lethal with Metformin due to NAD+ Depletion in Cancer Cells. Cell Rep. *25*, 3047–3058.e4.

Bergers, G., and Benjamin, L.E. (2003). Tumorigenesis and the angiogenic switch. Nat. Rev. Cancer *3*, 401–410.

Bhattacharyya, S., Brown, D.E., Brewer, J.A., Vogt, S.K., and Muglia, L.J. (2007). Macrophage glucocorticoid receptors regulate Toll-like receptor 4-mediated inflammatory responses by selective inhibition of p38 MAP kinase. Blood *109*, 4313–4319.

Biswas, S.K., and Mantovani, A. (2010). Macrophage plasticity and interaction with lymphocyte subsets: cancer as a paradigm. Nat. Immunol. *11*, 889–896.

Borges, J.S., and Johnson, W.D. (1975). Inhibition of multiplication of Toxoplasma gondii by human monocytes exposed to T-lymphocyte products. J. Exp. Med. *141*, 483–496.

Broz, M.L., Binnewies, M., Boldajipour, B., Nelson, A.E., Pollack, J.L., Erle, D.J., Barczak, A., Rosenblum, M.D., Daud, A., Barber, D.L., et al. (2014). Dissecting the tumor myeloid compartment reveals rare activating antigen-presenting cells critical for T cell immunity. Cancer Cell *26*, 638–652.

Bubna, A.K. (2015). Imiquimod - Its role in the treatment of cutaneous malignancies. Indian J

Pharmacol *47*, 354–359.

Burdette, D.L., and Vance, R.E. (2013). STING and the innate immune response to nucleic acids in the cytosol. Nat. Immunol. *14*, 19–26.

Burnet, F.M. (1971). Immunological surveillance in neoplasia. Transplant. Rev. *7*, 3–25.

Byeon, S.E., Yi, Y.-S., Oh, J., Yoo, B.C., Hong, S., and Cho, J.Y. (2012). The role of Src kinase in macrophage-mediated inflammatory responses. Mediators Inflamm. *2012*, 512926.

Cannarile, M.A., Weisser, M., Jacob, W., Jegg, A.-M., Ries, C.H., and Rüttinger, D. (2017). Colony-stimulating factor 1 receptor (CSF1R) inhibitors in cancer therapy. J. Immunother. Cancer *5*, 53.

Canton, J., Neculai, D., and Grinstein, S. (2013). Scavenger receptors in homeostasis and immunity. Nat. Rev. Immunol. *13*, 621–634.

Carrel, A., and Ebeling, A.H. (1922). Pure cultures of large mononuclear leucocytes. J. Exp. Med. *36*, 365–377.

Cassetta, L., and Pollard, J.W. (2018). Targeting macrophages: therapeutic approaches in cancer. Nat. Rev. Drug Discov. *17*, 887–904.

Cassetta, L., Fragkogianni, S., Sims, A.H., Swierczak, A., Forrester, L.M., Zhang, H., Soong, D.Y.H., Cotechini, T., Anur, P., Lin, E.Y., et al. (2019). Human Tumor-Associated Macrophage and Monocyte Transcriptional Landscapes Reveal Cancer-Specific Reprogramming, Biomarkers, and Therapeutic Targets. Cancer Cell *35*, 588–602.e10.

Cavaillon, J.-M. (2011). The historical milestones in the understanding of leukocyte biology initiated by Elie Metchnikoff. J. Leukoc. Biol. *90*, 413–424.

Certo, M., Tsai, C.-H., Pucino, V., Ho, P.-C., and Mauro, C. (2020). Lactate modulation of immune responses in inflammatory versus tumour microenvironments. Nat. Rev. Immunol.

Chakraborty, K., Veetil, A.T., Jaffrey, S.R., and Krishnan, Y. (2016). Nucleic Acid-Based Nanodevices in Biological Imaging. Annu. Rev. Biochem. *85*, 349–373.

Chakraborty, K., Leung, K., and Krishnan, Y. (2017). High lumenal chloride in the lysosome is critical for lysosome function. Elife *6*, e28862.

Chan, C.H., Fang, C., Yarilina, A., Prinjha, R.K., Qiao, Y., and Ivashkiv, L.B. (2015). BET bromodomain inhibition suppresses transcriptional responses to cytokine-Jak-STAT signaling in a gene-specific manner in human monocytes. Eur. J. Immunol. *45*, 287–297.

Chawla, A., Nguyen, K.D., and Goh, Y.P.S. (2011). Macrophage-mediated inflammation in metabolic disease. Nat. Rev. Immunol. *11*, 738–749.

Chen, Z., Feng, X., Herting, C.J., Garcia, V.A., Nie, K., Pong, W.W., Rasmussen, R., Dwivedi, B., Seby, S., Wolf, S.A., et al. (2017). Cellular and Molecular Identity of Tumor-Associated Macrophages in Glioblastoma. Cancer Res. *77*, 2266–2278.

Cheng, H.S., Lee, J.X.T., Wahli, W., and Tan, N.S. (2019). Exploiting vulnerabilities of cancer by targeting nuclear receptors of stromal cells in tumor microenvironment. Mol. Cancer *18*, 51.

Cho, Y., Lee, J.B., and Hong, J. (2014). Controlled release of an anti-cancer drug from DNA structured nano-films. Sci. Rep. *4*, 4078.

Clark, E.R., and Clark, E.L. (1930). Relation of monocytes of the blood to the tissue macrophages. Am. J. Anat. *46*, 149–185.

Clynes, R., Takechi, Y., Moroi, Y., Houghton, A., and Ravetch, J.V. (1998). Fc receptors are required in passive and active immunity to melanoma. Proc. Natl. Acad. Sci. USA *95*, 652–656.

Clynes, R.A., Towers, T.L., Presta, L.G., and Ravetch, J.V. (2000). Inhibitory Fc receptors modulate in vivo cytotoxicity against tumor targets. Nat. Med. *6*, 443–446.

Coats, B.R., Schoenfelt, K.Q., Barbosa-Lorenzi, V.C., Peris, E., Cui, C., Hoffman, A., Zhou, G., Fernandez, S., Zhai, L., Hall, B.A., et al. (2017). Metabolically Activated Adipose Tissue Macrophages Perform Detrimental and Beneficial Functions during Diet-Induced Obesity. Cell Rep. *20*, 3149–3161.

Colado, A., Genoula, M., Cougoule, C., Marín Franco, J.L., Almejún, M.B., Risnik, D., Kviatcovsky, D., Podaza, E., Elías, E.E., Fuentes, F., et al. (2018). Effect of the BTK inhibitor ibrutinib on macrophage- and γδ T cell-mediated response against Mycobacterium tuberculosis. Blood Cancer J. *8*, 100.

Colegio, O.R., Chu, N.-Q., Szabo, A.L., Chu, T., Rhebergen, A.M., Jairam, V., Cyrus, N., Brokowski, C.E., Eisenbarth, S.C., Phillips, G.M., et al. (2014). Functional polarization of tumour-associated macrophages by tumour-derived lactic acid. Nature *513*, 559–563.

Corbet, C., and Feron, O. (2017). Tumour acidosis: from the passenger to the driver's seat. Nat. Rev. Cancer *17*, 577–593.

Corrales, L., Glickman, L.H., McWhirter, S.M., Kanne, D.B., Sivick, K.E., Katibah, G.E., Woo, S.-R., Lemmens, E., Banda, T., Leong, J.J., et al. (2015). Direct activation of STING in the tumor microenvironment leads to potent and systemic tumor regression and immunity. Cell Rep. *11*, 1018–1030.

Cotechini, T., Medler, T.R., and Coussens, L.M. (2015). Myeloid cells as targets for therapy in solid tumors. Cancer J. *21*, 343–350.

Coussens, L.M., Zitvogel, L., and Palucka, A.K. (2013). Neutralizing tumor-promoting chronic inflammation: a magic bullet? Science *339*, 286–291.

Cruz-Leal, Y., Grubaugh, D., Nogueira, C.V., Lopetegui-González, I., Del Valle, A., Escalona, F., Laborde, R.J., Alvarez, C., Fernández, L.E., Starnbach, M.N., et al. (2018). The Vacuolar Pathway in Macrophages Plays a Major Role in Antigen Cross-Presentation Induced by the Pore-Forming Protein Sticholysin II Encapsulated Into Liposomes. Front. Immunol. *9*, 2473.

Cuddapah, S., Barski, A., Cui, K., Schones, D.E., Wang, Z., Wei, G., and Zhao, K. (2009). Native chromatin preparation and Illumina/Solexa library construction. Cold Spring Harb. Protoc. *2009*, pdb.prot5237.

Curiel, T.J., Coukos, G., Zou, L., Alvarez, X., Cheng, P., Mottram, P., Evdemon-Hogan, M., Conejo-Garcia, J.R., Zhang, L., Burow, M., et al. (2004). Specific recruitment of regulatory T cells in ovarian carcinoma fosters immune privilege and predicts reduced survival. Nat. Med. *10*, 942–949.

Cyrus, T., Witztum, J.L., Rader, D.J., Tangirala, R., Fazio, S., Linton, M.F., and Funk, C.D. (1999). Disruption of the 12/15-lipoxygenase gene diminishes atherosclerosis in apo E-deficient mice. J. Clin. Invest. *103*, 1597–1604.

Dan, K., Veetil, A.T., Chakraborty, K., and Krishnan, Y. (2019). DNA nanodevices map enzymatic activity in organelles. Nat. Nanotechnol. *14*, 252–259.

Dannenmann, S.R., Thielicke, J., Stöckli, M., Matter, C., von Boehmer, L., Cecconi, V., Hermanns, T., Hefermehl, L., Schraml, P., Moch, H., et al. (2013). Tumor-associated macrophages subvert T-cell function and correlate with reduced survival in clear cell renal cell carcinoma. Oncoimmunology *2*, e23562.

Daubiné, F., Le Gall, C., Gasser, J., Green, J., and Clézardin, P. (2007). Antitumor effects of clinical dosing regimens of bisphosphonates in experimental breast cancer bone metastasis. J. Natl. Cancer Inst. *99*, 322–330.

Daugherty, A., Tall, A.R., Daemen, M.J.A.P., Falk, E., Fisher, E.A., García-Cardeña, G., Lusis, A.J., Owens, A.P., Rosenfeld, M.E., Virmani, R., et al. (2017). Recommendation on design, execution, and reporting of animal atherosclerosis studies: A scientific statement from the american heart association. Arterioscler. Thromb. Vasc. Biol. *37*, e131–e157.

Delamarre, L., Pack, M., Chang, H., Mellman, I., and Trombetta, E.S. (2005). Differential lysosomal proteolysis in antigen-presenting cells determines antigen fate. Science *307*, 1630–1634.

DeNardo, D.G., and Ruffell, B. (2019). Macrophages as regulators of tumour immunity and immunotherapy. Nat. Rev. Immunol. *19*, 369–382.

Dengler, V.L., Galbraith, M.D., and Espinosa, J.M. (2014). Transcriptional regulation by

hypoxia inducible factors. Crit Rev Biochem Mol Biol *49*, 1–15.

Diment, S. (1990). Different roles for thiol and aspartyl proteases in antigen presentation of ovalbumin. J. Immunol. *145*, 417–422.

Divakaruni, A.S., Hsieh, W.Y., Minarrieta, L., Duong, T.N., Kim, K.K.O., Desousa, B.R., Andreyev, A.Y., Bowman, C.E., Caradonna, K., Dranka, B.P., et al. (2018). Etomoxir inhibits macrophage polarization by disrupting coa homeostasis. Cell Metab. *28*, 490–503.e7.

Doyle, A.G., Herbein, G., Montaner, L.J., Minty, A.J., Caput, D., Ferrara, P., and Gordon, S. (1994). Interleukin-13 alters the activation state of murine macrophages in vitro: comparison with interleukin-4 and interferon-gamma. Eur. J. Immunol. *24*, 1441–1445.

Dudek, A.Z., Yunis, C., Harrison, L.I., Kumar, S., Hawkinson, R., Cooley, S., Vasilakos, J.P., Gorski, K.S., and Miller, J.S. (2007). First in human phase I trial of 852A, a novel systemic toll-like receptor 7 agonist, to activate innate immune responses in patients with advanced cancer. Clin. Cancer Res. *13*, 7119–7125.

Dunn, G.P., Old, L.J., and Schreiber, R.D. (2004a). The three Es of cancer immunoediting. Annu. Rev. Immunol. *22*, 329–360.

Dunn, G.P., Old, L.J., and Schreiber, R.D. (2004b). The immunobiology of cancer immunosurveillance and immunoediting. Immunity *21*, 137–148.

Duong, L., Radley-Crabb, H.G., Gardner, J.K., Tomay, F., Dye, D.E., Grounds, M.D., Pixley, F.J., Nelson, D.J., and Jackaman, C. (2018). Macrophage Depletion in Elderly Mice Improves Response to Tumor Immunotherapy, Increases Anti-tumor T Cell Activity and Reduces Treatment-Induced Cachexia. Front. Genet. *9*, 526.

Eales, K.L., Hollinshead, K.E.R., and Tennant, D.A. (2016). Hypoxia and metabolic adaptation of cancer cells. Oncogenesis *5*, e190.

Ebert, R.H., and Florey, H.W. (1939). The Extravascular Development of the Monocyte Observed In vivo. British Journal of Experimental Pathology.

Edris, B., Weiskopf, K., Volkmer, A.K., Volkmer, J.-P., Willingham, S.B., Contreras-Trujillo, H., Liu, J., Majeti, R., West, R.B., Fletcher, J.A., et al. (2012). Antibody therapy targeting the CD47 protein is effective in a model of aggressive metastatic leiomyosarcoma. Proc. Natl. Acad. Sci. USA *109*, 6656–6661.

Ehrlich, P. (1909). Über den jetzigen Stand der Chemotherapie. Ber. Dtsch. Chem. Ges. *42*, 17–47.

Embgenbroich, M., and Burgdorf, S. (2018). Current Concepts of Antigen Cross-Presentation. Front. Immunol. *9*, 1643.

Eng, J.K., Hoopmann, M.R., Jahan, T.A., Egertson, J.D., Noble, W.S., and MacCoss, M.J. (2015). A deeper look into Comet--implementation and features. J Am Soc Mass Spectrom *26*, 1865–1874.

Epelman, S., Lavine, K.J., and Randolph, G.J. (2014). Origin and functions of tissue macrophages. Immunity *41*, 21–35.

Evans, R., and Alexander, P. (1970). Cooperation of immune lymphoid cells with macrophages in tumour immunity. Nature *228*, 620–622.

Faubert, B., Solmonson, A., and DeBerardinis, R.J. (2020). Metabolic reprogramming and cancer progression. Science *368*.

Fehres, C.M., Unger, W.W.J., Garcia-Vallejo, J.J., and van Kooyk, Y. (2014). Understanding the biology of antigen cross-presentation for the design of vaccines against cancer. Front. Immunol. *5*, 149.

Feng, Y., Xiong, Y., Qiao, T., Li, X., Jia, L., and Han, Y. (2018). Lactate dehydrogenase A: A key player in carcinogenesis and potential target in cancer therapy. Cancer Med *7*, 6124–6136.

Fowles, R.E., Fajardo, I.M., Leibowitch, J.L., and David, J.R. (1973). The enhancement of macrophage bacteriostasis by products of activated lymphocytes. J. Exp. Med. *138*, 952–964.

Gajewski, T.F., Schreiber, H., and Fu, Y.-X. (2013). Innate and adaptive immune cells in the tumor microenvironment. Nat. Immunol. *14*, 1014–1022.

Gautier, E.L., Shay, T., Miller, J., Greter, M., Jakubzick, C., Ivanov, S., Helft, J., Chow, A., Elpek, K.G., Gordonov, S., et al. (2012). Gene-expression profiles and transcriptional regulatory pathways that underlie the identity and diversity of mouse tissue macrophages. Nat. Immunol. *13*, 1118–1128.

Geeraerts, X., Bolli, E., Fendt, S.-M., and Van Ginderachter, J.A. (2017). Macrophage metabolism as therapeutic target for cancer, atherosclerosis, and obesity. Front. Immunol. *8*, 289.

Geissmann, F., Gordon, S., Hume, D.A., Mowat, A.M., and Randolph, G.J. (2010). Unravelling mononuclear phagocyte heterogeneity. Nat. Rev. Immunol. *10*, 453–460.

Gentles, A.J., Newman, A.M., Liu, C.L., Bratman, S.V., Feng, W., Kim, D., Nair, V.S., Xu, Y., Khuong, A., Hoang, C.D., et al. (2015). The prognostic landscape of genes and infiltrating immune cells across human cancers. Nat. Med. *21*, 938–945.

Georgoudaki, A.-M., Prokopec, K.E., Boura, V.F., Hellqvist, E., Sohn, S., Östling, J., Dahan, R., Harris, R.A., Rantalainen, M., Klevebring, D., et al. (2016). Reprogramming Tumor-Associated Macrophages by Antibody Targeting Inhibits Cancer Progression and Metastasis. Cell Rep. *15*, 2000–2011.

Germano, G., Frapolli, R., Belgiovine, C., Anselmo, A., Pesce, S., Liguori, M., Erba, E., Uboldi, S., Zucchetti, M., Pasqualini, F., et al. (2013). Role of macrophage targeting in the antitumor activity of trabectedin. Cancer Cell *23*, 249–262.

Gerner, M.Y., Casey, K.A., and Mescher, M.F. (2008). Defective MHC class II presentation by dendritic cells limits CD4 T cell help for antitumor CD8 T cell responses. J. Immunol. *181*, 155–164.

Gholamin, S., Mitra, S.S., Feroze, A.H., Liu, J., Kahn, S.A., Zhang, M., Esparza, R., Richard, C., Ramaswamy, V., Remke, M., et al. (2017). Disrupting the CD47-SIRPα anti-phagocytic axis by a humanized anti-CD47 antibody is an efficacious treatment for malignant pediatric brain tumors. Sci. Transl. Med. *9*.

Ginhoux, F., Greter, M., Leboeuf, M., Nandi, S., See, P., Gokhan, S., Mehler, M.F., Conway, S.J., Ng, L.G., Stanley, E.R., et al. (2010). Fate mapping analysis reveals that adult microglia derive from primitive macrophages. Science *330*, 841–845.

Gocheva, V., Wang, H.-W., Gadea, B.B., Shree, T., Hunter, K.E., Garfall, A.L., Berman, T., and Joyce, J.A. (2010). IL-4 induces cathepsin protease activity in tumor-associated macrophages to promote cancer growth and invasion. Genes Dev. *24*, 241–255.

Gopinathan, A., Denicola, G.M., Frese, K.K., Cook, N., Karreth, F.A., Mayerle, J., Lerch, M.M., Reinheckel, T., and Tuveson, D.A. (2012). Cathepsin B promotes the progression of pancreatic ductal adenocarcinoma in mice. Gut *61*, 877–884.

Gore, M.O., McGuire, D.K., Lingvay, I., and Rosenstock, J. (2015). Predicting cardiovascular risk in type 2 diabetes: the heterogeneity challenges. Curr. Cardiol. Rep. *17*, 607.

Green, J.E., Shibata, M.A., Yoshidome, K., Liu, M.L., Jorcyk, C., Anver, M.R., Wigginton, J., Wiltrout, R., Shibata, E., Kaczmarczyk, S., et al. (2000). The C3(1)/SV40 T-antigen transgenic mouse model of mammary cancer: ductal epithelial cell targeting with multistage progression to carcinoma. Oncogene *19*, 1020–1027.

Greten, F.R., and Grivennikov, S.I. (2019). Inflammation and cancer: triggers, mechanisms, and consequences. Immunity *51*, 27–41.

de Groot, A.E., and Pienta, K.J. (2018). Epigenetic control of macrophage polarization: implications for targeting tumor-associated macrophages. Oncotarget *9*, 20908–20927.

Grossman, J.G., Nywening, T.M., Belt, B.A., Panni, R.Z., Krasnick, B.A., DeNardo, D.G., Hawkins, W.G., Goedegebuure, S.P., Linehan, D.C., and Fields, R.C. (2018). Recruitment of CCR2+ tumor associated macrophage to sites of liver metastasis confers a poor prognosis in human colorectal cancer. Oncoimmunology *7*, e1470729.

Guerriero, J.L., Sotayo, A., Ponichtera, H.E., Castrillon, J.A., Pourzia, A.L., Schad, S., Johnson, S.F., Carrasco, R.D., Lazo, S., Bronson, R.T., et al. (2017). Class IIa HDAC inhibition reduces

breast tumours and metastases through anti-tumour macrophages. Nature *543*, 428–432.

Guerrini, V., and Gennaro, M.L. (2019). Foam cells: one size doesn't fit all. Trends Immunol. *40*, 1163–1179.

Gül, N., Babes, L., Siegmund, K., Korthouwer, R., Bögels, M., Braster, R., Vidarsson, G., Hagen, T.L.M. ten, Kubes, P., and van Egmond, M. (2014). Macrophages eliminate circulating tumor cells after monoclonal antibody therapy. J. Clin. Invest.

Haabeth, O.A.W., Fauskanger, M., Manzke, M., Lundin, K.U., Corthay, A., Bogen, B., and Tveita, A.A. (2018). CD4+ T-cell-Mediated Rejection of MHC Class II-Positive Tumor Cells Is Dependent on Antigen Secretion and Indirect Presentation on Host APCs. Cancer Res. *78*, 4573–4585.

Haffner, S.M., Lehto, S., Rönnemaa, T., Pyörälä, K., and Laakso, M. (1998). Mortality from coronary heart disease in subjects with type 2 diabetes and in nondiabetic subjects with and without prior myocardial infarction. N. Engl. J. Med. *339*, 229–234.

Han, M.S., Jung, D.Y., Morel, C., Lakhani, S.A., Kim, J.K., Flavell, R.A., and Davis, R.J. (2013). JNK expression by macrophages promotes obesity-induced insulin resistance and inflammation. Science *339*, 218–222.

Hanahan, D., and Weinberg, R.A. (2011). Hallmarks of cancer: the next generation. Cell *144*, 646–674.

Hardbower, D.M., Asim, M., Luis, P.B., Singh, K., Barry, D.P., Yang, C., Steeves, M.A., Cleveland, J.L., Schneider, C., Piazuelo, M.B., et al. (2017). Ornithine decarboxylase regulates M1 macrophage activation and mucosal inflammation via histone modifications. Proc. Natl. Acad. Sci. USA *114*, E751–E760.

Hartvigsen, K., Binder, C.J., Hansen, L.F., Rafia, A., Juliano, J., Hörkkö, S., Steinberg, D., Palinski, W., Witztum, J.L., and Li, A.C. (2007). A diet-induced hypercholesterolemic murine model to study atherogenesis without obesity and metabolic syndrome. Arterioscler. Thromb. Vasc. Biol. *27*, 878–885.

Heinecke, N.L., Pratt, B.S., Vaisar, T., and Becker, L. (2010). PepC: proteomics software for identifying differentially expressed proteins based on spectral counting. Bioinformatics *26*, 1574–1575.

Henke, E., Nandigama, R., and Ergün, S. (2019). Extracellular matrix in the tumor microenvironment and its impact on cancer therapy. Front. Mol. Biosci. *6*, 160.

Henze, A.-T., and Mazzone, M. (2016). The impact of hypoxia on tumor-associated macrophages. J. Clin. Invest. *126*, 3672–3679.

Hiraoka, K., Zenmyo, M., Watari, K., Iguchi, H., Fotovati, A., Kimura, Y.N., Hosoi, F., Shoda,

T., Nagata, K., Osada, H., et al. (2008). Inhibition of bone and muscle metastases of lung cancer cells by a decrease in the number of monocytes/macrophages. Cancer Sci. *99*, 1595–1602.

Hoeffel, G., Wang, Y., Greter, M., See, P., Teo, P., Malleret, B., Leboeuf, M., Low, D., Oller, G., Almeida, F., et al. (2012). Adult Langerhans cells derive predominantly from embryonic fetal liver monocytes with a minor contribution of yolk sac-derived macrophages. J. Exp. Med. *209*, 1167–1181.

Hotamisligil, G.S., Shargill, N.S., and Spiegelman, B.M. (1993). Adipose expression of tumor necrosis factor-alpha: direct role in obesity-linked insulin resistance. Science *259*, 87–91.

Hotamisligil, G.S., Peraldi, P., Budavari, A., Ellis, R., White, M.F., and Spiegelman, B.M. (1996). IRS-1-mediated inhibition of insulin receptor tyrosine kinase activity in TNF-alpha- and obesity-induced insulin resistance. Science *271*, 665–668.

Hoves, S., Ooi, C.-H., Wolter, C., Sade, H., Bissinger, S., Schmittnaegel, M., Ast, O., Giusti, A.M., Wartha, K., Runza, V., et al. (2018). Rapid activation of tumor-associated macrophages boosts preexisting tumor immunity. J. Exp. Med. *215*, 859–876.

Howard, D., Garcia-Parra, J., Healey, G.D., Amakiri, C., Margarit, L., Francis, L.W., Gonzalez, D., and Conlan, R.S. (2016). Antibody-drug conjugates and other nanomedicines: the frontier of gynaecological cancer treatment. Interface Focus *6*, 20160054.

Huang, D.W., Sherman, B.T., and Lempicki, R.A. (2009a). Bioinformatics enrichment tools: paths toward the comprehensive functional analysis of large gene lists. Nucleic Acids Res. *37*, 1–13.

Huang, D.W., Sherman, B.T., and Lempicki, R.A. (2009b). Systematic and integrative analysis of large gene lists using DAVID bioinformatics resources. Nat. Protoc. *4*, 44–57.

Hume, D.A. (2015). The many alternative faces of macrophage activation. Front. Immunol. *6*, 370.

Ivashkiv, L.B. (2020). The hypoxia-lactate axis tempers inflammation. Nat. Rev. Immunol. *20*, 85–86.

Joffre, O.P., Segura, E., Savina, A., and Amigorena, S. (2012). Cross-presentation by dendritic cells. Nat. Rev. Immunol. *12*, 557–569.

Joyce, J.A., and Pollard, J.W. (2009). Microenvironmental regulation of metastasis. Nat. Rev. Cancer *9*, 239–252.

Joyce, J.A., Baruch, A., Chehade, K., Meyer-Morse, N., Giraudo, E., Tsai, F.-Y., Greenbaum, D.C., Hager, J.H., Bogyo, M., and Hanahan, D. (2004). Cathepsin cysteine proteases are effectors of invasive growth and angiogenesis during multistage tumorigenesis. Cancer Cell *5*, 443–453.

Ju, C., McCoy, J.P., Chung, C.J., Graf, M.L.M., and Pohl, L.R. (2003). Tolerogenic role of Kupffer cells in allergic reactions. Chem. Res. Toxicol. *16*, 1514–1519.

Kai, F., Drain, A.P., and Weaver, V.M. (2019). The extracellular matrix modulates the metastatic journey. Dev. Cell *49*, 332–346.

Kaneda, M.M., Messer, K.S., Ralainirina, N., Li, H., Leem, C.J., Gorjestani, S., Woo, G., Nguyen, A.V., Figueiredo, C.C., Foubert, P., et al. (2016). PI3Kγ is a molecular switch that controls immune suppression. Nature *539*, 437–442.

Kang, T.H., and Jung, S.T. (2019). Boosting therapeutic potency of antibodies by taming Fc domain functions. Exp Mol Med *51*, 1–9.

Kanter, J.E., Hsu, C.-C., and Bornfeldt, K.E. (2020). Monocytes and macrophages as protagonists in vascular complications of diabetes. Front. Cardiovasc. Med. *7*, 10.

Kawanishi, S., Ohnishi, S., Ma, N., Hiraku, Y., and Murata, M. (2017). Crosstalk between DNA Damage and Inflammation in the Multiple Steps of Carcinogenesis. Int. J. Mol. Sci. *18*.

Kelly, B., and O'Neill, L.A.J. (2015). Metabolic reprogramming in macrophages and dendritic cells in innate immunity. Cell Res. *25*, 771–784.

Kerbel, R.S., and Kamen, B.A. (2004). The anti-angiogenic basis of metronomic chemotherapy. Nat. Rev. Cancer *4*, 423–436.

Kleinovink, J.W., Marijt, K.A., Schoonderwoerd, M.J.A., van Hall, T., Ossendorp, F., and Fransen, M.F. (2017). PD-L1 expression on malignant cells is no prerequisite for checkpoint therapy. Oncoimmunology *6*, e1294299.

Klug, F., Prakash, H., Huber, P.E., Seibel, T., Bender, N., Halama, N., Pfirschke, C., Voss, R.H., Timke, C., Umansky, L., et al. (2013). Low-dose irradiation programs macrophage differentiation to an iNOS^{+}/M1 phenotype that orchestrates effective T cell immunotherapy. Cancer Cell *24*, 589–602.

Kratz, M., Coats, B.R., Hisert, K.B., Hagman, D., Mutskov, V., Peris, E., Schoenfelt, K.Q., Kuzma, J.N., Larson, I., Billing, P.S., et al. (2014). Metabolic dysfunction drives a mechanistically distinct proinflammatory phenotype in adipose tissue macrophages. Cell Metab. *20*, 614–625.

Kroemer, G., Galluzzi, L., Kepp, O., and Zitvogel, L. (2013). Immunogenic cell death in cancer therapy. Annu. Rev. Immunol. *31*, 51–72.

Kumar, V., Cheng, P., Condamine, T., Mony, S., Languino, L.R., McCaffrey, J.C., Hockstein, N., Guarino, M., Masters, G., Penman, E., et al. (2016). CD45 Phosphatase Inhibits STAT3 Transcription Factor Activity in Myeloid Cells and Promotes Tumor-Associated Macrophage

Differentiation. Immunity *44*, 303–315.

Kurts, C., Robinson, B.W.S., and Knolle, P.A. (2010). Cross-priming in health and disease. Nat. Rev. Immunol. *10*, 403–414.

Kusmartsev, S., and Gabrilovich, D.I. (2005). STAT1 signaling regulates tumor-associated macrophage-mediated T cell deletion. J. Immunol. *174*, 4880–4891.

Lavin, Y., Winter, D., Blecher-Gonen, R., David, E., Keren-Shaul, H., Merad, M., Jung, S., and Amit, I. (2014). Tissue-resident macrophage enhancer landscapes are shaped by the local microenvironment. Cell *159*, 1312–1326.

Lee, H., Lytton-Jean, A.K.R., Chen, Y., Love, K.T., Park, A.I., Karagiannis, E.D., Sehgal, A., Querbes, W., Zurenko, C.S., Jayaraman, M., et al. (2012). Molecularly self-assembled nucleic acid nanoparticles for targeted in vivo siRNA delivery. Nat. Nanotechnol. *7*, 389–393.

Lengauer, C., Kinzler, K.W., and Vogelstein, B. (1998). Genetic instabilities in human cancers. Nature *396*, 643–649.

Leopold Wager, C.M., Arnett, E., and Schlesinger, L.S. (2019). Macrophage nuclear receptors: Emerging key players in infectious diseases. PLoS Pathog. *15*, e1007585.

Leung, K., Chakraborty, K., Saminathan, A., and Krishnan, Y. (2019). A DNA nanomachine chemically resolves lysosomes in live cells. Nat. Nanotechnol. *14*, 176–183.

Li, A.C., and Glass, C.K. (2002). The macrophage foam cell as a target for therapeutic intervention. Nat. Med. *8*, 1235–1242.

Li, F., Lv, B., Liu, Y., Hua, T., Han, J., Sun, C., Xu, L., Zhang, Z., Feng, Z., Cai, Y., et al. (2018a). Blocking the CD47-SIRPα axis by delivery of anti-CD47 antibody induces antitumor effects in glioma and glioma stem cells. Oncoimmunology *7*, e1391973.

Li, H., Sorenson, A.L., Poczobutt, J., Amin, J., Joyal, T., Sullivan, T., Crossno, J.T., Weiser-Evans, M.C.M., and Nemenoff, R.A. (2011). Activation of PPARγ in myeloid cells promotes lung cancer progression and metastasis. PLoS One *6*, e28133.

Li, S., Jiang, Q., Liu, S., Zhang, Y., Tian, Y., Song, C., Wang, J., Zou, Y., Anderson, G.J., Han, J.-Y., et al. (2018b). A DNA nanorobot functions as a cancer therapeutic in response to a molecular trigger in vivo. Nat. Biotechnol. *36*, 258–264.

Li, Z., He, X., Luo, X., Wang, L., and Ma, N. (2016). DNA-Programmed Quantum Dot Polymerization for Ultrasensitive Molecular Imaging of Cancer Cells. Anal. Chem. *88*, 9355–9358.

Liguori, M., Buracchi, C., Pasqualini, F., Bergomas, F., Pesce, S., Sironi, M., Grizzi, F., Mantovani, A., Belgiovine, C., and Allavena, P. (2016). Functional TRAIL receptors in

monocytes and tumor-associated macrophages: A possible targeting pathway in the tumor microenvironment. Oncotarget *7*, 41662–41676.

Lin, E.Y., and Pollard, J.W. (2007). Tumor-associated macrophages press the angiogenic switch in breast cancer. Cancer Res. *67*, 5064–5066.

Lin, N., and Simon, M.C. (2016). Hypoxia-inducible factors: key regulators of myeloid cells during inflammation. J. Clin. Invest. *126*, 3661–3671.

Lin, E.Y., Nguyen, A.V., Russell, R.G., and Pollard, J.W. (2001). Colony-stimulating factor 1 promotes progression of mammary tumors to malignancy. J. Exp. Med. *193*, 727–740.

Lin, E.Y., Li, J.-F., Gnatovskiy, L., Deng, Y., Zhu, L., Grzesik, D.A., Qian, H., Xue, X., and Pollard, J.W. (2006). Macrophages regulate the angiogenic switch in a mouse model of breast cancer. Cancer Res. *66*, 11238–11246.

Liu, J., Zhang, N., Li, Q., Zhang, W., Ke, F., Leng, Q., Wang, H., Chen, J., and Wang, H. (2011). Tumor-associated macrophages recruit CCR6+ regulatory T cells and promote the development of colorectal cancer via enhancing CCL20 production in mice. PLoS One *6*, e19495.

Liu, J., Wang, L., Zhao, F., Tseng, S., Narayanan, C., Shura, L., Willingham, S., Howard, M., Prohaska, S., Volkmer, J., et al. (2015). Pre-Clinical Development of a Humanized Anti-CD47 Antibody with Anti-Cancer Therapeutic Potential. PLoS One *10*, e0137345.

Liu, M., O'Connor, R.S., Trefely, S., Graham, K., Snyder, N.W., and Beatty, G.L. (2019). Metabolic rewiring of macrophages by CpG potentiates clearance of cancer cells and overcomes tumor-expressed CD47-mediated "don't-eat-me" signal. Nat. Immunol. *20*, 265–275.

Liu, X., Kwon, H., Li, Z., and Fu, Y.-X. (2017). Is CD47 an innate immune checkpoint for tumor evasion? J Hematol Oncol *10*, 12.

Loeb, L.A., Loeb, K.R., and Anderson, J.P. (2003). Multiple mutations and cancer. Proc. Natl. Acad. Sci. USA *100*, 776–781.

Lund, A.W., Duraes, F.V., Hirosue, S., Raghavan, V.R., Nembrini, C., Thomas, S.N., Issa, A., Hugues, S., and Swartz, M.A. (2012). VEGF-C promotes immune tolerance in B16 melanomas and cross-presentation of tumor antigen by lymph node lymphatics. Cell Rep. *1*, 191–199.

Mackaness, G.B. (1962). Cellular resistance to infection. J. Exp. Med. *116*, 381–406.

Madsen, D.H., Jürgensen, H.J., Siersbæk, M.S., Kuczek, D.E., Grey Cloud, L., Liu, S., Behrendt, N., Grøntved, L., Weigert, R., and Bugge, T.H. (2017). Tumor-Associated Macrophages Derived from Circulating Inflammatory Monocytes Degrade Collagen through Cellular Uptake. Cell Rep. *21*, 3662–3671.

Maiti, R. (2014). Metronomic chemotherapy. J Pharmacol Pharmacother *5*, 186–192.

Manthey, C.L., Johnson, D.L., Illig, C.R., Tuman, R.W., Zhou, Z., Baker, J.F., Chaikin, M.A., Donatelli, R.R., Franks, C.F., Zeng, L., et al. (2009). JNJ-28312141, a novel orally active colony-stimulating factor-1 receptor/FMS-related receptor tyrosine kinase-3 receptor tyrosine kinase inhibitor with potential utility in solid tumors, bone metastases, and acute myeloid leukemia. Mol. Cancer Ther. *8*, 3151–3161.

Mantovani, A., Sozzani, S., Locati, M., Allavena, P., and Sica, A. (2002). Macrophage polarization: tumor-associated macrophages as a paradigm for polarized M2 mononuclear phagocytes. Trends Immunol. *23*, 549–555.

Mantovani, A., Sica, A., Sozzani, S., Allavena, P., Vecchi, A., and Locati, M. (2004). The chemokine system in diverse forms of macrophage activation and polarization. Trends Immunol. *25*, 677–686.

Mantovani, A., Allavena, P., Sica, A., and Balkwill, F. (2008). Cancer-related inflammation. Nature *454*, 436–444.

Mantovani, A., Marchesi, F., Malesci, A., Laghi, L., and Allavena, P. (2017). Tumour-associated macrophages as treatment targets in oncology. Nat. Rev. Clin. Oncol. *14*, 399–416.

Marra, M., Salzano, G., Leonetti, C., Tassone, P., Scarsella, M., Zappavigna, S., Calimeri, T., Franco, R., Liguori, G., Cigliana, G., et al. (2011). Nanotechnologies to use bisphosphonates as potent anticancer agents: the effects of zoledronic acid encapsulated into liposomes. Nanomedicine *7*, 955–964.

Martinez, F.O., and Gordon, S. (2014). The M1 and M2 paradigm of macrophage activation: time for reassessment. F1000Prime Rep. *6*, 13.

Matsumoto, K., Mizoue, K., Kitamura, K., Tse, W.C., Huber, C.P., and Ishida, T. (1999). Structural basis of inhibition of cysteine proteases by E-64 and its derivatives. Biopolymers *51*, 99–107.

Medzhitov, R., and Janeway, C. (2000). The Toll receptor family and microbial recognition. Trends Microbiol. *8*, 452–456.

Mei, J., Xiao, Z., Guo, C., Pu, Q., Ma, L., Liu, C., Lin, F., Liao, H., You, Z., and Liu, L. (2016). Prognostic impact of tumor-associated macrophage infiltration in non-small cell lung cancer: A systemic review and meta-analysis. Oncotarget *7*, 34217–34228.

Melisi, D., Frizziero, M., Tamburrino, A., Zanotto, M., Carbone, C., Piro, G., and Tortora, G. (2014). Toll-Like Receptor 9 Agonists for Cancer Therapy. Biomedicines *2*, 211–228.

Meric-Bernstam, F., Sandhu, S.K., Hamid, O., Spreafico, A., Kasper, S., Dummer, R., Shimizu, T., Steeghs, N., Lewis, N., Talluto, C.C., et al. (2019). Phase Ib study of MIW815 (ADU-S100) in combination with spartalizumab (PDR001) in patients (pts) with advanced/metastatic solid

tumors or lymphomas. J. Clin. Oncol. *37*, 2507–2507.

Metchnikoff, M.E., and Metchnikoff, E. (1873). Untersuchungen über die intracelluläre Verdauung bei wirbellosen Tieren.

Metschnikoff, E. (1884). Ueber eine Sprosspilzkrankheit der Daphnien. Beitrag zur Lehre über den Kampf der Phagocyten gegen Krankheitserreger. Archiv f. Pathol. Anat. *96*, 177–195.

Miao, P., Sheng, S., Sun, X., Liu, J., and Huang, G. (2013). Lactate dehydrogenase A in cancer: a promising target for diagnosis and therapy. IUBMB Life *65*, 904–910.

Mills, C.D., Kincaid, K., Alt, J.M., Heilman, M.J., and Hill, A.M. (2000). M-1/M-2 macrophages and the Th1/Th2 paradigm. J. Immunol. *164*, 6166–6173.

Mills, C.D., Thomas, A.C., Lenz, L.L., and Munder, M. (2014). Macrophage: SHIP of immunity. Front. Immunol. *5*, 620.

Miselis, N.R., Wu, Z.J., Van Rooijen, N., and Kane, A.B. (2008). Targeting tumor-associated macrophages in an orthotopic murine model of diffuse malignant mesothelioma. Mol. Cancer Ther. *7*, 788–799.

Mizuochi, T., Yee, S.T., Kasai, M., Kakiuchi, T., Muno, D., and Kominami, E. (1994). Both cathepsin B and cathepsin D are necessary for processing of ovalbumin as well as for degradation of class II MHC invariant chain. Immunol. Lett. *43*, 189–193.

Mohamed, M.M., and Sloane, B.F. (2006). Cysteine cathepsins: multifunctional enzymes in cancer. Nat. Rev. Cancer *6*, 764–775.

Moore, K.J., and Tabas, I. (2011). Macrophages in the pathogenesis of atherosclerosis. Cell *145*, 341–355.

Moore, K.J., Sheedy, F.J., and Fisher, E.A. (2013). Macrophages in atherosclerosis: a dynamic balance. Nat. Rev. Immunol. *13*, 709–721.

Morandi, F., and Pistoia, V. (2014). Interactions between HLA-G and HLA-E in Physiological and Pathological Conditions. Front. Immunol. *5*, 394.

Mosmann, T.R., Cherwinski, H., Bond, M.W., Giedlin, M.A., and Coffman, R.L. (1986). Two types of murine helper T cell clone. I. Definition according to profiles of lymphokine activities and secreted proteins. J. Immunol. *136*, 2348–2357.

Muller, P.A., Koscsó, B., Rajani, G.M., Stevanovic, K., Berres, M.-L., Hashimoto, D., Mortha, A., Leboeuf, M., Li, X.-M., Mucida, D., et al. (2014). Crosstalk between muscularis macrophages and enteric neurons regulates gastrointestinal motility. Cell *158*, 300–313.

Munn, D.H., and Cheung, N.K. (1990). Phagocytosis of tumor cells by human monocytes

cultured in recombinant macrophage colony-stimulating factor. J. Exp. Med. *172*, 231–237.

Munn, D.H., Shafizadeh, E., Attwood, J.T., Bondarev, I., Pashine, A., and Mellor, A.L. (1999). Inhibition of T cell proliferation by macrophage tryptophan catabolism. J. Exp. Med. *189*, 1363–1372.

Murray, P.J. (2017). Macrophage Polarization. Annu. Rev. Physiol. *79*, 541–566.

Murray, P.J., Allen, J.E., Biswas, S.K., Fisher, E.A., Gilroy, D.W., Goerdt, S., Gordon, S., Hamilton, J.A., Ivashkiv, L.B., Lawrence, T., et al. (2014). Macrophage activation and polarization: nomenclature and experimental guidelines. Immunity *41*, 14–20.

Nakagawa, T.Y., and Rudensky, A.Y. (1999). The role of lysosomal proteinases in MHC class II-mediated antigen processing and presentation. Immunol. Rev. *172*, 121–129.

Napoletano, C., Zizzari, I.G., Rughetti, A., Rahimi, H., Irimura, T., Clausen, H., Wandall, H.H., Belleudi, F., Bellati, F., Pierelli, L., et al. (2012). Targeting of macrophage galactose-type C-type lectin (MGL) induces DC signaling and activation. Eur. J. Immunol. *42*, 936–945.

Napolitano, G., and Ballabio, A. (2016). TFEB at a glance. J. Cell Sci. *129*, 2475–2481.

Nathan, C.F. (1983). Mechanisms of macrophage antimicrobial activity. Trans. R. Soc. Trop. Med. Hyg. *77*, 620–630.

Nathan, C., and Ding, A. (2010). Nonresolving inflammation. Cell *140*, 871–882.

Nathan, C.F., Karnovsky, M.L., and David, J.R. (1971). Alterations of macrophage functions by mediators from lymphocytes. J. Exp. Med. *133*, 1356–1376.

Nathan, C.F., Remold, H.G., and David, J.R. (1973). Characterization of a lymphocyte factor which alters macrophage functions. J. Exp. Med. *137*, 275–290.

North, R.J., and Mackaness, G.B. (1963). Electron microscopical observations on the peritoneal macrophages of normal mice and mice immunised with listeria monocytogenes. ii. structure of macrophages from immune mice and early cytoplasmic response to the presence of ingested bacteria. Br J Exp Pathol *44*, 608–611.

Noy, R., and Pollard, J.W. (2014). Tumor-associated macrophages: from mechanisms to therapy. Immunity *41*, 49–61.

Odegaard, J.I., Ricardo-Gonzalez, R.R., Goforth, M.H., Morel, C.R., Subramanian, V., Mukundan, L., Red Eagle, A., Vats, D., Brombacher, F., Ferrante, A.W., et al. (2007). Macrophage-specific PPARgamma controls alternative activation and improves insulin resistance. Nature *447*, 1116–1120.

Oh, K.-S., Patel, H., Gottschalk, R.A., Lee, W.S., Baek, S., Fraser, I.D.C., Hager, G.L., and

Sung, M.-H. (2017). Anti-Inflammatory Chromatinscape Suggests Alternative Mechanisms of Glucocorticoid Receptor Action. Immunity *47*, 298–309.e5.

Okabe, Y., and Medzhitov, R. (2016). Tissue biology perspective on macrophages. Nat. Immunol. *17*, 9–17.

Okazawa, H., Motegi, S., Ohyama, N., Ohnishi, H., Tomizawa, T., Kaneko, Y., Oldenborg, P.-A., Ishikawa, O., and Matozaki, T. (2005). Negative regulation of phagocytosis in macrophages by the CD47-SHPS-1 system. J. Immunol. *174*, 2004–2011.

Olefsky, J.M., and Glass, C.K. (2010). Macrophages, inflammation, and insulin resistance. Annu. Rev. Physiol. *72*, 219–246.

Olson, O.C., and Joyce, J.A. (2015). Cysteine cathepsin proteases: regulators of cancer progression and therapeutic response. Nat. Rev. Cancer *15*, 712–729.

O'Neill, L.A.J., and Hardie, D.G. (2013). Metabolism of inflammation limited by AMPK and pseudo-starvation. Nature *493*, 346–355.

Ong, S.-M., Tan, Y.-C., Beretta, O., Jiang, D., Yeap, W.-H., Tai, J.J.Y., Wong, W.-C., Yang, H., Schwarz, H., Lim, K.-H., et al. (2012). Macrophages in human colorectal cancer are pro-inflammatory and prime T cells towards an anti-tumour type-1 inflammatory response. Eur. J. Immunol. *42*, 89–100.

O'Sullivan, T., Saddawi-Konefka, R., Vermi, W., Koebel, C.M., Arthur, C., White, J.M., Uppaluri, R., Andrews, D.M., Ngiow, S.F., Teng, M.W.L., et al. (2012). Cancer immunoediting by the innate immune system in the absence of adaptive immunity. J. Exp. Med. *209*, 1869–1882.

Owen, J.L., and Mohamadzadeh, M. (2013). Macrophages and chemokines as mediators of angiogenesis. Front. Physiol. *4*, 159.

Palucka, A.K., and Coussens, L.M. (2016). The basis of oncoimmunology. Cell *164*, 1233–1247.

Paolicelli, R.C., Bolasco, G., Pagani, F., Maggi, L., Scianni, M., Panzanelli, P., Giustetto, M., Ferreira, T.A., Guiducci, E., Dumas, L., et al. (2011). Synaptic pruning by microglia is necessary for normal brain development. Science *333*, 1456–1458.

Parkhurst, C.N., Yang, G., Ninan, I., Savas, J.N., Yates, J.R., Lafaille, J.J., Hempstead, B.L., Littman, D.R., and Gan, W.-B. (2013). Microglia promote learning-dependent synapse formation through brain-derived neurotrophic factor. Cell *155*, 1596–1609.

Pastor, F., Kolonias, D., McNamara, J.O., and Gilboa, E. (2011). Targeting 4-1BB costimulation to disseminated tumor lesions with bi-specific oligonucleotide aptamers. Mol. Ther. *19*, 1878–1886.

Penny, H.L., Sieow, J.L., Adriani, G., Yeap, W.H., See Chi Ee, P., San Luis, B., Lee, B., Lee, T., Mak, S.Y., Ho, Y.S., et al. (2016). Warburg metabolism in tumor-conditioned macrophages promotes metastasis in human pancreatic ductal adenocarcinoma. Oncoimmunology *5*, e1191731.

Perry, C.J., Muñoz-Rojas, A.R., Meeth, K.M., Kellman, L.N., Amezquita, R.A., Thakral, D., Du, V.Y., Wang, J.X., Damsky, W., Kuhlmann, A.L., et al. (2018). Myeloid-targeted immunotherapies act in synergy to induce inflammation and antitumor immunity. J. Exp. Med. *215*, 877–893.

Petersen, M.C., and Shulman, G.I. (2018). Mechanisms of insulin action and insulin resistance. Physiol. Rev. *98*, 2133–2223.

Petrova, V., Annicchiarico-Petruzzelli, M., Melino, G., and Amelio, I. (2018). The hypoxic tumour microenvironment. Oncogenesis *7*, 10.

Poh, A.R., and Ernst, M. (2018). Targeting macrophages in cancer: from bench to bedside. Front. Oncol. *8*, 49.

Powers, J.C., Asgian, J.L., Ekici, Ö.D., and James, K.E. (2002). Irreversible Inhibitors of Serine, Cysteine, and Threonine Proteases. Chem. Rev. *102*, 4639–4750.

Qian, B.-Z., and Pollard, J.W. (2010). Macrophage diversity enhances tumor progression and metastasis. Cell *141*, 39–51.

Qian, B.-Z., Li, J., Zhang, H., Kitamura, T., Zhang, J., Campion, L.R., Kaiser, E.A., Snyder, L.A., and Pollard, J.W. (2011). CCL2 recruits inflammatory monocytes to facilitate breast-tumour metastasis. Nature *475*, 222–225.

Reardon, C.A., Lingaraju, A., Schoenfelt, K.Q., Zhou, G., Cui, C., Jacobs-El, H., Babenko, I., Hoofnagle, A., Czyz, D., Shuman, H., et al. (2018). Obesity and Insulin Resistance Promote Atherosclerosis through an IFNγ-Regulated Macrophage Protein Network. Cell Rep. *23*, 3021–3030.

Remmerie, A., and Scott, C.L. (2018). Macrophages and lipid metabolism. Cell Immunol. *330*, 27–42.

Ries, C.H., Cannarile, M.A., Hoves, S., Benz, J., Wartha, K., Runza, V., Rey-Giraud, F., Pradel, L.P., Feuerhake, F., Klaman, I., et al. (2014). Targeting tumor-associated macrophages with anti-CSF-1R antibody reveals a strategy for cancer therapy. Cancer Cell *25*, 846–859.

Roberts, E.W., Broz, M.L., Binnewies, M., Headley, M.B., Nelson, A.E., Wolf, D.M., Kaisho, T., Bogunovic, D., Bhardwaj, N., and Krummel, M.F. (2016). Critical role for CD103(+)/CD141(+) dendritic cells bearing CCR7 for tumor antigen trafficking and priming of T cell immunity in melanoma. Cancer Cell *30*, 324–336.

Roche, P.A., and Furuta, K. (2015). The ins and outs of MHC class II-mediated antigen processing and presentation. Nat. Rev. Immunol. *15*, 203–216.

Rodell, C.B., Arlauckas, S.P., Cuccarese, M.F., Garris, C.S., Li, R., Ahmed, M.S., Kohler, R.H., Pittet, M.J., and Weissleder, R. (2018). TLR7/8-agonist-loaded nanoparticles promote the polarization of tumour-associated macrophages to enhance cancer immunotherapy. Nat. Biomed. Eng. *2*, 578–588.

Rodriguez, G.M., and Diment, S. (1995). Destructive proteolysis by cysteine proteases in antigen presentation of ovalbumin. Eur. J. Immunol. *25*, 1823–1827.

Rodriguez, P.C., Zea, A.H., DeSalvo, J., Culotta, K.S., Zabaleta, J., Quiceno, D.G., Ochoa, J.B., and Ochoa, A.C. (2003). L-arginine consumption by macrophages modulates the expression of CD3 zeta chain in T lymphocytes. J. Immunol. *171*, 1232–1239.

Rodriguez, P.C., Quiceno, D.G., Zabaleta, J., Ortiz, B., Zea, A.H., Piazuelo, M.B., Delgado, A., Correa, P., Brayer, J., Sotomayor, E.M., et al. (2004). Arginase I production in the tumor microenvironment by mature myeloid cells inhibits T-cell receptor expression and antigen-specific T-cell responses. Cancer Res. *64*, 5839–5849.

Rodríguez-Prados, J.-C., Través, P.G., Cuenca, J., Rico, D., Aragonés, J., Martín-Sanz, P., Cascante, M., and Boscá, L. (2010). Substrate fate in activated macrophages: a comparison between innate, classic, and alternative activation. J. Immunol. *185*, 605–614.

Rogers, T.L., and Holen, I. (2011). Tumour macrophages as potential targets of bisphosphonates. J. Transl. Med. *9*, 177.

Saberi, M., Woods, N.-B., de Luca, C., Schenk, S., Lu, J.C., Bandyopadhyay, G., Verma, I.M., and Olefsky, J.M. (2009). Hematopoietic cell-specific deletion of toll-like receptor 4 ameliorates hepatic and adipose tissue insulin resistance in high-fat-fed mice. Cell Metab. *10*, 419–429.

Sagiv-Barfi, I., Czerwinski, D.K., Levy, S., Alam, I.S., Mayer, A.T., Gambhir, S.S., and Levy, R. (2018). Eradication of spontaneous malignancy by local immunotherapy. Sci. Transl. Med. *10*.

Saio, M., Radoja, S., Marino, M., and Frey, A.B. (2001). Tumor-infiltrating macrophages induce apoptosis in activated CD8(+) T cells by a mechanism requiring cell contact and mediated by both the cell-associated form of TNF and nitric oxide. J. Immunol. *167*, 5583–5593.

Salmi, M. (2017). Macrophages and cancer. Duodecim *133*, 829–837.

Samie, M., and Cresswell, P. (2015). The transcription factor TFEB acts as a molecular switch that regulates exogenous antigen-presentation pathways. Nat. Immunol. *16*, 729–736.

Sardiello, M., Palmieri, M., di Ronza, A., Medina, D.L., Valenza, M., Gennarino, V.A., Di Malta, C., Donaudy, F., Embrione, V., Polishchuk, R.S., et al. (2009). A gene network regulating lysosomal biogenesis and function. Science *325*, 473–477.

Satpathy, A.T., Kc, W., Albring, J.C., Edelson, B.T., Kretzer, N.M., Bhattacharya, D., Murphy, T.L., and Murphy, K.M. (2012). Zbtb46 expression distinguishes classical dendritic cells and their committed progenitors from other immune lineages. J. Exp. Med. *209*, 1135–1152.

Sawyer, R.T., Strausbauch, P.H., and Volkman, A. (1982). Resident macrophage proliferation in mice depleted of blood monocytes by strontium-89. Lab. Invest. *46*, 165–170.

Schroder, K., Irvine, K.M., Taylor, M.S., Bokil, N.J., Le Cao, K.-A., Masterman, K.-A., Labzin, L.I., Semple, C.A., Kapetanovic, R., Fairbairn, L., et al. (2012). Conservation and divergence in Toll-like receptor 4-regulated gene expression in primary human versus mouse macrophages. Proc. Natl. Acad. Sci. USA *109*, E944-53.

Schulz, C., Gomez Perdiguero, E., Chorro, L., Szabo-Rogers, H., Cagnard, N., Kierdorf, K., Prinz, M., Wu, B., Jacobsen, S.E.W., Pollard, J.W., et al. (2012). A lineage of myeloid cells independent of Myb and hematopoietic stem cells. Science *336*, 86–90.

Seimon, T.A., Nadolski, M.J., Liao, X., Magallon, J., Nguyen, M., Feric, N.T., Koschinsky, M.L., Harkewicz, R., Witztum, J.L., Tsimikas, S., et al. (2010). Atherogenic lipids and lipoproteins trigger CD36-TLR2-dependent apoptosis in macrophages undergoing endoplasmic reticulum stress. Cell Metab. *12*, 467–482.

Seki, S., Habu, Y., Kawamura, T., Takeda, K., Dobashi, H., Ohkawa, T., and Hiraide, H. (2000). The liver as a crucial organ in the first line of host defense: the roles of Kupffer cells, natural killer (NK) cells and NK1.1 Ag+ T cells in T helper 1 immune responses. Immunol. Rev. *174*, 35–46.

Serafini, P., Mgebroff, S., Noonan, K., and Borrello, I. (2008). Myeloid-derived suppressor cells promote cross-tolerance in B-cell lymphoma by expanding regulatory T cells. Cancer Res. *68*, 5439–5449.

Seth, P., Csizmadia, E., Hedblom, A., Vuerich, M., Xie, H., Li, M., Longhi, M.S., and Wegiel, B. (2017). Deletion of Lactate Dehydrogenase-A in Myeloid Cells Triggers Antitumor Immunity. Cancer Res. *77*, 3632–3643.

Settembre, C., Di Malta, C., Polito, V.A., Garcia Arencibia, M., Vetrini, F., Erdin, S., Erdin, S.U., Huynh, T., Medina, D., Colella, P., et al. (2011). TFEB links autophagy to lysosomal biogenesis. Science *332*, 1429–1433.

Sharma, P., and Allison, J.P. (2015). Immune checkpoint targeting in cancer therapy: toward combination strategies with curative potential. Cell *161*, 205–214.

Shen, L., Sigal, L.J., Boes, M., and Rock, K.L. (2004). Important role of cathepsin S in generating peptides for TAP-independent MHC class I crosspresentation in vivo. Immunity *21*, 155–165.

Shi, C., and Pamer, E.G. (2011). Monocyte recruitment during infection and inflammation. Nat. Rev. Immunol. *11*, 762–774.

Shi, Y., Oeh, J., Hitz, A., Hedehus, M., Eastham-Anderson, J., Peale, F.V., Hamilton, P., O'Brien, T., Sampath, D., and Carano, R.A.D. (2017). Monitoring and Targeting Anti-VEGF Induced Hypoxia within the Viable Tumor by 19F-MRI and Multispectral Analysis. Neoplasia *19*, 950–959.

Sigal, L.J., Crotty, S., Andino, R., and Rock, K.L. (1999). Cytotoxic T-cell immunity to virus-infected non-haematopoietic cells requires presentation of exogenous antigen. Nature *398*, 77–80.

Singhal, S., Stadanlick, J., Annunziata, M.J., Rao, A.S., Bhojnagarwala, P.S., O'Brien, S., Moon, E.K., Cantu, E., Danet-Desnoyers, G., Ra, H.-J., et al. (2019). Human tumor-associated monocytes/macrophages and their regulation of T cell responses in early-stage lung cancer. Sci. Transl. Med. *11*.

Sistigu, A., Viaud, S., Chaput, N., Bracci, L., Proietti, E., and Zitvogel, L. (2011). Immunomodulatory effects of cyclophosphamide and implementations for vaccine design. Semin Immunopathol *33*, 369–383.

Stankovic, B., Bjørhovde, H.A.K., Skarshaug, R., Aamodt, H., Frafjord, A., Müller, E., Hammarström, C., Beraki, K., Bækkevold, E.S., Woldbæk, P.R., et al. (2018). Immune Cell Composition in Human Non-small Cell Lung Cancer. Front. Immunol. *9*, 3101.

Stanley, E.R., Berg, K.L., Einstein, D.B., Lee, P.S.W., Pixley, F.J., Wang, Y., and Yeung, Y.-G. (1997). Biology and action of colony-stimulating factor-1. Mol. Reprod. Dev. *46*, 4–10.

Steggerda, S.M., Bennett, M.K., Chen, J., Emberley, E., Huang, T., Janes, J.R., Li, W., MacKinnon, A.L., Makkouk, A., Marguier, G., et al. (2017). Inhibition of arginase by CB-1158 blocks myeloid cell-mediated immune suppression in the tumor microenvironment. J. Immunother. Cancer *5*, 101.

Stein, M., Keshav, S., Harris, N., and Gordon, S. (1992). Interleukin 4 potently enhances murine macrophage mannose receptor activity: a marker of alternative immunologic macrophage activation. J. Exp. Med. *176*, 287–292.

Strachan, D.C., Ruffell, B., Oei, Y., Bissell, M.J., Coussens, L.M., Pryer, N., and Daniel, D. (2013). CSF1R inhibition delays cervical and mammary tumor growth in murine models by attenuating the turnover of tumor-associated macrophages and enhancing infiltration by CD8+ T cells. Oncoimmunology *2*, e26968.

Strauss, L., Sangaletti, S., Consonni, F.M., Szebeni, G., Morlacchi, S., Totaro, M.G., Porta, C., Anselmo, A., Tartari, S., Doni, A., et al. (2015). RORC1 Regulates Tumor-Promoting "Emergency" Granulo-Monocytopoiesis. Cancer Cell *28*, 253–269.

Sullivan, M.R., Danai, L.V., Lewis, C.A., Chan, S.H., Gui, D.Y., Kunchok, T., Dennstedt, E.A., Vander Heiden, M.G., and Muir, A. (2019). Quantification of microenvironmental metabolites in murine cancers reveals determinants of tumor nutrient availability. Elife *8*.

Surana, S., Bhat, J.M., Koushika, S.P., and Krishnan, Y. (2011). An autonomous DNA nanomachine maps spatiotemporal pH changes in a multicellular living organism. Nat. Commun. *2*, 340.

Tachibana, K., Yamasaki, D., Ishimoto, K., and Doi, T. (2008). The role of ppars in cancer. PPAR Res *2008*, 102737.

Takeya, M., and Komohara, Y. (2016). Role of tumor-associated macrophages in human malignancies: friend or foe? Pathol Int *66*, 491–505.

Tang, X. (2013). Tumor-associated macrophages as potential diagnostic and prognostic biomarkers in breast cancer. Cancer Lett. *332*, 3–10.

Tauber, A.I. (2003). Metchnikoff and the phagocytosis theory. Nat. Rev. Mol. Cell Biol. *4*, 897–901.

Tauber, A.I., and Chernyak, L. (1991). Metchnikoff and the Origins of Immunology: From Metaphor to Theory (Monographs on the History and Philosophy of Biology) (Oxford University Press).

Teitelbaum, S.L., and Ross, F.P. (2003). Genetic regulation of osteoclast development and function. Nat. Rev. Genet. *4*, 638–649.

Thomas, A.C., and Mattila, J.T. (2014). "Of mice and men": arginine metabolism in macrophages. Front. Immunol. *5*, 479.

Thorsson, V., Gibbs, D.L., Brown, S.D., Wolf, D., Bortone, D.S., Ou Yang, T.-H., Porta-Pardo, E., Gao, G.F., Plaisier, C.L., Eddy, J.A., et al. (2018). The immune landscape of cancer. Immunity *48*, 812–830.e14.

Tikhanovich, I., Zhao, J., Olson, J., Adams, A., Taylor, R., Bridges, B., Marshall, L., Roberts, B., and Weinman, S.A. (2017). Protein arginine methyltransferase 1 modulates innate immune responses through regulation of peroxisome proliferator-activated receptor γ-dependent macrophage differentiation. J. Biol. Chem. *292*, 6882–6894.

Tomura, M., Yoshida, N., Tanaka, J., Karasawa, S., Miwa, Y., Miyawaki, A., and Kanagawa, O. (2008). Monitoring cellular movement in vivo with photoconvertible fluorescence protein "Kaede" transgenic mice. Proc. Natl. Acad. Sci. USA *105*, 10871–10876.

Travers, M., Brown, S.M., Dunworth, M., Holbert, C.E., Wiehagen, K.R., Bachman, K.E., Foley, J.R., Stone, M.L., Baylin, S.B., Casero, R.A., et al. (2019). DFMO and 5-Azacytidine Increase M1 Macrophages in the Tumor Microenvironment of Murine Ovarian Cancer. Cancer Res. *79*,

3445–3454.

Triozzi, P.L., Aldrich, W., Achberger, S., Ponnazhagan, S., Alcazar, O., and Saunthararajah, Y. (2012). Differential effects of low-dose decitabine on immune effector and suppressor responses in melanoma-bearing mice. Cancer Immunol. Immunother. *61*, 1441–1450.

Trombetta, E.S., and Mellman, I. (2005). Cell biology of antigen processing in vitro and in vivo. Annu. Rev. Immunol. *23*, 975–1028.

Trombetta, E.S., Ebersold, M., Garrett, W., Pypaert, M., and Mellman, I. (2003). Activation of lysosomal function during dendritic cell maturation. Science *299*, 1400–1403.

Tsung, K., Dolan, J.P., Tsung, Y.L., and Norton, J.A. (2002). Macrophages as effector cells in interleukin 12-induced T cell-dependent tumor rejection. Cancer Res. *62*, 5069–5075.

Uderhardt, S., Herrmann, M., Oskolkova, O.V., Aschermann, S., Bicker, W., Ipseiz, N., Sarter, K., Frey, B., Rothe, T., Voll, R., et al. (2012). 12/15-lipoxygenase orchestrates the clearance of apoptotic cells and maintains immunologic tolerance. Immunity *36*, 834–846.

Van Acker, H.H., Anguille, S., Willemen, Y., Smits, E.L., and Van Tendeloo, V.F. (2016). Bisphosphonates for cancer treatment: Mechanisms of action and lessons from clinical trials. Pharmacol. Ther. *158*, 24–40.

Veetil, A.T., Chakraborty, K., Xiao, K., Minter, M.R., Sisodia, S.S., and Krishnan, Y. (2017). Cell-targetable DNA nanocapsules for spatiotemporal release of caged bioactive small molecules. Nat. Nanotechnol. *12*, 1183–1189.

Vergadi, E., Ieronymaki, E., Lyroni, K., Vaporidi, K., and Tsatsanis, C. (2017). Akt signaling pathway in macrophage activation and M1/M2 polarization. J. Immunol. *198*, 1006–1014.

Villadangos, J.A., Bryant, R.A., Deussing, J., Driessen, C., Lennon-Duménil, A.M., Riese, R.J., Roth, W., Saftig, P., Shi, G.P., Chapman, H.A., et al. (1999). Proteases involved in MHC class II antigen presentation. Immunol. Rev. *172*, 109–120.

Vitale, I., Manic, G., Coussens, L.M., Kroemer, G., and Galluzzi, L. (2019). Macrophages and metabolism in the tumor microenvironment. Cell Metab. *30*, 36–50.

Vonderheide, R.H. (2018). The immune revolution: A case for priming, not checkpoint. Cancer Cell *33*, 563–569.

Waldman, A.D., Fritz, J.M., and Lenardo, M.J. (2020). A guide to cancer immunotherapy: from T cell basic science to clinical practice. Nat. Rev. Immunol. *20*, 651–668.

Wang, J., Li, D., Cang, H., and Guo, B. (2019). Crosstalk between cancer and immune cells: Role of tumor-associated macrophages in the tumor microenvironment. Cancer Med *8*, 4709–4721.

Ward, P.S., and Thompson, C.B. (2012). Metabolic reprogramming: a cancer hallmark even warburg did not anticipate. Cancer Cell *21*, 297–308.

Wculek, S.K., Cueto, F.J., Mujal, A.M., Melero, I., Krummel, M.F., and Sancho, D. (2020). Dendritic cells in cancer immunology and immunotherapy. Nat. Rev. Immunol. *20*, 7–24.

Wei, X., Song, H., Yin, L., Rizzo, M.G., Sidhu, R., Covey, D.F., Ory, D.S., and Semenkovich, C.F. (2016). Fatty acid synthesis configures the plasma membrane for inflammation in diabetes. Nature *539*, 294–298.

Weigert, A., von Knethen, A., Fuhrmann, D., Dehne, N., and Brüne, B. (2018). Redox-signals and macrophage biology. Mol. Aspects Med. *63*, 70–87.

Weisberg, S.P., McCann, D., Desai, M., Rosenbaum, M., Leibel, R.L., and Ferrante, A.W. (2003). Obesity is associated with macrophage accumulation in adipose tissue. J. Clin. Invest. *112*, 1796–1808.

Wenes, M., Shang, M., Di Matteo, M., Goveia, J., Martín-Pérez, R., Serneels, J., Prenen, H., Ghesquière, B., Carmeliet, P., and Mazzone, M. (2016). Macrophage metabolism controls tumor blood vessel morphogenesis and metastasis. Cell Metab. *24*, 701–715.

Winkler, J., Abisoye-Ogunniyan, A., Metcalf, K.J., and Werb, Z. (2020). Concepts of extracellular matrix remodelling in tumour progression and metastasis. Nat. Commun. *11*, 5120.

Wynn, T.A., and Barron, L. (2010). Macrophages: master regulators of inflammation and fibrosis. Semin Liver Dis *30*, 245–257.

Wynn, T.A., Chawla, A., and Pollard, J.W. (2013). Macrophage biology in development, homeostasis and disease. Nature *496*, 445–455.

Xiao, Z., Chung, H., Banan, B., Manning, P.T., Ott, K.C., Lin, S., Capoccia, B.J., Subramanian, V., Hiebsch, R.R., Upadhya, G.A., et al. (2015). Antibody mediated therapy targeting CD47 inhibits tumor progression of hepatocellular carcinoma. Cancer Lett. *360*, 302–309.

Xie, Y., Tolmeijer, S., Oskam, J.M., Tonkens, T., Meijer, A.H., and Schaaf, M.J.M. (2019). Glucocorticoids inhibit macrophage differentiation towards a pro-inflammatory phenotype upon wounding without affecting their migration. Dis. Model. Mech. *12*.

Xin, H., Zhang, C., Herrmann, A., Du, Y., Figlin, R., and Yu, H. (2009). Sunitinib inhibition of Stat3 induces renal cell carcinoma tumor cell apoptosis and reduces immunosuppressive cells. Cancer Res. *69*, 2506–2513.

Xu, H., Barnes, G.T., Yang, Q., Tan, G., Yang, D., Chou, C.J., Sole, J., Nichols, A., Ross, J.S., Tartaglia, L.A., et al. (2003). Chronic inflammation in fat plays a crucial role in the development of obesity-related insulin resistance. J. Clin. Invest. *112*, 1821–1830.

Xu, Q., Choksi, S., Qu, J., Jang, J., Choe, M., Banfi, B., Engelhardt, J.F., and Liu, Z.-G. (2016). NADPH oxidases are essential for macrophage differentiation. J. Biol. Chem. *291*, 20030–20041.

Yan, D., Wang, H.-W., Bowman, R.L., and Joyce, J.A. (2016). STAT3 and STAT6 Signaling Pathways Synergize to Promote Cathepsin Secretion from Macrophages via IRE1α Activation. Cell Rep. *16*, 2914–2927.

Yin, S., Huang, J., Li, Z., Zhang, J., Luo, J., Lu, C., Xu, H., and Xu, H. (2017). The Prognostic and Clinicopathological Significance of Tumor-Associated Macrophages in Patients with Gastric Cancer: A Meta-Analysis. PLoS One *12*, e0170042.

Zeisberger, S.M., Odermatt, B., Marty, C., Zehnder-Fjällman, A.H.M., Ballmer-Hofer, K., and Schwendener, R.A. (2006). Clodronate-liposome-mediated depletion of tumour-associated macrophages: a new and highly effective antiangiogenic therapy approach. Br. J. Cancer *95*, 272–281.

Zhang, L., and Li, S. (2020). Lactic acid promotes macrophage polarization through MCT-HIF1α signaling in gastric cancer. Exp. Cell Res. *388*, 111846.

Zhang, D., Tang, Z., Huang, H., Zhou, G., Cui, C., Weng, Y., Liu, W., Kim, S., Lee, S., Perez-Neut, M., et al. (2019). Metabolic regulation of gene expression by histone lactylation. Nature *574*, 575–580.

Zhang, P., Wang, C., Zhao, J., Xiao, A., Shen, Q., Li, L., Li, J., Zhang, J., Min, Q., Chen, J., et al. (2016). Near Infrared-Guided Smart Nanocarriers for MicroRNA-Controlled Release of Doxorubicin/siRNA with Intracellular ATP as Fuel. ACS Nano *10*, 3637–3647.

Zhao, X., Qu, J., Sun, Y., Wang, J., Liu, X., Wang, F., Zhang, H., Wang, W., Ma, X., Gao, X., et al. (2017). Prognostic significance of tumor-associated macrophages in breast cancer: a meta-analysis of the literature. Oncotarget *8*, 30576–30586.

Zhu, Y., Herndon, J.M., Sojka, D.K., Kim, K.-W., Knolhoff, B.L., Zuo, C., Cullinan, D.R., Luo, J., Bearden, A.R., Lavine, K.J., et al. (2017). Tissue-Resident Macrophages in Pancreatic Ductal Adenocarcinoma Originate from Embryonic Hematopoiesis and Promote Tumor Progression. Immunity *47*, 323–338.e6.

Zizzo, G., and Cohen, P.L. (2015). The PPAR-γ antagonist GW9662 elicits differentiation of M2c-like cells and upregulation of the MerTK/Gas6 axis: a key role for PPAR-γ in human macrophage polarization. J. Inflamm. (Lond.) *12*, 36.

(1998). Tamoxifen for early breast cancer: an overview of the randomised trials. Early Breast Cancer Trialists' Collaborative Group. Lancet *351*, 1451–1467.